NOTICE



Printed in the United States of America
Available from
National Technical Information Service
U.S. Department of Commerce
5285 Port Royal Road
Springfield, VA 22161

NTIS Price codes
Printed copy: A06
Microfiche copy: A01

# Chaos and Simple Determinism in Reversed Field Pinch Plasmas

## Nonlinear Analysis of Numerical Simulation and Experimental Data

by

Christopher A. Watts

A thesis submitted in partial fulfillment of the requirements for the degree of

Doctor Of Philosophy

(Physics)

at the

UNIVERSITY OF WISCONSIN - MADISON

1993

**Abstract**

In this dissertation the possibility that chaos and simple determinism are governing the dynamics of reversed field pinch (RFP) plasmas is investigated. To properly assess this possibility, data from both numerical simulations and experiment are analyzed. A large repertoire of nonlinear analysis techniques is used to identify low dimensional chaos in the data. These tools include phase portraits and Poincaré sections, correlation dimension, the spectrum of Lyapunov exponents and short term predictability. In addition, nonlinear noise reduction techniques are applied to the experimental data in an attempt to extract any underlying deterministic dynamics.

Two model systems are used to simulate the plasma dynamics. These are the DEBS code, which models global RFP dynamics, and the dissipative trapped electron mode (DTEM) model, which models drift wave turbulence. Data from both simulations show strong indications of low dimensional chaos and simple determinism. Experimental data were obtained from the Madison Symmetric Torus RFP and consist of a wide array of both global and local diagnostic signals. None of the signals shows any indication of low dimensional chaos or other simple determinism. Moreover, most of the analysis tools indicate the experimental system is very high dimensional with properties similar to noise. Nonlinear noise reduction is unsuccessful at extracting an underlying deterministic system.

**Acknowledgments**

To keep this brief I'll confine it just to physics. I begin with the two devils, each sitting by an ear, one who whispers "theory" and the other "experiment". David Newman and Sam Hokin, I will sorely miss having you close at hand to bounce ideas off and realign my guidance systems. I thank Clint Sprott, my advisor, who continually amazes me with his insightful, qualitative understanding of nonlinear dynamics. There is Earl Scime, whom I admire because he isn't afraid to ask when he doesn't understand (a disease common to graduate students). I will miss the inertial rangers office lads: Brett, Edwardo, Jim, Matt and Kevin. Thanks to Carl Sovinec and Liz Zita for help with the DEBS code. And thanks to Keith Briggs for his Lyapunov exponent code.

Finally, hats off to the U.S. Department of Energy, who supported this research.

**Table of Contents**

# 1. Introduction

> **Chaos:** "...deterministic chaos denotes the irregular or chaotic motion which is generated by nonlinear systems whose dynamical laws determine the evolution of a state of the system ..."[1]

Figure 1.1 compares three time series. One of the traces is data produced by a numerical random number generator, one trace is data from one of the standard diagnostics on the Madison Symmetric Torus (MST), and the third is generated from a simple deterministic equation. It is not obvious which signal/s is/are deterministic simply from inspection. Moreover, the data from the deterministic system is indistinguishable from random data using most conventional tests for randomness. Advances in nonlinear analysis techniques within the last decade however, now make it possible to distinguish the two using only their time records. It is the goal of the work presented in this dissertation to establish whether the signal from the MST may also be governed by simple deterministic equations or is better described as a stochastic process.

## 1.1. Brief History of Nonlinear Dynamics

Complex behavior in a system has traditionally required complex systems of equations to describe this behavior. Work over the past 30 years or so has demonstrated that extraordinarily rich and complex behavior can result from trivially simple systems of equations. The term "chaos" first came into use in the late '70s. However, long before this the dynamics of nonlinear equations of motion were explored by a few hardy souls. The most influential of these, the likely father of nonlinear dynamics, was Henri Poincaré (1854-1912). His work stressed global, qualitative understanding of a system's dynamics. Other important characters during this early analytical period include A.M. Lyapunov and G.D. Birkhoff. Most of this work remained largely unnoticed by the general scientific community for much of this century. The advent of electronic computers helped promote the field. In 1961, Edward Lorenz, using a

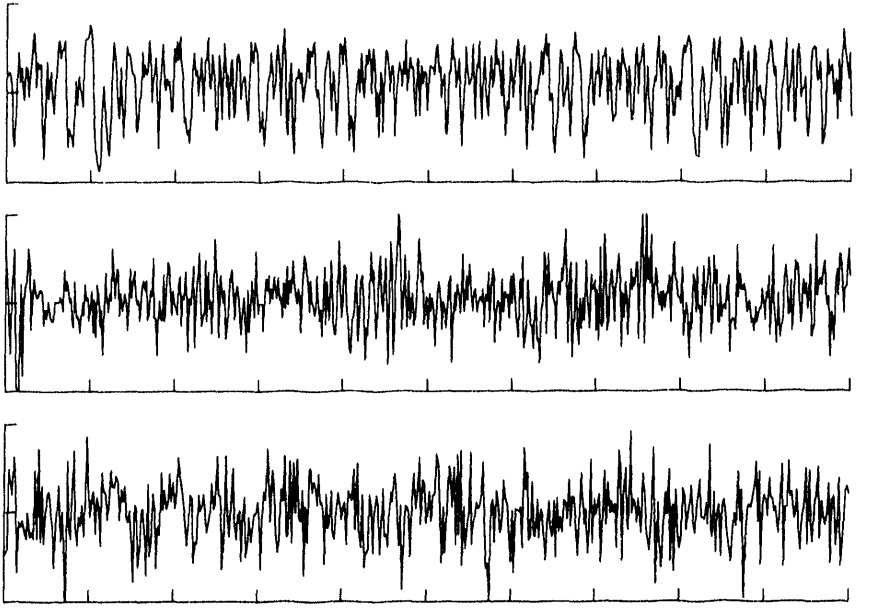

**Figure 1.1.** Depicted are three time traces, one from a known chaotic system, one from Gaussian distributed random numbers and one is a measurement signal from an MST discharge.†

primitive digital computer, accidentally discovered the sensitivity to initial conditions of a simple set of nonlinear equations used to model atmospheric convection. This set of equations now bears his name. Using computer graphics B. Mandelbrot "discovered" the fractal set which bears his name. M.J. Feigenbaum discovered a number of features universally present in a certain class of chaotic maps. Around 1980 work began to turn towards identifying chaotic systems and quantifying the degree of chaos, which is where we stand now.

This work has led to the identification of several real systems which are governed by low dimensional

---

† The signals shown in figure 1.1 are; top: Mackey-Glass system; middle: toroidal magnetic field fluctuations in MST; and bottom: Gaussian random numbers.

chaotic dynamics. Low dimensional chaos and simple determinism have been identified in the electrical activity of the brain, heartbeats, the pattern of childhood epidemics and stellar pulsar activity.[2] Equally important are those studies which find no evidence of a low chaotic dimension or simple determinism. A good example is the business cycle.[3]

### 1.2. Chaos in Plasmas

The search for evidence of chaos in plasmas has yielded mixed results. A wide range of chaotic processes has been reported, including the transition to turbulence and the formation of magnetic islands.[4] Several groups have reported identifying chaos and period doubling behavior in glow discharges and pulsed machines.[5,6,7,8] Low dimensional chaos has also been identified with drift wave turbulence both in experiment and simulations.[9,10] In toroidal, fusion caliber devices chaos has been reported in low frequency Mirnov oscillations in the DITE tokamak.[11] In TFTR low dimensional chaos has been reported in density fluctuations measured by $CO_2$ laser scattering.[12] The dimension of the system is wavenumber dependent. Finally, chaos of dimension near 7 has been reported in broadband (0-100kHz) oscillations of both the poloidal and toroidal magnetic fields in the HBTX1A reversed field pinch.[13] In contrast, a group measuring broadband magnetic and density fluctuations in the TCA tokamak finds no evidence of low dimensional chaos.[14]

These results provide a starting point for a better understanding of plasma processes using the tools of nonlinear dynamics. Most of these results were obtained nearly a decade ago when these tools were new or nonexistent. In the intervening time a better understanding of the application of these methods exists and several new techniques for identifying low dimensional chaos have been developed. Initial reports of chaos in other systems have been reexamined and found to be lacking. Without being specific, I think in light of this new understanding that several of the reported positive results may not stand up to more rigorous tests.

The Madison Symmetric Torus (MST) reversed field pinch (RFP) provides a particularly good instrument for investigations in nonlinear dynamics in fusion plasmas. It is a large toroidal confinement device with

discharges characterized by a spontaneous reversal of the toroidal magnetic field at the edge of the plasma. Discharges exhibit broadband fluctuations in most measured quantities. However, most of the fluctuation power (~ 90%) is concentrated in a few long wavelength modes. We believe we understand the mechanism behind these tearing mode fluctuations well, both on the basis of experimental evidence and from numerical simulations using magnetohydrodynamic (MHD) models of RFP discharges. Bispectral analysis of magnetic fluctuations from experiment and simulations indicate a three wave coupling process, linking two $m$ =1 modes to an $m$ =2 mode.[15] The point is, that although the signals appear stochastic, the principal dynamics of the device can be modeled computationally. Hence, they may be the result of a chaotic or other simple deterministic process.

One of the major obstacles in achieving viable thermonuclear power is the fluctuation-driven particle and energy transport. The past decade has seen a tremendous effort towards correlating experimentally observed transport with hydrodynamic models. Drift wave models in particular have shown promise towards explaining the anomalous ion heat loss in tokamaks. Studies of these models indicate that the dynamics are low dimensional, despite the large number of interacting modes in the system. Essentially, a system of $4 \times 10^3$ equations, one for each mode, can be reduced to a system with a topological dimension of less than 3.[10] This is a very important result: Although the original phase space is 1000 dimensional the dynamics of the system contract to a three dimensional object, an enormous simplification. This identification of a low dimensional attractor could mean a significant reduction in the complexity of the models needed to accurately describe the system. The applicability of drift wave models to RFP transport is more tenuous. However, the models are sufficiently general that many of the results are relevant to RFP physics.

Once chaos has been identified in a system, one is led to ask, aside from purely academic interest, what good is it? Three benefits can immediately be cited. The most useful and ambitious objective would be to simplify the equations describing the system. A plasma comprised of $N$ particles can be described by $O(6N)$ ordinary differential equations. MHD simplifies this by restricting the system to a

set of partial differential equations with only a finite number of modes. Nonlinear processes considerably complicate this approach, yet MHD has been particularly successful in describing the essentials of plasma dynamics. If, however, a low dimensional chaotic attractor is identified, a lower bound can be placed on the number of equations needed to adequately describe the system. Empirical evidence suggests that this number scales in some fashion with the dimension of the system, although no concrete law exists. With such a set of equations, one could determine the parameter space for best confinement or heating, determine scaling laws, etc.

An objective in harnessing fusion power is control of the system. One method of control which has recently received a lot of attention is the phenomenon of entrainment.[16,17,18,19] An important example of entrainment is the action of a pacemaker on the heart. Chaotic systems are densely interwoven with nearby periodic orbits. Small, periodic perturbations can sometime force a system to oscillate around a periodic trajectory rather than its natural chaotic one. The converse is also true, where it may be the objective to drive a system away from an undesirable stable trajectory. The applicability of entrainment to plasma systems is untested, however it could have important consequences in controlling the growth of certain unstable modes.

A final benefit is short term predictability. If the system shows evidence of low dimensional chaos, then the system is deterministic, which implies that it has short term predictability. As will be discussed, prediction is possible even without the governing equations. This property may be used in conjunction with the above in order to control the system, and may be particularly applicable to RFP plasmas. Most RFP discharges are characterized by aperiodic flux jumps: bursts of magnetic activity. These flux jumps are both a boon and a bane. During flux jump activity the ions are strongly heated. However, transport is also enhanced, resulting in tremendous particle and energy loss. In order to improve confinement, it seems desirable to control the most severe of these flux jumps. Assuming there is a chaotic process governing this discharge behavior, one could predict the next flux jump occurrence a short time in the future and possibly use feedback to suppress it.

[illegible] low [illegible] and the first task is simply to identify low dimensional chaos and simple periodicity in MST fluctuations. Despite simulations which suggest that chaos is present in RFP fluctuations, experimental data is shown all tests for identification. As will be discussed in this dissertation, identification is particularly sensitive to the presence of noise and the stationarity of the system. This is additionally complicated by the fact that standard linear filtering techniques are not appropriate to signals generated by chaotic systems. Thus, although low dimensional chaos may govern MST fluctuations, it presents challenges to the analysis techniques.

This dissertation is organized as follows. Chapter two presents a basic introduction to the jargon of nonlinear dynamics and the essentials of the analysis techniques used on the data. Chapter three shows the application of these techniques to a few known systems for comparison with the results presented later. Chapter four deals with the complications of analyzing unknown data sets, in particular data which may be noise corrupted. Chapter five presents the results from analysis of two numerical simulations. The DEBS code simulates RFP plasmas, and is thought to model the dominant tearing mode fluctuations correctly. The dissipative trapped electron mode (DTEM) model is designed to model ion scale turbulence thought to be a major contributor to transport in the core of tokamaks. Chapter six presents the results of analysis of experimental data from the MST. The final chapter presents conclusions and future perspectives.

## 2. Essential Chaos Theory

In light of the fact that chaos is a relatively new field of study I present here a brief overview of the essentials of nonlinear dynamics. The concepts presented here are the foundation of the rest of the dissertation. For a more detailed treatment, the reader is invited to refer to the bibliography presented at the end of the dissertation.

### 2.1. Chaotic Systems

#### 2.1.1. Maps

The simplest form of equations exhibiting chaos is the class of maps: $x_{t+1}=f(x_t)$. An example is the shift map given by:

$$x_{t+1} = 2x_t \quad \text{mod1} \ . \tag{2.1}$$

Figure 2.1 shows the behavior of this system as time progresses. The time series shows erratic, random-like behavior with no detectable pattern. The signal generated by this map would pass most tests for uniformly distributed random numbers: a histogram plot is essentially flat, as is the power spectrum.

Not all maps, however, exhibit chaotic behavior. For example, the map

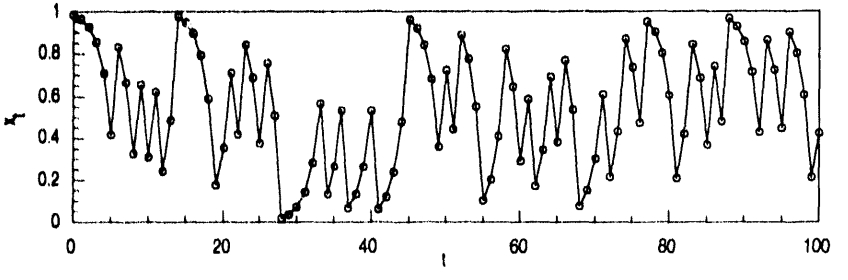


**Figure 2.1.** Time evolution of the shift map for the first 100 points. The system is difficult to distinguish from random white noise.

$$x_{t+1} = x_t + a \quad \text{mod1} \tag{2.2}$$

is not chaotic. In order for an equation to be chaotic the system must exhibit some form of "mixing" behavior. The equation (2.2) does not mix in the sense that two neighboring points will always be spatially close together as the system evolves. For the shift map eq. (2.1) however, points quickly separate within the confines of the system. This mixing usually manifests itself as stretching and folding. The system expands in one direction, while folding back on itself at the same time. Figure 2.2 demonstrates this behavior for the shift map. The factor of 2 stretches the system, while mod 1 folds the range back onto the domain, effectively mixing the system.

Critical in this type of system is that there exists a set of unstable points which map back to themselves after a finite number of iterations. Any point satisfying $x = p/2^m$, where $p$ and $m$ are integers, will be mapped onto 0 and remain there. These points are unstable in the sense that a small perturbation will destroy this mapping and result in a chaotic mapping instead. Although there are an infinite number of such points, they comprise a set of measure zero; the likelihood of arbitrarily choosing any one is infinitesimally small. Nonetheless it is this density of non-chaotic initial conditions which guarantees effective mixing. These points effectively work as rocks in the flow of the system.[20]

In order to illustrate the more general behavior of chaotic systems I will use a system known as the

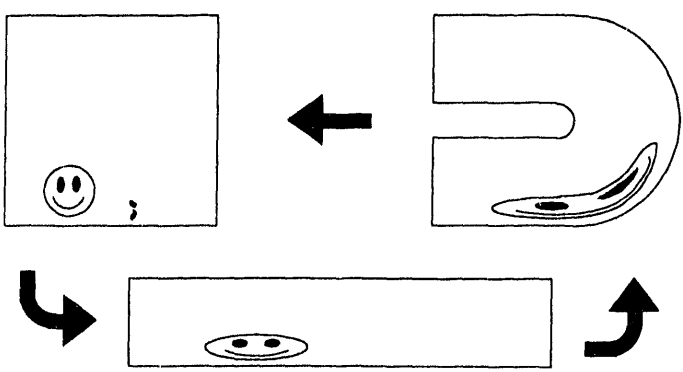

**Figure 2.2** The schematic illustrates the stretching and folding of a system which results in chaotic dynamics. The two black dots represent points initially close which separate exponentially.

logistic map. This map was first developed as a model for population growth of a species constrained by finite available resources. The map is given by:

$$x_{t+1} = a x_t (1 - x_t) \,. \tag{2.3}$$

$a$ is called the *control parameter.* Changing the value of the control parameter dramatically changes the dynamics of the system, as shown in Fig. 2.3. For $a < 3$ the system approaches a fixed value. For $a$ slightly greater than 3, the system exhibits periodic behavior. This spontaneous transition to periodic behavior is known as *period doubling.* For $a = 1+\sqrt{6}$ the period two solutions again double in period to give stable period 4 solutions. This period doubling behavior continues as $a$ is increased until $a$ = 3.569..., at which point the period becomes infinite. The solution is chaotic, exhibiting random like, non repeating behavior. The period doubling behavior can be made clearer by plotting the limiting solutions of x versus the control parameter $a$, as in Fig 2.4. One can graphically see why points where period doubling occurs are known as *pitchfork bifurcations.*

An important feature of chaotic dynamics is the sensitivity to initial conditions. Points spatially close

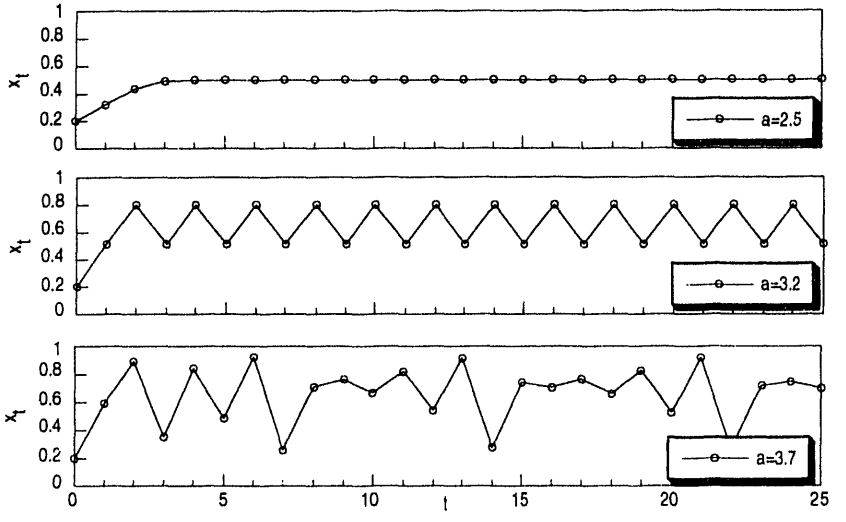


**Figure 2.3** The time behavior of the logistic map for 3 values of the control parameter $a$. The system exhibits stable, periodic and chaotic behavior.

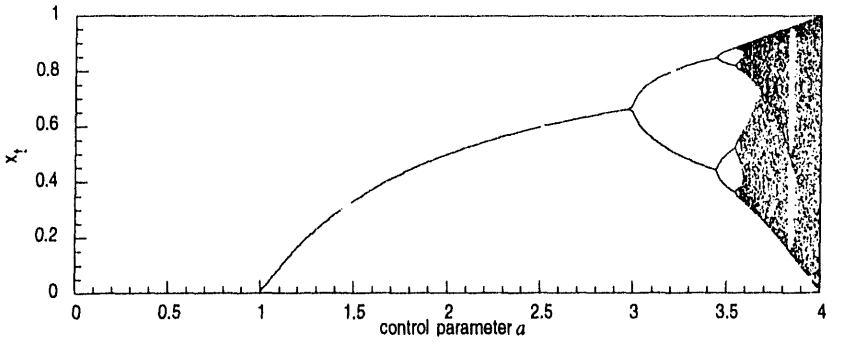


**Figure 2.4** The stable solutions of the logistic map plotted as a function of the control parameter $a$. The pitchfork bifurcations are clearly visible. There is a period 3 window distinguishable at $a$≈3.8.

together initially will, on average, diverge exponentially in time within the confines of the system. This phenomena is illustrated in Fig. 2.5. Two points separated by a distance of $1x10^{-5}$ have completely uncorrelated behavior after about 15 iterations of the logistic map. This sensitivity to initial conditions has become the standard criterion for chaotic behavior. It is characterized by the Lyapunov exponent to be discussed later.

Although the logistic map provides an excellent illustration of several of the basic properties of chaotic systems, both it and the shift map are examples of symplectic chaos. This is a term applied specifically to maps which denotes systems which have no dissipation. In this dissertation I will be concerned with

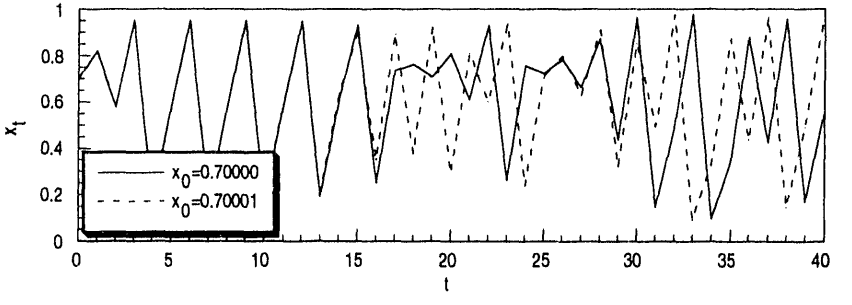


**Figure 2.5**. The evolution of the logistic map for two closely spaced initial conditions. This illustrates the exponential divergence of chaotic trajectories.

dissipative dynamical systems: systems whose phase space volume contracts in time. Hamiltonian systems, though they may be chaotic, have phase space volumes which do not contract. As such, there is no region of space, an *attractor*, to which nearby trajectories of the system evolve.

An example of a dissipative two dimensional map exhibiting chaos is the Hénon map introduced by M. Hénon in 1976.[21] It is defined by

$$x_{t+1} = 1 - ax_t^2 + y_t$$
$$y_{t+1} = bx_t \tag{2.4}$$

The map is a quadratic map very similar to the logistic map. If $b = 0$, $a \neq 0$, the map can in fact be transformed into the logistic map. For $a$ and $b$ both small and positive the map exhibits the same period doubling behavior in two space as $a$ is increased. For large enough values of $a$, and $b < 1$, (for $b > 1$ trajectories are unbounded) the map has chaotic solutions. Solutions of the map in the $x$ $y$ plane are plotted in figure 2.6. The object depicted is known as a *strange attractor*. The attractor is embedded on the *inertial manifold* which is the contiguous region of space on which all trajectories lie. As shown in the right half of figure 2.6, the attractor shows self similar structure on small scales, a property typical of *fractals*. Fractals are geometric objects which usually have a non-integer dimension.

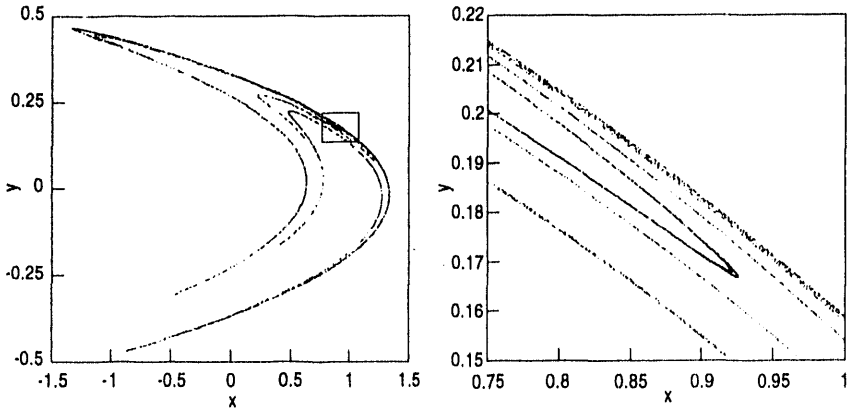


**Figure 2.6.** The two dimensional Hénon map for $a = 1.3$ and $b = 0.35$. The right figure shows an expanded scale detailing the self similar fractal structure of the strange attractor.

The same stretching and folding that takes place in Hamiltonian systems is evident in dissipative systems. However, because they are dissipative, the stretching takes place in only one dimension, while the total phase space volume decreases. An illustration of the process for the Hénon equation is given in figure 2.7. It shows the action of two successive iterations of the Hénon equations on a circle of initial conditions. The stretching and folding of the circle are evident, as is the overall volume decrease.

### 2.1.2. Ordinary Differential Equations and Strange Attractors

Although maps provide simple systems for numerical studies of chaos, they are inappropriate models for most real systems because they are not continuous. Real systems are usually described by systems of differential equations. The chaotic behavior evident in one and two dimensional maps results from the fact that the systems do not have to deform continuously from one state to the next in time. Mapping allows the system to "jump" from one state to the next state, avoiding the intervening points. In actuality maps are infinite dimensional systems. The restriction that the system be continuous in time severely limits the dynamics in one and two dimensions.

A system $\dot{x} = F(x,t,c)$, where $x$ is an $d$ dimensional vector and $c$ is a set of $k$ control parameters, will have an orbit or trajectory through the $d$ dimensional space describing its motion as the system

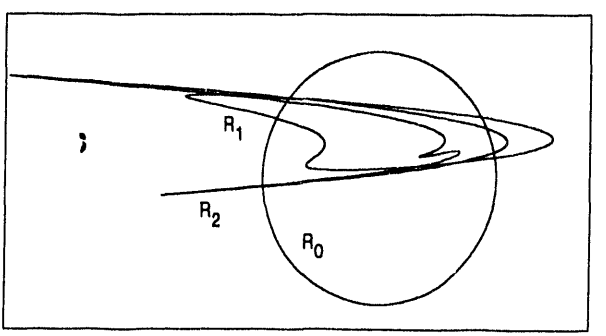


**Figure 2.7.** The action of two successive iterations of the Hénon equations on a circle. The stretching and folding of the circle are evident, as is the overall volume decrease.

progresses with time. (In keeping with current literature, bold notation is no longer used to indicate vectors.) For any autonomous system, one which does not depend explicitly on time, this trajectory cannot cross itself in space. Were the case otherwise, orbits would not be unique.

If a system of ODEs is confined to one dimension, regardless of how complex the equations, it can exhibit only one of two behaviors as time progresses. The trajectory of the system is either attracted to a point, known as a *fixed point* (some authors use the terms critical point or equilibrium point) usually denoted by $x^*$, or the trajectory tends towards infinity. The system may have several fixed points, each with its own *basin of attraction* which defines the set of points, the limit of whose trajectory is the fixed point. A simple example would be radioactive decay, $\dot{x} = -ax$, which has a fixed point at $x^* = 0$, though $x^*$ is only attainable after an infinite time.

Fixed points may be either stable or unstable. Any (noise free) system which finds itself at the fixed point will remain there forever. However nearby points will either tend towards the fixed point, in which case the fixed point is stable, or away from the fixed point, making it unstable. There is a third class of fixed points called semi-stable or saddle points where the fixed point is stable when approached from one direction and unstable when approached from the other.

In two dimensions the additional degree of freedom allows for a third type of behavior: the *limit cycle*. A limit cycle is essentially a two dimensional fixed point. Any system that finds itself on the limit cycle will remain on that trajectory. As with fixed points, limit cycles may be either stable, unstable or semi-stable depending on the trajectory of nearby orbits. The van der Pol equations $\dot{x} = y$, $\dot{y} = \varepsilon(1 - x^2)y - x$, provide an example of a limit cycle for small $\varepsilon$. The limit cycle is stable for $\varepsilon > 0$, and unstable for $\varepsilon < 0$. An example of a stable cycle is shown in figure 2.8.

In three dimensions the dynamics become far more rich. The simplest extension of the dynamics of one and two dimensions is the two torus. This is the superposition of two limit cycles in perpendicular directions, which spiral around a torus. If the frequencies are commensurate, the trajectory is periodic. They need not be commensurate though, and the trajectory will cover the torus in the limit of infinite

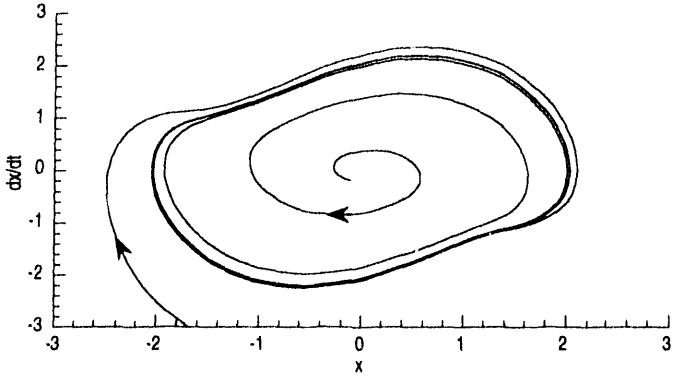


**Figure 2.8.** A stable limit cycle generated by the van der Pol equations with $\varepsilon = 0.5$. The trajectory of nearby orbits is depicted as they spiral onto the limit cycle.

time. An example of a system whose trajectory is confined to a two torus is a double pendulum – a mass attached to a ridged rod in turn attached to a second mass and rod – confined to a plane. The equations of motion are:

$$\dot{\omega}_1 = \frac{2m_2\omega_1\omega_2 rz}{m_1\ell_1^2 + m_2 r^2}$$

$$\dot{\omega}_2 = \frac{\omega_1^2 rz}{\ell_2^2}$$

$$\dot{r} = \omega_2 z \quad ; \quad \dot{z} = \omega_2(r - \ell_1) \qquad (2.5)$$

where $r = \sqrt{x^2+y^2}$, $m$ are the masses of the pendulums, $\ell$ the lengths and $\omega$ the frequencies of oscillation. Note that this system has no dissipation, and hence the torus on which the trajectory lies is not an attractor.

The novel situation in three dimensions is the strange attractor. A strange attractor shows no periodic behavior. For maps, as with the Hénon map above (fig. 2.6), this means the attracting set becomes an infinite set of discrete points. (The set is finite for periodic solutions.) For ODEs, however, all trajectories, periodic or chaotic, must be continuous. The trajectory of a strange attractor thus traces

out a complicated pattern in the three space, never crossing itself, but still remaining confined to a finite region. The trajectory has infinite length, yet never fills the bounded space it occupies. In addition to infinite period, strange attractors exhibit fractal structure; they are self similar in the limit of small scales.

A classic example of a strange attractor is the Lorenz attractor. The attractor is generated by a set of equations introduced in 1963 by Edward Lorenz as simple model of Rayleigh-Benard convection in the atmosphere.[22] They are:

$$\begin{aligned} \dot{x} &= \sigma(y - x) \\ \dot{y} &= x(r - z) - y \\ \dot{z} &= xy - bz \end{aligned} \tag{2.6}$$

The system will be described in more detail in chapter 3. A 2D projection of the attractor is plotted in figure 2.9. As can be seen in the figure, the orbit spends most of its time around either of a pair of conjugate unstable fixed points. The trajectory is extremely sensitive to initial conditions. However, any set of initial conditions within the basin of the attractor will quickly converge onto the inertial manifold generating an attractor similar to the one depicted. As with the Hénon map, the structure is fractal, and the self similarity is evident with sufficient magnification.

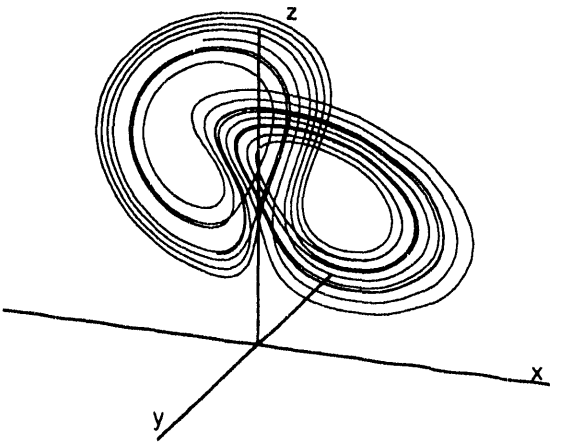


**Figure 2.9.** The Lorenz strange attractor.

## 2.2. Quantifying Chaos

### 2.2.1. Phase Delay Plots and Poincaré Sections

The definition of chaos given in the introduction is a rather qualitative one. On simple inspection a sequence of values may appear "chaotic", but this is not sufficient to establish that the signal is chaotic. One needs to be able to show that the signal is a) deterministic, and b) not periodic. What is needed is a way to quantify chaos. Hopefully one can, on the basis of this, estimate how many equations are needed to describe the essential dynamics of the system, and ultimately to reproduce these equations.

One method of determining whether a system exhibits low dimensional chaos was alluded to in the previous sections. Simply plotting the trajectory in space can indicate chaos by visual inspection. If the trajectory spirals to a fixed point or limit cycle, chaos can be ruled out. If the orbit is bounded but never closes, chaos is a possibility.

In general, one does not have access to all the independent variables of the system, and for experimental data, it may not at all be clear *which* variables are independent. An alternative is to plot a single variable in a phase-delay plot. One plots $x(t)$ versus $x(t+\tau)$ versus $x(t+2\tau)$, etc. where $\tau$ is some appropriately chosen time constant. F. Takens has proven that for chaotic systems, a single variable will capture all the relevant dynamics of the system subject to certain conditions.[23] Specifically, given a system $F(t) = [x(t), y(t), z(t), \ldots]$ there is a diffeomorphism – a differentiable, reversible mapping – from the manifold containing the attractor to that containing the attractor in delayed coordinates $X(t) = [x(t), x(t+\tau), x(t+2\tau), \ldots, x(t+m\tau)]$, so long as $m \geq 2d+1$, where $d$ is the dimension containing the original attractor. The $m$ dimension space is known as the *embedding space* of the attractor. The necessity of $2d+1$ components is to insure that the embedding space is orthogonal. Often values of $m$ less than $2d+1$ suffice for proper reconstruction of the original system.

Unfortunately, for systems with dimensions greater than two phase-delay plots are of limited use; the projection of a four dimensional attractor onto a plane usually looks like a ball of wool. Another useful

method of visualizing a chaotic system is the Poincaré section or puncture plot. The dimension of the system can be reduced by one by passing a hyperplane through the orbit and marking the trajectory each time it crosses the plane. This is schematically illustrated for three dimensions in fig. 2.10. Note that a Poincaré section is distinctly different from strobing a time signal at regular intervals. In general, strobing will not reduce the dimension of the system unless one fortuitously chooses a time increment related to a natural frequency of the system. Often Poincaré sections give strong indications of chaotic behavior. The Takens theorem can of course be applied, and a single time record used for creating the Poincaré section. A method for reducing the dimension by 2 using a "double" Poincaré section has been developed for periodically driven systems.[24] The method does not appear to be generally applicable, however.

### 2.2.2. Fractals

One characteristic property of chaotic systems mentioned earlier is their geometric structure. For strange attractors, this structure is self similar at small scales. Such objects are known as *fractals*, a term coined by Mandelbrot to indicate the fact that the topological structure usually has a fractional dimension.[25] The Hénon map, for example, has an attractor greater than dimension 1; however, it fails to fill a two dimensional space. Thus its fractal dimension is somewhere between 1 and 2.

As an example of a simple fractal, consider the triadic Cantor set. It consists of a line segment from which the middle third has been removed, and the middle third of the remaining two segments has

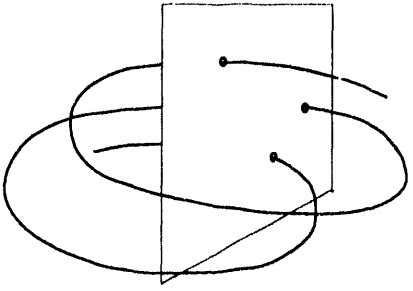

**Figure 2.10.** Schematic illustration of the process in creating a Poincaré section of an attractor.

been removed, *ad infinitum* (see Fig. 2.11). The set is obviously more than a simple collection of points (dimension 0), but is not a complete line segment (dimension 1). Its fractal dimension lies somewhere between the two. A well known example of a more complex fractal structure is the boundary of the Mandelbrot set. This set is generated by the equation:

$$x_{n+1} = x_n^2 + c \quad , \tag{2.7}$$

where $x$ and $c$ are complex. All points that do not diverge are members of the set (see Fig. 2.11).

### 2.2.3. Spatial Measures

Fractal structure has been identified and used to characterize a variety of phenomena in nature, from cloud shapes to coastlines. In order to be useful though, there must be a quantitative way to compute the fractal dimension. The most basic and intuitive measure is the Hausdorff dimension, which measures a fractal's space filling ability. One subdivides the region of space containing the fractal into equal volume sub-regions and counts what fraction of the regions contain part of the fractal. Because an ideal fractal is self-similar, as one continues to subdivide the region into smaller and smaller volumes the fraction containing the fractal will approach a constant. One would expect $N(r) \propto (1/r)^D$ in the limit of small $r$. The Hausdorff dimension is then defined as:

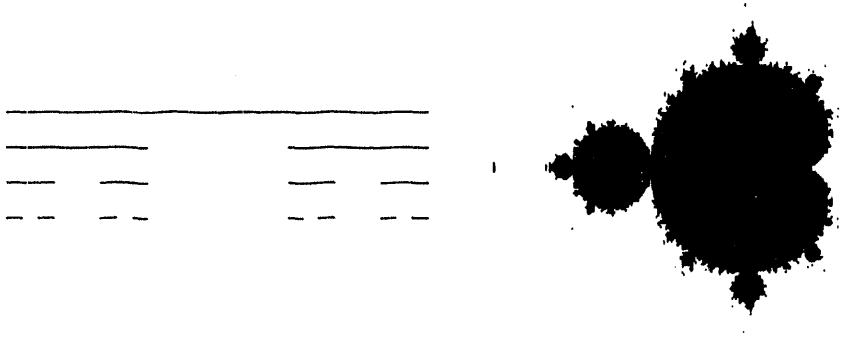

**Figure 2.11.** The triadic Cantor set and Mandelbrot set are examples of fractals.

$$D_0 = \lim_{r \to 0} \frac{\ln N(r)}{\ln (1/r)} \quad , \tag{2.8}$$

where $N(r)$ is the number of hyperspheres or hypercubes of linear dimension $r$ needed to cover the attractor.

In the example above of the Cantor set, the fractal dimension is easily computed analytically. In the first step, 2 boxes of length 1/3 are needed. For the $n^{th}$ successive step, $2^n$ boxes of length $(1/3)^n$ are needed. Thus the fractal dimension of the Cantor set is $D_0 = \ln 2^n / \ln 3^n \approx 0.631$.

For most systems the Hausdorff dimension is not so straightforward to calculate. Additionally, rarely does one have the governing equations to perform an analytical calculation. Typically one measures a time series record from one or a few of the system variables. In order to calculate the fractal dimension, one must first embed the data in a space presumed to contain the dynamics of the system. This space is then partitioned and the number of hypercubes containing points is counted. If for several embeddings the calculated dimension remains constant, this value can be assigned as the fractal dimension. If, on the other hand, the attractor continues to fill the space, the data must be assumed to represent a higher dimensional or possibly random system. In either case, computation of the Hausdorff dimension is extremely computationally intensive, and other, simpler methods have been found to estimate the fractal dimension.

For dynamical systems one can define a hierarchy of generalized fractal dimensions, $D_q$, each characterizing different properties of the fractal geometry of the attractor.[28] Given the region containing the attractor, subdivide it into cells. Count the number of points $N_i$ in each cell. The probability of finding a point in a given cell is then:

$$p_i = \lim_{N \to \infty} \frac{N_i}{N} \quad , \tag{2.9}$$

where $N$ is the total number of points. From this one can define the fractal dimensions as:

$$D_q = \lim_{r \to 0} \frac{1}{q-1} \frac{\ln \sum_{i=1}^{M} p_i^q}{\ln r} \qquad (2.10)$$

when subdividing the region into $M$ cells. This definition of dimension is formally equivalent to the free energy from equilibrium thermodynamics. $p_i$ is the probability that a particle (point) of the system is in energy state (box) $i$, and $q$ corresponds to the inverse temperature.[1] For $q=0$ this yields the Hausdorff dimension, where $\sum p^0 = M(r)$ is simply the number of boxes containing a point of the attractor. For larger values of $q$ one can characterize the space filling properties and inhomogeneity of the attractor in more detail. $D_1$ is known as the information dimension

$$D_1 = \lim_{r \to 0} \frac{\sum_{i=1}^{M} p_i \ln p_i}{\ln r} \qquad (2.11)$$

The quantity $p_i \ln p_i$ from Shannon's information theory, characterizes the amount of information gained by knowing the trajectory is in the $N_i^{th}$ cell, given one knows $p_i$.[27] For a completely homogeneous attractor $p_i = 1/M$, and thus $D_1 = D_0$. The information dimension then characterizes the non uniformity of the attractor, and for non-homogeneous attractors, $D_0 > D_1$.

Of particular interest is the dimension defined by $q=2$. Known as the correlation dimension, it represents the probability that any two points will be found within a given hypersphere and measures the 'clumpiness' of the orbit.[28] The correlation dimension $D_2$ is defined by

$$D_2 = \lim_{r \to 0} \frac{\ln \sum_{i=1}^{M} p_i^2}{\ln r} = \lim_{r \to 0} \frac{\ln C(r)}{\ln r} \qquad (2.12)$$

The correlation integral $C(r)$ can be recast as

$$C(r) = \lim_{N \to \infty} \frac{1}{N^2} \sum_{i \neq j} \Theta(r - |x_i - x_j|) \qquad (2.13)$$

$\Theta(r)$ is the Heavyside function whose value is one for $r > 0$, and zero otherwise. In this form, the correlation integral and $D_2$ are easily calculated for large data sets using a computer, hence the appeal of the correlation dimension as the most common measure of fractal dimension in the literature. One

can show that $D_{q-1} \geq D_q$, and thus the correlation dimension provides a lower bound on the Hausdorff dimension. The Hausdorff and correlation dimensions usually agree closely, and often differ by no more than a few percent.

Typically, in computing the correlation dimension, one computes the correlation integral for various radii $r$ and plots log $C(r)$ vs. log $r$. Over some region in log $r$, known as the scaling region, the slope is constant, and the value of this slope is taken as the correlation dimension. The correlation integral is said to saturate at a constant slope. For clarity, in this dissertation I will plot the two point slope $\delta[\log C(r)] / \delta[\log r]$ versus log $r$. This yields a plateau at the value of the correlation dimension, allowing a better determination of the scaling region. Examples illustrating the application of this technique will be given in the next chapter.

### 2.2.4. Dynamical Measures

In addition to fractal dimension, another property of chaotic systems alluded to earlier is sensitive dependence on initial conditions. This property can be characterized quantitatively by the Lyapunov exponents which measure the average divergence and convergence of the attractor in phase space. Trajectories of chaotic systems spatially close at some time $t_0$ will, on average, diverge (converge) exponentially in time. For the one dimensional continuous map $x(t) = f_t(x_0)$, with two initial conditions separated by $\delta x$ the average separation after a time $t$ is $\delta x_t \approx \delta x_0 e^{\lambda t}$. Taking the limit of infinitesimally separated points and infinite time the characteristic or Lyapunov exponent $\lambda$ is defined by

$$\lambda = \lim_{t\to\infty} \frac{1}{t} \lim_{\delta x_0 \to 0} \ln\left|\frac{\delta x_t}{\delta x_0}\right| = \lim_{t\to\infty} \frac{1}{t} \ln\left|\frac{df_t(x)}{dx}\right| . \qquad (2.14)$$

If this exponent $\lambda$ is greater than zero, trajectories separate exponentially in time within the confines of the system. This criterion, a positive largest Lyapunov exponent, has become the standard definition of a chaotic system.

Any dissipative system is bounded, hence the exponential expansion cannot occur indefinitely. After

few exponents, although negative values show very sensitive behavior. The subtleties of calculation of the Lyapunov exponents will be discussed in the next chapter.

Kaplan and Yorke have conjectured a general formula which relates the Lyapunov exponents to the fractal dimension:[32]

$$D_{KY} = j + \frac{\sum_{i=1}^{j} \lambda_i}{|\lambda_{j+1}|} \approx D_0 \ . \qquad (2.16)$$

$D_{KY}$ is the Kaplan-Yorke or Lyapunov dimension. The Lyapunov exponents are ordered such that $\lambda_i > \lambda_{i+1}$, and $j$ is the largest index for which $\sum_{i=1}^{j} \lambda_i > 0$. The conjecture appears to hold rigorously only for homogeneous attractors. However, it does hold approximately for many cases.

## 2.3. Nonlinear Prediction

Ultimately, the goal of identifying and characterizing chaotic behavior in experimental data is to develop a set of model equations for the system. These equations can never hope to yield an exact replica of the time series being analyzed, owing to the sensitivity on initial conditions. However, global properties of the system – average Lyapunov exponents, dimensions and power spectra – should be preserved. In addition, because these systems are not random but governed by deterministic dynamics, short term prediction must be possible. Given a set of initial conditions approximating those of the experimental system in question, the next several time steps of the model system should mimic those of the actual data.

Unfortunately, even though a system may have been fully characterized with regards to its chaotic properties, developing a set of nonlinear model equations is not a trivial exercise. Although much research has been devoted to extracting model equations from the data of the system, no general method has yet been found.[33,34] A less ambitious goal is simply to predict the short term behavior of a system without knowing the governing equations explicitly. With this goal in mind, several methods of doing so have been developed.

some time the expansion crosses the fold in the attractor and the trajectories may converge again. The exponential divergence characterized by the Lyapunov exponent is still reflected in the information loss of the system, despite the fact that spatial trajectories are no longer diverging. For example, the shift map, in computer lingo, represents a left shift, leading digit truncation. Even with double precision accuracy of $10^{-18}$ after 23 iterations all information about the initial conditions is lost. It is this information loss that the Lyapunov exponents measure.

For systems of more than one dimension there is a collection of Lyapunov exponents, one for each dimension of the system. Each exponent corresponds to one of the principle axes of an ellipsoid centered on the trajectory and characterizes the local expansion or contraction of the attractor. The orientation of this ellipsoid changes as the trajectory evolves in time. The spectrum of Lyapunov exponents is given by:

$$\lambda^{(i)} = \lim_{t\to\infty} \frac{1}{t} \ln\left|\frac{\partial f_t(x^{(i)})}{\partial x^{(i)}}\right| \quad , i = 1,2,\ldots n \quad . \tag{2.15}$$

Any continuous system must have at least three dimensions and hence three Lyapunov exponents. If the system is dissipative their sum must be negative to reflect the contraction of phase space. The least negative exponent controls the flow of perturbed trajectories onto the inertial manifold.[29] A chaotic system has a positive largest exponent, and any system continuous in time must have at least one Lyapunov exponent equal to zero corresponding to the lack of divergence (on average) tangent to the flow.[30] Thus a three dimensional chaotic system has Lyapunov exponents (+,0,–).

Calculation of the largest Lyapunov exponent is relatively straightforward, though computationally intensive. Wolf, *et al.* have developed a method for calculation of the largest exponent from the time series of a single variable of the chaotic system.[29] Essentially, it follows the trajectory of neighboring points and calculates the average separation as they progress in time. The spectrum of Lyapunov exponents is more difficult. Ruelle and Eckmann have developed a method whereby one estimates the Jacobian from the tangent space matrix.[31] This can usually lead to reasonable estimates of the first

All of the methods developed thus far use essentially the same procedure, with more or less sophistication.[35,36] The time series is first embedded in an appropriate space using the method of time lags. The initial point for prediction is chosen, and the space is searched for its nearest neighbors. In the simplest method, the average of the neighbors' short term trajectory becomes the basis for predicting the evolution of the initial point. The neighbors of this predicted point are then found and the process is repeated. More sophisticated methods fit higher order polynomials to the local space which can result in better prediction accuracy.

In addition to actual prediction, one can characterize the determinism of a system with a quantity known as the *translation error*.[37] The translation error quantifies the coherence of the flow of the system through phase space. In simple deterministic systems nearby trajectories should parallel each other, at least in the short term. The translation error measures the deviation of nearby points from the average flow of the group. More concisely,

$$e_{\text{trans}} = \frac{1}{k+1} \sum_{j=0}^{k} \frac{\left| v_j - \bar{v} \right|^2}{\left\| \bar{v} \right\|^2} \quad , \tag{2.17}$$

where $v_j$ is the translation $f(x_j) - x_j$ and $f(x_j)$ is the map of $x_j$ in the embedding space. $\bar{v}$ is the average translation of the set of $k$ neighbors. The normalization $\|\bar{v}\|^2$ makes the measure $e_{trans}$ insensitive to attractor size. For a random signal, the value of $e_{\text{trans}}$ should remain a constant value of about one, regardless of the embedding dimension; random signals fill the embedding space they occupy. Deterministic signal will have low values of $e_{\text{trans}}$ for embeddings near the proper dimension of the system, reflecting the coherent flow of the neighboring trajectories. For embeddings much below the dimension of the system the translation error will be larger; in the truncated space distant points may be artificially close. In higher embeddings, the finite number of points in the data record means that the space will be more sparsely filled, and nearby points will not be as well correlated. Unfortunately, the translation error is a poor measure for high dimensional attractors, as will be shown in the next chapter.

## 2.4. Summary

As outlined in this chapter, a number of techniques exist for identifying and quantifying low dimensional chaos and simple determinism. These include phase delay plots and Poincaré sections, fractal dimensions, Lyapunov exponents and short term predictability. There are some subtleties in applying these techniques to data, as will be discussed in the following two chapters. These are the tools, then, with which I will analyze numerical and experimental plasma systems for evidence of simple determinism.

## 3. Analysis Techniques Applied to Known Numerical Systems

Three numerical systems whose chaotic properties are well understood are presented here to illustrate the techniques for nonlinear analysis. These analysis techniques will then be applied to the data from numerical simulations of plasmas, as well as experimental data from MST. Two of the systems, the Lorenz equations and the Mackey-Glass equation are known chaotic systems. The third system is Gaussian distributed random noise. The results obtained from investigation of these systems provide a standard by which to compare unknown data records.

### 3.1. Phase Delay Plots and Poincaré Sections

#### 3.1.1. Lorenz Attractor

As mentioned in chapter 2, the Lorenz attractor is generated by a set of equations introduced in 1963 by Edward Lorenz as a simple model of Rayleigh-Benard convection in the atmosphere. Once again:

$$\begin{aligned} \dot{x} &= \sigma(y - x) \\ \dot{y} &= x(r - z) - y \\ \dot{z} &= xy - bz \end{aligned} \tag{3.1}$$

The equations are in Fourier space, with $x$ representing a single mode of the velocity flow, and $y$ and $z$ two Fourier components of the temperature field. $r$ is the normalized Rayleigh number, $\sigma$ is the Prandtl number, and $b$ is a geometrical factor. The system has three fixed points, one at the origin, and two at $z = r - 1$, $x = y = \pm\sqrt{b(r-1)}$. For $r < 1$ only the fixed point at the origin exists and is stable. For $r > 1$, the origin becomes unstable and the two other stable fixed points emerge. These fixed points become unstable for appropriate values of $r$, $b$, and $\sigma$, and the Lorenz strange attractor emerges.

The left plot in Figure 3.1 shows a two dimensional projection of the phase-delay reconstruction of the attractor for the standard parameters $r = 28$, $b = 8/3$ and $\sigma = 10$, plotting $x(t)$ versus $x(t + .15)$ versus $x(t + .3)$. Comparing this with figure 2.9 one can see that the phase delay plot captures the basic structure

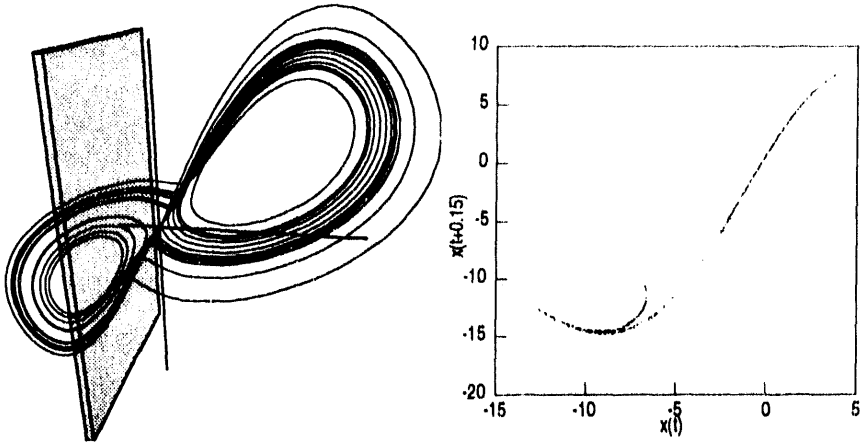


**Figure 3.1.** The Lorenz attractor. The left plot shows the $x$ component of the attractor in phase delay representation. The right is a Poincaré section taken at the gray plane on the left.

of the attractor: a pair of conjugate unstable fixed points about which the trajectory spirals. The gray plane cutting through the attractor is the plane of the Poincaré section in the right figure. Structure is evident, indicating the low dimensional simple determinism. There are a few spurious points which are the result of poor polynomial fits used to determine the point where the trajectory crosses the plane.

### 3.1.2. Mackey Glass

A second example of a strange attractor is generated by the Mackey-Glass equation.[38] The Mackey-Glass equation is a single delay-differential equation developed to model hematopoiesis, the process by which the bone marrow creates blood cells.

$$\dot{P} = \frac{\beta_0 \theta^n P(t-T)}{\theta^n + P(t-T)^n} - \gamma P(t) \tag{3.2}$$

$P$ is the density of circulating mature cells and $T$ is the delay time between initiation of cell production and the release of mature cells into the bloodstream. $\beta_0$, $\theta$, $n$, and $\gamma$, are constants. The system is actually infinite dimensional: one needs to specify an infinite number of initial conditions for the function between $x(t)$ and $x(t+T)$. In practice, however, the system collapses to a much smaller

dimension, and adjusting the delay time $T$ determines the fractal dimension of the system over a wide range of values. The system is thus especially useful as a model in studies of relatively high dimensional dynamics.

Figure 3.2 shows a phase-delay plot (the only possible option!) for the Mackey-Glass attractor with a delay of $T$ = 20s. Equation (3.2) was solved using a $4^{th}$ order Runga-Kutta integration scheme using a step size of 0.01 and storing every $10^{th}$ point. The attractor appears to have structure, an indication that the system is probably low dimensional. The left plot of figure 3.3 shows a Poincaré section of the attractor for the same parameters. The attractor was delay-embedded in 3 dimensions with a delay time of $\tau$=8s, and the section was taken at the plane $x(t+2\tau)$ =1.1. The value of $\tau$ was chosen as will be discussed in section 3.2. Because the attractor is low dimensional (about 2.1) for this value of $T$, structure is readily apparent. The right plot is a Poincaré section for a system with identical parameters, except the delay time $T$ = 50s. No obvious structure is apparent here because the attractor has a dimension greater than four. Phase delay plots and Poincaré sections are of limited usefulness for

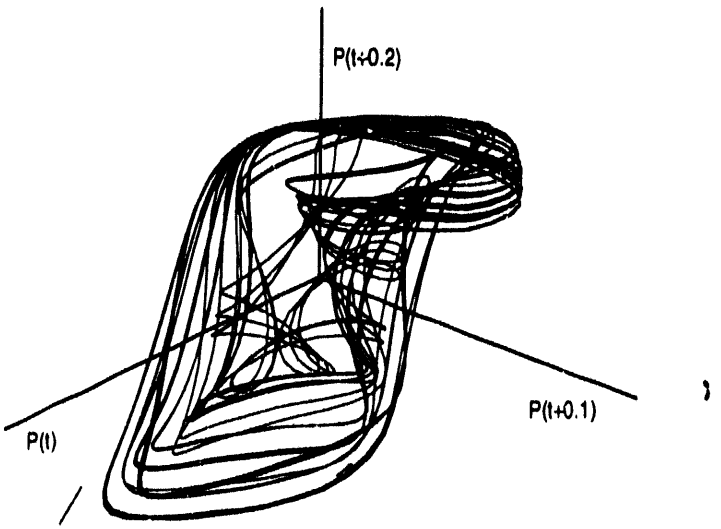


**Figure 3.2.** Phase-delay plot of the Mackey-Glass attractor for delay time $T$ = 20s.

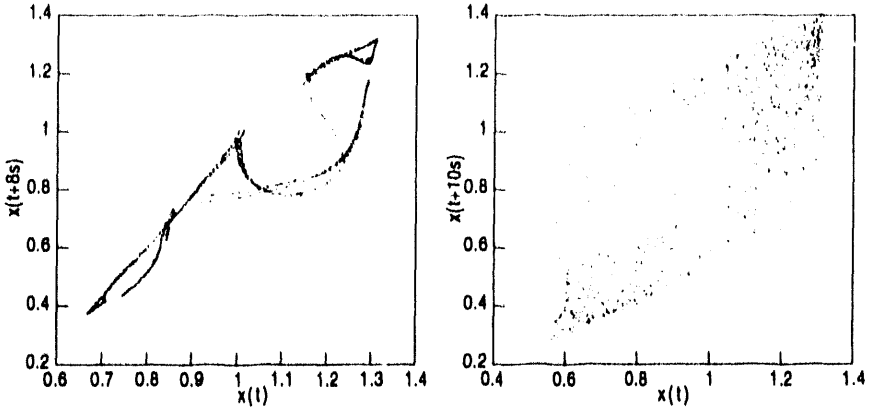


**Figure 3.3.** Poincaré sections of the Mackey-Glass attractor. The left plot is for an equation delay time of $T = 20s$ which has a fractal dimension of about 2.1. The right plot is for $T = 50s$ which has a fractal dimension greater than 4.

attractors with dimension greater than 3.

### 3.1.3. Random Numbers

The final numerical system to be analyzed is a system of random noise. There are several types of noise, the most familiar being Gaussian distributed white noise. The power spectrum of such a time record is flat, having equal power at all frequencies, hence the name. Colored noise, also known as fractional Brownian motion, has a preponderance of low frequencies, and the power spectrum is proportional to $f^{-\alpha}$, where $f$ is the frequency. A simple method for generating colored noise with such a spectral density is given by.[39]

$$x_l = \sum_{k=1}^{N/2} \left[ A k^{-\alpha} \left( \frac{2\pi}{N} \right)^{1-\alpha} \right]^{1/2} \cos\left( \frac{2\pi i k}{N} + \phi_k \right) . \qquad (3.3)$$

$A$ is the amplitude and $\phi_k$ are $N/2$ random phases.

Random systems provide a comparison for a truly high (infinite) dimensional system. The data are also a check against spurious indications of chaos resulting from severe data manipulation. In particular, noise

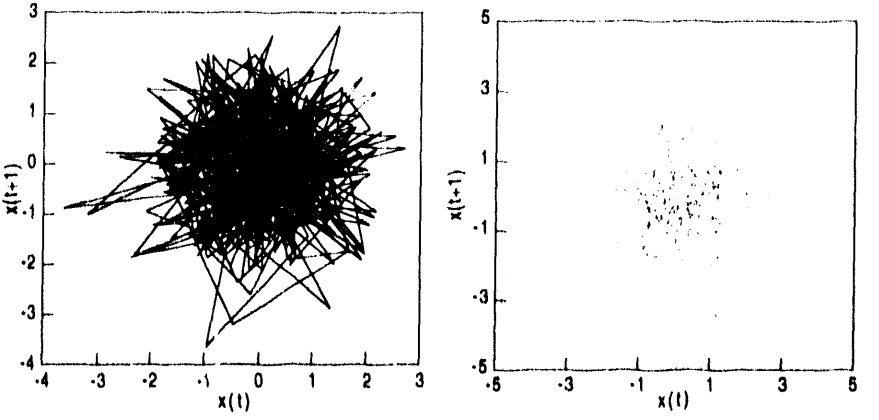


**Figure 3.4.** Phase-delay plot and Poincaré section of Gaussian distributed random numbers.

with some degree of short term correlation -- either colored noise or noise which has been lowpass filtered – will give spurious indications of simple determinism. I will use the term "correlated noise" when speaking of such systems in general. Methods for distinguishing between correlated noise and systems which are truly chaotic will be discussed in this chapter and the next.

In figure 3.4 is plotted a phase-delay plot of Gaussian white noise plotting $x(t)$ versus $x(t+1)$ . As expected, no structure is apparent; random numbers will densely fill the space they occupy. A Poincaré section taken at the plane $x(t+2)=0$ is no improvement.

### 3.2. Correlation Dimension

Calculation of the correlation dimension $D_2$ has become a standard technique in the repertoire of tools for analyzing chaotic systems because it not only identifies a system as having underlying simple determinism, it also quantifies the degree to which the system is chaotic. Conventional wisdom has it that the number of independent equations needed to describe the system is only slightly greater than its correlation dimension, i.e. an unknown system with dimension 3.2 would need four or possibly five equations to describe it. Thus, determination of the correlation dimension is a first step in

reconstructing the system's governing equations. Work by Sprott[40], however, has shown for a certain class of systems – maps and ODEs described by polynomial and other simple functions – that the average correlation dimension is of the order of the square root of the number of equations. The number of equations needed may be far greater than the fractal dimension indicates.

That notwithstanding, the correlation dimension is still widely used as measure of the degree of chaos in a system. Unfortunately, although it is simple to implement, calculation is computationally intensive, often requiring many CPU hours for large data sets. Several methods have been developed to speed computation, most of which favor calculation of only some distance pairs – the closest ones – and omitting most others. I prefer another method which makes use of certain redundancies in the calculation to speed computation.[41] Although not as fast as some of the other methods, it computes all distance pairs, which can be important in determining the parameters for proper calculation of $D_2$.

Figure 3.5 presents typical results for the Lorenz attractor. 10,000 points were analyzed. The top plot shows the correlation integral log $C(r)$ plotted versus log $r$ (logarithm base 10), where $r$ is the radius of the hypersphere, for several embedding dimensions. The scaling region of constant slope is indicated by a straight line fit. The slope of this line should be the same for all embeddings. The lower plot is the two point slope of the upper one. Here the scaling region, now a plateau, is much more apparent, and it can be seen that all embeddings do indeed saturate to the same slope. For clarity, only some of the points are indicated by symbols. At large radii the slope falls to zero indicating that the hyperspheres are encompassing the entire attractor. At small radii one is limited by the number of points in the finite data record; statistics get poorer and the dimension increases. The best fit to a straight line over this scaling region (admitting a somewhat arbitrary determination) yields a value for the correlation dimension of $D_2 = 2.000 \pm .003$, where the error is from the goodness of fit. This is close to the accepted value of the Hausdorff fractal dimension of 2.05.

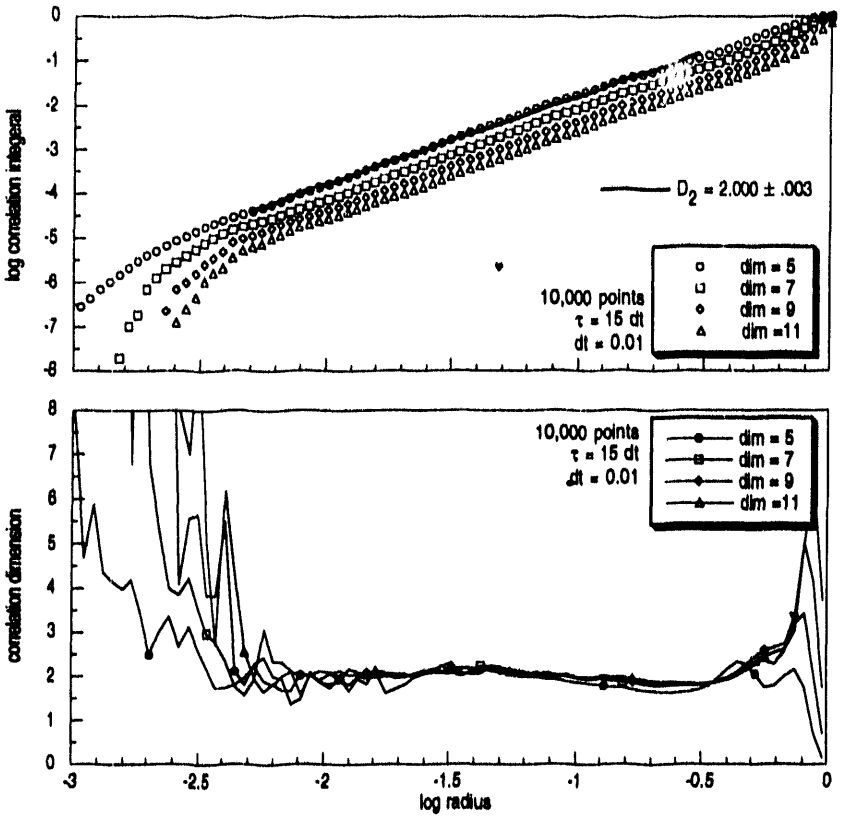


**Figure 3.5.** Plots used in determining the correlation dimension of the Lorenz attractor. The solid line in the top figure is a best fit to the constant slope scaling region. As seen in the bottom plot, the correlation dimension remains constant in several embedding dimensions over a region of at least a decade in $r$.

The subtleties of determining the correlation dimension are discussed in some detail in [42], however two important points are worth mentioning here. Critical in calculating the correlation dimension is the value of the time lag $\tau$. The time lag must be chosen appropriately such that vector components are independent. Choosing $\tau$ too small can result in spurious correlation and an artificially low correlation dimension. At the other extreme, due to the finite length of any real data record and sensitivity to initial

conditions, too large a value of $\tau$ leads to decorrelation and an overestimate of the correlation dimension. The autocorrelation function generally provides a good criterion for the choice of choice of time lag: $\tau$ times the embedding dimension should be 2 to 3 times the $e$ -folding time. However, the correlation dimension should be computed for various $\tau$ in order to find an optimal value. Over some range of $\tau$ the slopes of the log $C(r)$ versus log $r$ plots overlay in a given embedding. The time lag must be chosen somewhere within this range. There is an excellent discussion in Albano, *et al.* where they show that there is a range of "window lengths" $(m\text{-}1)\tau$ over which the Grassberger-Proccacia algorithm provides an accurate estimate of the correlation dimension.[43]

Typically, one wants to sample data frequently enough so that the autocorrelation time is several time steps. Sampling infrequently will yield data that is not properly correlated; sampling too often will confine the dynamics to only a portion of the attractor. Best results for $D_2$, and all other analysis methods presented here, are obtained when the autocorrelation time is between 10 and 20 time steps.

Another possible source of error is described by Thieler.[44] In addition to vector *components* being correlated, *vectors* close in time may be correlated to each other. This results in a spurious $D_2 = 0$ region of the correlation plot. Thieler suggests introducing a parameter $W$ and computing the correlation function only for vectors such that $t_j > t_i + W$. An appropriate choice for $W$ is indicated by the disappearance of the $D_2 = 0$ region; usually $W$ is small, on the order of $5\tau$.

As mentioned previously, the fractal dimension, and hence correlation dimension of the Mackey-Glass attractor is dependent on the equation delay time $T$. The behavior is evident in the two plots of figure 3.6 which show correlation dimension for $T = 23$s and 100s. As expected from figure 3.2, the Mackey-Glass attractor is low dimensional for $T = 23$s. The accepted value is $D_2 = 2.44 \pm 0.5$. For $T = 100$s the dimension increases to $D_2 = 7.5$, which is the accepted value.[45] For the latter case, the correlation dimension drops at small radii indicating enhanced correlation on small scales. This can be attributed to the relatively small number of points used. In high dimensional embedding spaces there are only a few nearby trajectories. Thus, at small radii trajectories are correlated only with themselves, which results

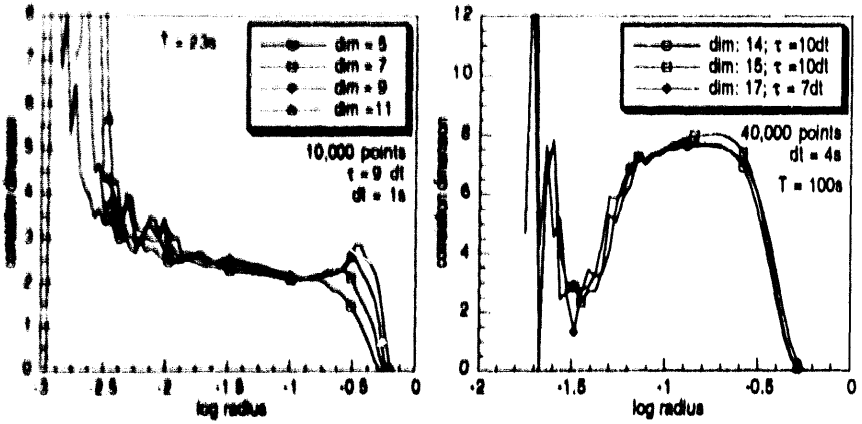


**Figure 3.6.** The correlation dimension of the Mackey-Glass attractor for two different values of the equation delay time $T$.

in an artificially high correlation fraction relative to the total.

A significant drawback of the correlation dimension is that it can make no estimate of the degree of accuracy of the computed dimension (no error bars). Another problem is apparent when comparing the two Mackey-Glass attractors: the scaling region for the $T$= 100s case is significantly shorter than for $T$= 23s. This is due to the number of points required to obtain adequate saturation in higher dimensions: *points are more sparse in higher dimensional spaces.* Several groups have estimated the number of points required for a reliable estimation of the correlation dimension. Estimates range from several hundred to $42^{D}$.[46,47] Tsonis provides a more reasonable rule of thumb : $N_{min} \propto 10^{2+0.4D}$, which also coincides with my experience.[39] Perhaps the best rule is: For adequate confidence in a correlation dimension determination a scaling region which spans at least a decade in $r$ is required.[48]

Random numbers densely fill the space they occupy, and this is reflected in the correlation dimension plot 3.7. At each embedding the correlation dimension asymptotes to the dimension of the embedding space. No clear scaling region is evident.

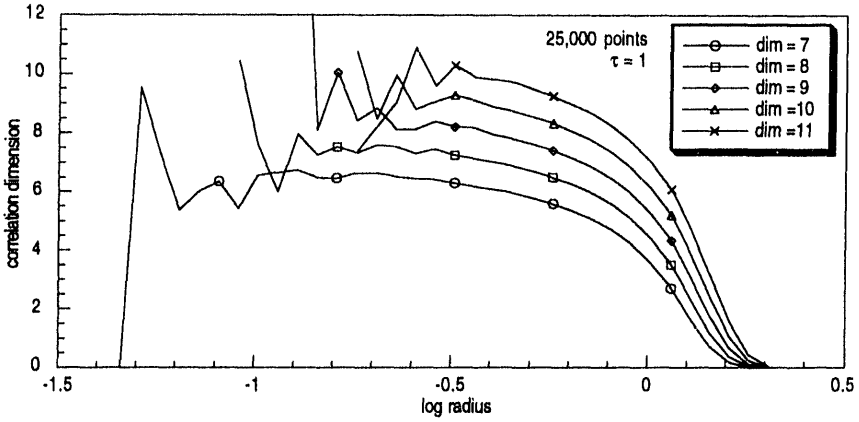


**Figure 3.7.** Correlation dimension for Gaussian distributed random numbers. No clear scaling region exists.

### 3.3. Lyapunov Exponents

As mentioned in chapter 2, computation of the largest Lyapunov exponent is relatively straightforward. The method of Wolf, *et al.*[29] follows the trajectory of a single component in phase delay space, known as the *fiducial* trajectory. A nearby orbit is found, and their average divergence over some time period is measured. Because all chaotic attractors are, on average, contracting in phase space, the exponential divergence cannot continue indefinitely. Consequently, after some time period a new orbit closer to the fiducial trajectory must be found. The vector connecting this new orbit to the fiducial trajectory must preserve the orientation in phase space of the original vector in order to compute the Lyapunov exponent properly. This procedure amounts to a reorthonormalization of the tangent space vectors describing the expansion/contraction of the attractor. This process continues throughout the time record, and is illustrated schematically in figure 3.8.

Although the procedure is effective, it is incomplete. A single Lyapunov exponent can only indicate that a system is chaotic, but tells nothing about the dimension of the system. Noise also has a positive largest Lyapunov exponent. One really needs the entire spectrum of exponents to ascertain whether

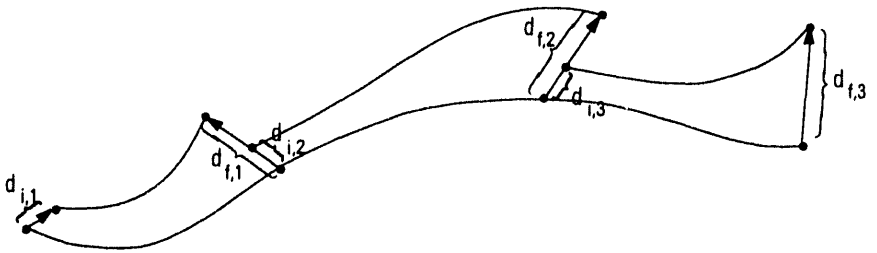


**Figure 3.8.** The figure schematically depicts the computation of the largest Lyapunov exponent by following a fiducial trajectory in time and calculating the divergence of nearby trajectories.

underlying simple determinism exists. A positive Lyapunov exponent accompanied by a negative one would indicate the presence of chaos.

A method proposed by Eckmann, *et al.* and modified by Briggs computes the spectrum of exponents by approximating the Jacobian of the local trajectory of the dynamical system.[31,49] In the method of Briggs, the time series is embedded in phase delay-space, a group of nearest neighbors is found, and their trajectory is fit to a polynomial function. This function can then be differentiated analytically to obtain the Jacobian of the local dynamics. The Lyapunov exponents are then given by:

$$\lambda^{(i)} = \lim_{t\to\infty} \frac{1}{t} \ln \left\| J_t^{(i)} \right\| , \qquad (3.4)$$

where $\left\| J_t^{(i)} \right\|$ is the $i^{th}$ eigenvalue of the Jacobian after advancing the system a time $t$ (see [26] for a thorough discussion).

Finding the eigenvalues of real, nonsymmetric matrices is not trivial, and often the eigenvalues are complex, whereas Lyapunov exponents are real. This is because the tangent space of the system is not necessarily aligned with our (arbitrary) coordinate system. Computation of the Lyapunov exponents is facilitated by *QR* decomposition. Any matrix can be written as **M=QR** where **Q** is an orthogonal matrix and **R** is upper right triangular with positive diagonal elements. This is known as the "skinny" decomposition, and it is unique. We can write $x(t) = f_t(x_0)$, and since the time series to be analyzed is descretized, by the chain rule, $\mathbf{J}_{t+1} = [\partial f_{t+1}/\partial x] = \mathbf{J}_t \mathbf{J}_{t-1} \ldots \mathbf{J}_0$. Given a set of matrices $\mathbf{J}_1, \mathbf{J}_2, \ldots \mathbf{J}_t$, one

can decompose them as:

$$\begin{aligned} \mathbf{J}_1 &= \mathbf{Q}_{(1)}\mathbf{R}_{(1)} \\ \mathbf{J}_2\mathbf{Q}_{(1)} &= \mathbf{Q}_{(2)}\mathbf{R}_{(2)} \\ &\vdots \\ \mathbf{J}_t\mathbf{Q}_{(t-1)} &= \mathbf{Q}_{(t)}\mathbf{R}_{(t)} \end{aligned} \qquad (3.5)$$

The Jacobian then becomes $\mathbf{J}_{t+1} = \mathbf{J}_t \ldots \mathbf{J}_2\mathbf{J}_1 = \mathbf{Q}_{(t)}\mathbf{R}_{(t)} \ldots \mathbf{R}_{(2)}\mathbf{R}_{(1)}$. The effect of the products $\mathbf{JQ}$ is to successively orient the Jacobian matrices along the principal axes of the tangent space of the attractor. The Lyapunov exponents can be computed from:

$$\lambda_i = \frac{1}{\tau n}\sum_{j=1}^{n} \ln R_{ii(j)} \quad . \qquad (3.6)$$

Implementation of the algorithm is not difficult on a computer, and several routines exist to do the *QR* decomposition.[50,51] Most of the CPU time is spent searching for nearest neighbors rather than in actual calculation of the exponent. The Briggs method gives superior results to the original method proposed by Eckmann and Ruelle, because in fitting an arbitrary polynomial it includes the curvature of the local space. This is particularly true in embedding dimensions higher than the spatial dimension of the attractor. A sample of the results are contained in table 3.1. The Kaplan-Yorke dimension is also presented for comparison.

Critical in obtaining accurate results is the choice of the component delay time $\tau$ and the number of time steps to evolve the trajectory before measuring the expansion. In all cases, the best results are obtained by evolving $\tau$ time steps before computing each Jacobian. The optimum choice of $\tau$ is made in the same way as for the correlation dimension: $\tau$ times the embedding dimension is 2 to 3 times the $e$-folding time of the autocorrelation function. The number of neighbors is also important, but it does not influence the results as strongly. I have found that it is best to use all neighbors up to a predefined maximum within a given fixed radius, rather than a fixed number of neighbors; choosing too many neighbors in sparsely populated regions can skew the predicted trajectory, and choosing too few in densely populated regions may mean most points lie on the same trajectory. A radius of about 10% of

| system | $\tau$ | $D_{KY}$ | Lyapunov exponents | | |
|---|---|---|---|---|---|
| Lorenz | 0.9s | 2.09 | 1.387 ± 9.1% | -0.067 ± >100% | -14.874 ± 2.6% |
| accepted $\lambda$ :[29] | 0.8s | 2.09 | 1.633 ± 6.8% | 0.067 ± >100% | -18.352 ± 1.4% |
| 1.497, 0.0, -22.46 | | | -45 | | |
| Mackey-Glass, $T$ = 23 | 6s | 2.68 | 0.0965 ± 11.5% | -0.007 ± >100% | -0.131 ± 15.4% |
| accepted $\lambda$ :[45] | dt=0.5s | | -0.391 ± 8.2% | | |
| .0956, 0.0, -.119, -.344 | | | | | |
| Mackey-Glass, $T$ = 100 | 5s | 8.95 | 1.4293 ± 0.9% | 0.7830 ± 1.3% | 0.4133 ± 1.8% |
| | dt=1s | | 0.1871± 3.6% | 0.0095 ± 74.6% | -0.0790 ± 10.5% |
| | | | -0.3186 ± 3.2% | -0.7277± 1.9% | -1.7798 ± 1.4% |
| Random Numbers | 2 | 3.86 | 0.258 ± 1.0% | 0.093 ± 4.8% | -0.068 ± 8.2% |
| | | | -0.327 ± 3.1% | | |
| | | 4.61 | 0.200 ± 2.1% | 0.094 ± 3.8% | 0.011 ± 33.7% |
| | | | -0.101 ± 5.1% | -0.337 ± 2.9% | |
| | | 5.47 | 0.199 ± 2.2% | 0.105 ± 3.2% | 0.031 ± 10.1% |
| | | | -0.040 ± 9.3% | -0.133 ± 4.2% | -0.348 ± 2.9% |

**Table 3.1.** Computed Lyapunov exponents for several systems. The parameters for the Lorenz system were: $r$=45.92, $b$= 4.0, $\sigma$= 16.0. For the Mackey-Glass system: $\beta_0$ = 0.2, $\gamma$=0.1, $n$ =10.

the maximum extent of the attractor usually gives good results.

Results for the Lorenz system are in excellent agreement with the accepted values, even the large negative value. Negative exponents are notoriously difficult to calculate because of their extreme sensitivity to the quality of the data. The zero exponent is easily identifiable both by its small absolute value relative to the others and the large standard deviation. Typically, the "zero" exponent has a magnitude about a factor of 10 smaller that the next largest value. During computation this value fluctuates wildly, sometimes positive sometimes negative, and has a very large (>100%) standard deviation. In the next largest embedding space, the first three exponents remain constant and a fourth negative exponent appears. The Kaplan-Yorke dimension remains essentially constant, indicating that an embedding of 4 is unnecessary.

The Mackey-Glass system proved more difficult to analyze; the system is fairly sensitive to the value of $\tau$. Results are nonetheless good, with the largest exponent being within 4% of the accepted value. Choosing a shorter sampling time (more data points per time step) can make the system less sensitive to the choice of $\tau$, though the number of matrices available, and hence the statistics, is thus decreased. For the system with an equation delay time $T$ = 100s, no saturation in the Kaplan-Yorke dimension is seen up to an embedding of 10. However, the values of the exponents remain essentially unchanged as the embedding dimension is increased. This indicates that the positive exponents are probably nearly correct. It has been estimated that $D_{KY}$ is greater than 10.[45]

Random numbers can be identified by several characteristics. First, they continue to fill the space they are embedded in, as evidenced by the KY dimension. In fact, for some cases, the $D_{KY}$ is actually greater than the embedding dimension. Second, although there are negative exponents, no convincing zero exponent exists. The fact that there are negative exponents indicates that the set is bounded ( $|x| <$ 6 in this case), so that points near the edge are pulled back into the set. This is not, however, evidence of an attractor. Finally, during the calculation of the exponents, finding sufficient nearest neighbors is a problem, even for rather large radii. Random points are evenly and sparsely distributed in the embedding space. The positive exponents do not change appreciably as the embedding increases, which indicates that they may be correct.

### 3.4. Predictability

Both the Lorenz and Mackey-Glass systems are governed by simple deterministic equations, and as such should be predictable in the short term. Sugihara and May have proposed a very simple method for predicting the short term behavior of such systems.[36] In their method one finds the *minimum* number of nearest neighbors to a "predictee" needed to form a simplex – $D$ +1 points – in the embedding. The simplex is then evolved a number of time steps into the future. The predicted evolution of the predictee is then the weighted mean of the simplex, where the weights are the exponentiated original predictee-neighbor distances. In practice, a portion of the data record is deemed the database

of neighbors and the remaining points are the predictee values. Each predictee is evolved several time steps into the future, and one then compares the predicted trajectory with the actual trajectory.

In order to characterize the degree of short term predictability Sugihara and May use the linear correlation coefficient to measure the correlation between the original trajectory and the predicted one. This is a poor measure for several reasons. The linear correlation coefficient will give a value of 1 if the predicted trajectory ($y$) equals the actual trajectory ($x$) for all points considered. Unfortunately, it will also give a value of 1 if $y = ax$. We are *assuming* the attractor is chaotic, and trajectories diverge exponentially rather than linearly. Secondly, the correlation coefficient does not indicate whether the observed correlation is *significant* because it contains no information about the distributions of $x$ and $y$. Finally, it is generally only a reasonable measure for large (>20) sample populations. Typically, because of the exponential divergence of chaotic trajectories, predicted trajectories are reasonable for only about ten time steps. A better measure simply computes the average deviation of the predicted from the actual values, normalized to the distance propagated. Because a single poor prediction (say in a sparsely populated region of phase space) can strongly skew the mean, the median is a better measure of the average normalized deviation.

As a result of its simplicity, the Sugihara-May method is not a very good predictor even for short times. It is a $0^{th}$ order method, in that there is no $x$ dependence, and it does not even attempt to capture the underlying dynamics of the system. A superior method fits a linear or higher order polynomial to the local trajectory in order to do the prediction. The method is similar to one proposed by Farmer and Sidorowich[35] except that a generalized polynomial is fit to the local trajectory. The generalized polynomial can be written as

$$F_i(x) = f_{i0} + \sum f_{i1}x + \sum f_{i2}xx + \ldots \quad . \tag{3.7}$$

$F_i(x)$ is the map of the $i^{th}$ component and the sums are over all components in the embedding space ($f_{i1}$ is an $m$ dimensional vector, $f_{i2}$ is an $mxm$ tensor, etc.). To implement the method, one (as usual) chooses an appropriate time-delay embedding based on the autocorrelation function. A window length

1 1/2 to 2 times the autocorrelation time usually works best. Shorter window lengths will give better predictions, but this is artificial, since points close in time may retain spurious correlations. Correlated noise is notorious for this property. As with the Sugihara-May method, the degree of predictability is characterized by the normalized deviation.

Results for the systems presented in this chapter are summarized in figure 3.9. Time steps are measured in units of $\tau$ . Correlated noise, if it is frequently sampled, can give very small prediction errors if one chooses time steps equal to the sampling time rather than $\tau$. One can see the short term predictability for all three chaotic systems is reasonably good (small error), while white noise consistently has 100% error. Predictability of the Lorenz system is extremely good. The reason for this is reflected in the Lyapunov exponents. The least negative exponent (smallest in absolute value) governs the contraction of the system onto the inertial manifold containing the attractor. For the Lorenz system, this is very large, and the attractor is extremely stable to perturbations. This also accounts for its predictability. In the random signal, the initial error of less than 100% is an artifact of advancing $\tau$ time steps. Because a delay embedding is used, after $\tau$ time steps many of the vector components are identical. The error is nonetheless large (~50%), and after 2 time steps it is equal to 100%.

The translation error (Eq. (2.17)) for these systems is plotted as a function of embedding dimension in

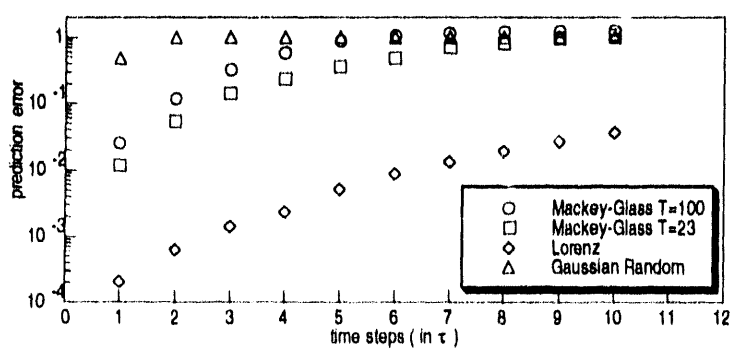


**Figure 3.9.** The prediction error for several systems versus the number of time steps into the future measured in units of $\tau$ . The deterministic systems show a high degree of predictability while random noise does not.

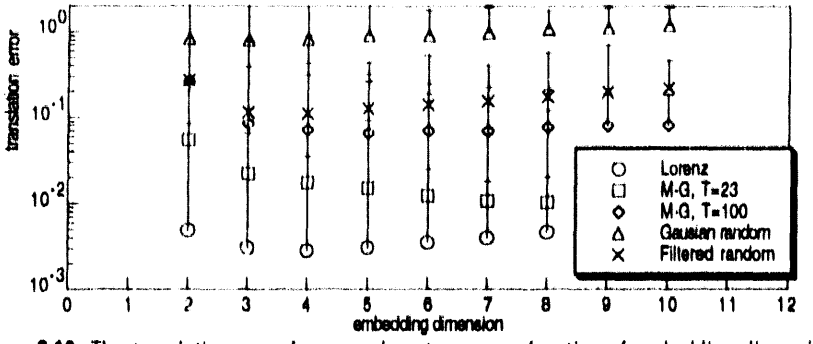


**Figure 3.10.** The translation error for several systems as a function of embedding dimension. Deterministic systems have low values which increase with embedding. Random noise has values near 1, and shows no such increase. Filtered noise also shows some degree of predictability although it is not deterministic.

figure 3.10. The simple deterministic systems, Lorenz and Mackey-Glass, both show low values for the translation error, indicating coherent flow. The error decreases until the system is properly embedded and then increases again in higher embeddings where points are more sparsely distributed. Gaussian random noise gives consistently high values, close to or equal to 1, in all embeddings. In addition, there is no strong trend in the data. Also plotted is a correlated noise series created by lowpass filtering Gaussian white noise. The data show short term predictability due to the finite autocorrelation time of the data, although the system is not deterministic. This effect will be discussed at length in the next chapter.

### 3.5. Summary

I have discussed the application of the analysis methods used to identify chaotic and simple deterministic systems using two systems know to be chaotic, the Lorenz and Mackey-Glass systems, and Gaussian random noise. Low dimensional systems may show structure in phase-delay reconstruction plot and Poincaré sections. High dimensional systems usually show no structure, as is true of noise. For chaotic systems, the correlation dimension plots show a clear plateau over the scaling region which corresponds to the dimension of the system. Random noise fills the embedding space and

show no saturation in any embedding dimension. The spectrum of Lyapunov exponents for chaotic systems is marked by consistent exponents in larger embeddings, the Kaplan-Yorke dimension approaching a constant value, and a clear "zero" exponent indicated by both a small magnitude and large standard deviation. Proper estimation of the exponents is more difficult for higher dimensional system. For random system, $D_{KY}$ does not saturate and there is no clear zero exponent. Chaotic systems are characterized by good short term predictability and coherence of flow. These are measured by the prediction error and translation error, respectively. Random noise has poor predictability and flow coherence.

## 4. Extracting Simple Determinism from Intransigent Data

The techniques outlined in section 2.2 for identifying underlying simple determinism are robust in theory. Practical application of the methods is rarely straightforward. One must be certain that the presumed simple determinism is real and not a result of improper analysis technique. In addition, all systems *real or numerical* suffer from noise corruption. This chapter deals with the practical application, precautions and pitfalls of applying the methods of chapter 2 to real systems. The first section addresses the issue of spurious low dimensionality in high dimensional systems. The next two sections deal with techniques for resolving a corrupted underlying attractor.

### 4.1. Surrogate Data Sets

Once a chaotic system has been identified, one needs to confirm that the identification is indeed correct and not an artifact of the analysis procedure. A simple method for doing so involves the creation of surrogate data sets. A surrogate set is similar to the original attractor, but randomized in some way to destroy the simple determinism. The analysis methods should then be reapplied to this new data set. All tests should yield very different (negative!) results, thereby confirming the original assessment of simple determinism. If there still remain indications of simple determinism, more than likely one is witnessing an artifact of the analysis method.

One method of creating a surrogate data record is simply to shuffle all the data points in the record. This will create a random signal, all moments of which are the same as the original, but will destroy any correlation in the original signal. The method is too drastic, however. It destroys essentially all information contained in the original system: power spectrum, structure, etc. The method is little better than generating a random noise system of the appropriate amplitude. A better method involves using the data from the original system and randomizing the phases of the Fourier components. This preserves the original power spectrum, but creates a data set in which small scale correlation is lost.

The method preserves global quantities of the system: the power spectrum (obviously), macrostructure in all embeddings (similar periodicity and amplitude) and also the autocorrelation time. Yet any simple determinism is destroyed.

Figure 4.1 depicts a time record of the original Lorenz system and a surrogate data set created by phase randomization. The neighboring plot depicts the two dimensional phase-delay reconstruction of the surrogate. This should be compared with figure 3.1. It is evident that the two signals are structurally similar, though the phase-randomized data does not show the same coherency of flow as the original data. Figure 4.2 shows the correlation dimension for the phase-randomized surrogate of the Lorenz system on the left and of the Mackey-Glass system with $T = 100s$ on the right. The surrogate sets show the same behavior as random noise; there is no scaling region because the system fills the embedding space. These plots should be compared with those of the original systems shown in figures 3.5 and 3.6.

Figure 4.3 compares the prediction error and translation error for the two systems with their surrogates. The prediction error measures the short term predictability of the system while the translation error

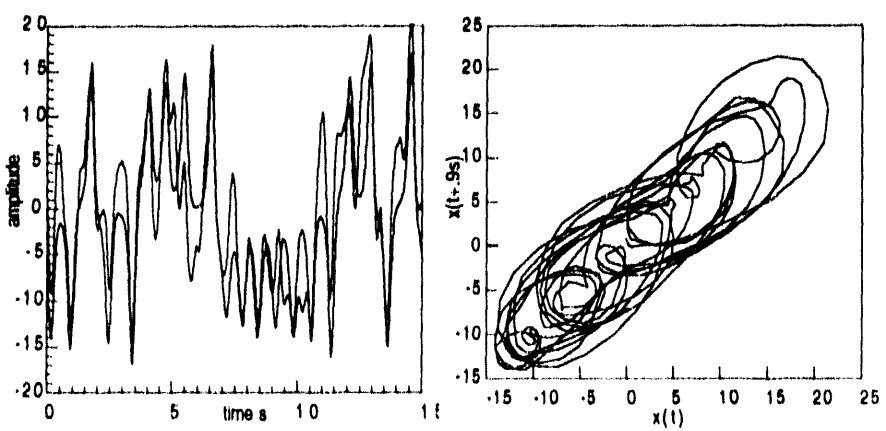


**Figure 4.1.** The left figure shows the time series of a phase-randomized surrogate for the Lorenz attractor. The original signal is in gray. The right figure shows the 2 dimensional phase-delay plot of just the surrogate. This should be compared with figure 3.1 The two appear structurally very similar, but the surrogate does not have simple determinism.

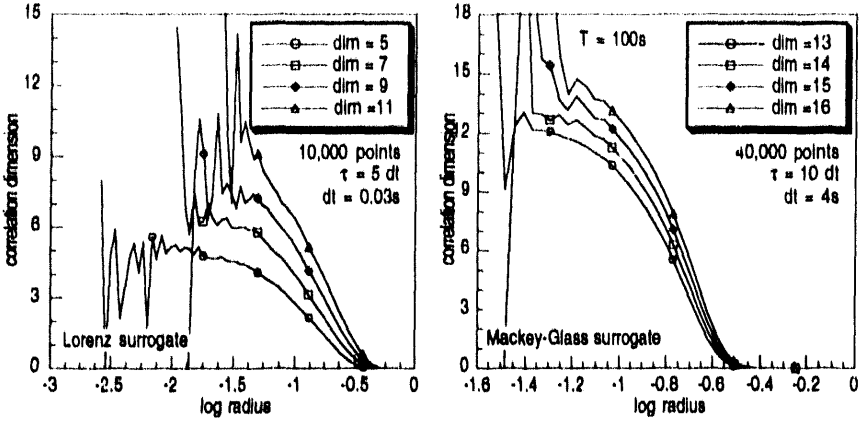


**Figure 4.2.** The correlation dimension of the surrogate data sets for the Lorenz attractor and the Mackey-Glass system with $T$ =100s. Neither show any evidence of low dimensional chaos. The plots should be compared with figures 3.5 and 3.6.

measures the coherence of flow. The two are closely related. The surrogate systems exhibit behavior similar to random numbers: There is a steep rise over 1-2 prediction steps in error from modest values (20-30%) to 100% error. The initial correlation is artificial. Since prediction error is measured in units of $\tau$, the component time lag, all signals will show initial spurious predictability because components are shared among successive points. For the Lorenz system the surrogate shows worse predictability by several orders of magnitude. This is typical of low dimensional systems. Higher dimensional systems show a less dramatic change. It is nonetheless significant (over a factor of 3) for the Mackey-Glass system with $T$ =100. The fact that the translation error for the Mackey-Glass system is so close to that of its surrogate is disconcerting. As will be discussed later, the translation error is an unreliable measure of simple determinism for high dimensional systems.

Table 4.1 shows the Lyapunov exponents of the Mackey-Glass and Lorenz systems compared with their surrogate data sets. The Kaplan-Yorke dimension of the surrogates continues to increase with larger embeddings. There is no clear zero exponent, normally characterized by its small magnitude and large standard deviation, which would indicate that the system is continuous in time. The positive exponents

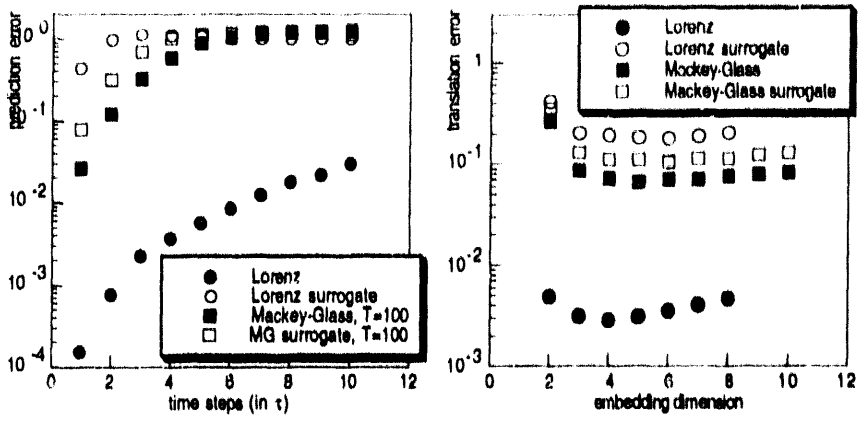


**Figure 4.3.** The prediction error and translation error plotted for the Lorenz attractor and the Mackey-Glass attractor and their phase-randomized surrogates. The prediction error clearly distinguishes the original data from the surrogates for both systems. There is a marked difference in translation error for the Lorenz data, but the higher dimensional ($T$ =100s) Mackey-Glass data is not as clearly distinguishable from its surrogate.

of the surrogate systems may be correct, however, reflecting the space-filling properties of the random data.

An additional use for surrogate data sets was described recently by Bauer, *et al.*[52] They use dimension densities to characterize high dimensional chaotic systems. Using the usual correlation dimension, they define the dimension density as

$$D_2 / m = \frac{\Delta \log C(r)}{\Delta \log \tilde{C}(r)} \tag{4.1}$$

where $m$ is the embedding dimension. $\tilde{C}(r)$ is the correlation integral of an attractor with the same macrostructure as the original system, but without the small scale coherent structure. To this end, the phase randomized surrogate is ideally suited. (For reasons of simplicity, they advocate a different method for obtaining a surrogate data set and computing $D_2$, which is not strictly correct.)† In their

† In creating their surrogate, they measure the probability distribution of the points of the original system in the embedding $m$, and then randomize this distribution. In order to simplify calculations, they use the maximum norm in computing the

| system | $\tau$ | $D_{KY}$ | Lyapunov exponents | | |
|---|---|---|---|---|---|
| Mackey-Glass, $T$ =23s | 1 s | 2.66 | 0.1043 ±16.6% | -0.0050 ±99.9% | -0.1495 ±20.4% |
| | | | -0.3643 ±10.9% | -1.0808 ± 5.4% | |
| Mackey-Glass surrogate | 1 s | 4.04 | 0.7326 ± 3.2% | 0.2254 ±11.1% | -0.1627 ±19.9% |
| | | | -0.6977 ± 7.0% | -2.1967 ± 3.8% | |
| Lorenz | 0.03 | 2.12 | 0.1537 ± 6.6% | 0.0335 ±40.0% | -1.5605 ± 2.1% |
| | | | -4.9448 ± 1.3% | -10.7600 ± 0.6% | |
| Lorenz surrogate | 0.03 | 5.16 | 12.9658 ± 1.6% | 5.8749 ± 2.9% | 0.8818 ±18.7% |
| | | | -4.1618 ± 5.1% | -13.4014 ± 2.9% | |
| Filtered Gaussian noise | 1 | 7.13 | 2.0223 ± 1.0% | 1.3121 ± 1.6% | 0.6516 ± 3.5% |
| | | | 0.1557±19.2% | -0.4627 ± 8.8% | -1.0514 ± 5.5% |
| | | | -2.0718 ± 3.9% | -4.1227± 2.6% | -9.2322 ± 1.5% |

**Table 4.1.** The Lyapunov exponents the Mackey-Glass system, Lorenz system and their surrogates. The surrogates show no saturation in the Kaplan-Yorke dimension with higher embeddings, and no clear zero exponent. The exponents of a filtered noise data set are discussed in section 4.3.

article, they measure a dimension density of about 0.8 in an embedding of 15, which for their system of 1000 coupled oscillators corresponds to a dimension of 800. They have not as yet tried applying the method to low dimensional systems, but they intend to use it to study Taylor-Couette fluid flow (a known real system with low dimension).[53] Unfortunately, my studies using the Lorenz attractor with both randomized and phase randomized surrogates indicate that the method is not very effective for this case. The plateau length is extremely short (ca. 0.5 decades), and no plateau exists at large radii, the very region the method is supposed to compensate for. It does show some promise, though much research still needs to be done.

## 4.2. Noise Reduction

All systems, numerical or experimental, are corrupted by some degree of noise. Its simplest, most benign form is measurement noise. By this I mean that by some non-invasive process one measures the

---

correlation dimension, rather than the Euclidean norm. In a private communication they acknowledged that this does not accurately measure $D_2$ at all scales, but justified it on the grounds that at small scales $\tilde{C}(r)$ is not as limited by statistics.

dynamics of a system, however the instrumentation used in the measurement adds a noise component to the signal. Given a system $x_{t+1} = f(x_t)$, this additive noise process can be modeled as $y = x + r$, where $r$ is the added noise, and $y$ is the measured signal. In computational systems this may occur unintentionally by truncating the data when storing it. In a more insidious process the diagnostic tool may distort the signal through filtering or other means, i.e. $y=g(x)$. Nonetheless, the diagnostic is separate from the system, and in theory – though not in practice – one can extract the relevant signal by "reverse processing" the data. A different problem is the one of dynamical noise or stationarity of the system. In this instance, the system itself is noisy, which alters the (noise-free) dynamics as the system evolves. In this case, $x_{t+1} = f(x_t + r)$, and the measured signal is $x$. For example, a control parameter, ostensibly constant, may fluctuate as the system evolves. If conditions affecting the dynamics of the system change in time identification of the underlying attractor may be impossible because no stationary attractor exists. This can be true even for the seemingly benign situation of small, slow perturbations to the system. In numerical systems the "noise" process may be as subtle as computational roundoff error. In all cases, the noise tends to increase the true dimension of the system, and may corrupt the underlying system so strongly that no dimension is identifiable at all. As a further complication, in addition to the destruction of underlying simple determinism, often the analysis techniques can identify spurious low dimensional chaos where none actually exists. This is especially true for systems which have been subjected to linear filtering and other noise reduction techniques.

Very recently, Schreiber has developed a method for estimation of the noise level in chaotic systems.[54] His analytical results indicate that a noise level of more than about 2% can be catastrophic, obscuring any scaling region and making estimation of the correlation dimension impossible. Fortunately, there exist noise reduction methods for nonlinear systems which can help to overcome this problem. These will be discussed in the next three sections.

### 4.2.1. Principal Component Analysis

Principal component analysis (PCA) is a technique that relies on singular value decomposition (SVD) to

extract the dominant dynamics of a system. It can be a powerful noise reduction technique. In contrast to Fourier decomposition which approximates the system as a finite subset of sine and cosine functions, SVD will decompose the system into a unique set of orthonormal eigenfunctions and eigenvalues. In applying this technique, it is hoped that the dominant eigenfunctions – those with the largest eigenvalues – will capture the relevant dynamics of the system. The set is then truncated, retaining only those eigenfunctions with the largest eigenvalues. From this set any of the techniques outlined in chapter 2 can be applied to describe quantitatively the chaotic dynamics of the original system.

SVD is based on a theorem of linear algebra, which states that any $m$ by $n$ matrix **A** with $m > n$, can be decomposed into the product of an $m$ by $n$ column-orthogonal matrix **U** and two $n$ dimensional square matrices: one diagonal with positive elements **W**, and the transpose of an orthogonal matrix **V**. This is illustrated schematically in fig. 4.4. This decomposition is unique up to a corresponding permutation of the columns of **U**, **W**, and **V**.

Typically this technique is applied to time records of a single system variable. An $n$-dimensional system is created using the Takens method of lags. This matrix is then decomposed with SVD. The eigenfunctions are contained in the matrix **V**, the eigenvalues in **W**. **UW** is then the projection of the original system onto the eigenvector space. The columns of **UW** represent the dominant dynamics of the system. By retaining only the first few columns of **UW** it is hoped that noise, which tends to be uniformly distributed in eigenvector space, can be reduced and the relevant dynamics extracted.

The process of principal component analysis is depicted in figure 4.5. The top left plot shows the

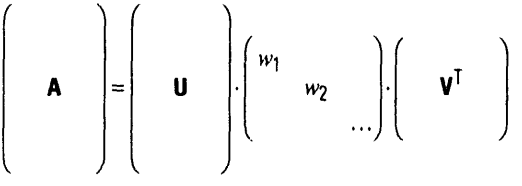


**Figure 4.4.** Schematic illustration of the singular value decomposition of a matrix (after [55]).

original signal from the Lorenz attractor and the neighboring plot shows the same signal corrupted by 50% rms additive Gaussian white noise. Singular value decomposition in an embedding dimension of seven identifies 3-4 large eigenvalues, shown in the center plot, two of whose corresponding eigenvectors are depicted in the lower left plot. An offset has been added to separate the two. The sum of these two largest eigenvectors results in a signal considerably cleaner than the original noise contaminated one as shown in the lower right plot. Note that by using only some of the principal components to recreate the signal a slight time shift is introduced.

### 4.2.2. Lowpass filtering

The most obvious and basic method of noise reduction is simple, linear lowpass filtering. In most all experimental situations some level of filtering takes place. This can be either unintentional, i.e. the finite bandpass capability of the diagnostic equipment, or intentional filtering to extract desired low frequency dynamics. Of the latter, there are two methods to achieve the desired results. Causal filtering filters in the time domain, and is typically implemented with hardware before the signal is recorded. The second method is acausal. Data are post-processed, after being recorded, in the frequency domain with software. Work with chaotic systems has shown that acausal filtering is generally better than causal filtering.[56] While it is impossible to eliminate unintentional filtering effects of the diagnostic equipment, one should avoid hardware filtering when possible. This places a restriction on the sampling frequency, requiring a sampling rate fast enough to avoid aliasing the signal.

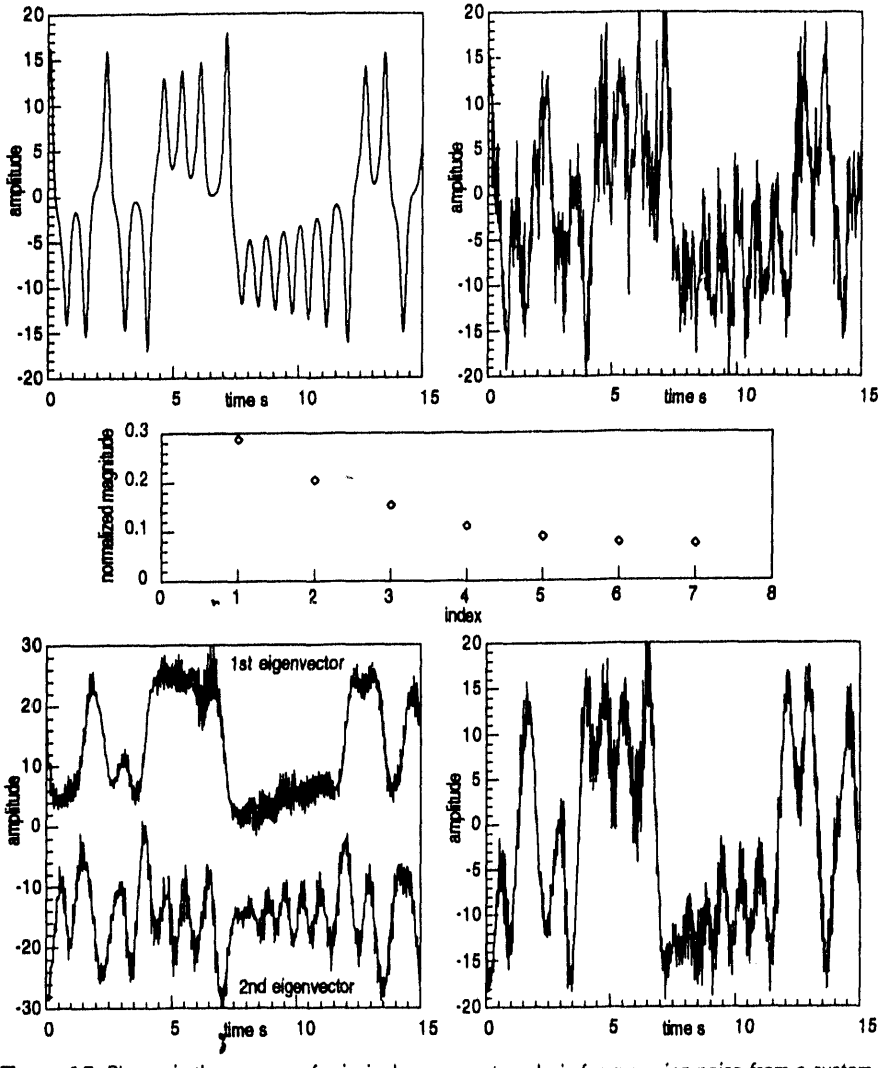


**Figure 4.5.** Shown is the process of principal component analysis for removing noise from a system. The top left plot show the uncorrupted signal from the Lorenz system. The neighboring plot is the same series corrupted by 50% rms Gaussian white noise. Principal component analysis identifies 3-4 major eigenvalues, two of whose component vectors are depicted in the lower left plot. Their sum (lower right) gives a cleaned version of the noisy signal which better approximates the original. The normalized eigenvalues are plotted in the center graph.

Actually, one should avoid linear lowpass filtering altogether. When applying a linear filter to data, one tacitly assumes that the relevant dynamics for the system are confined to a particular frequency range and the noise to a separate regime. This is rarely the case with chaotic systems because their Fourier spectra are typically broadband. In addition, when one attempts to filter a signal one is usually primarily concerned with amplitude reduction. As a consequence linear filtering can distort the phase information of the Fourier components of the signal. As should be apparent from the previous section, phase is crucial to the dynamics of a chaotic system. Another problem is that heavily filtered data can artificially show evidence of low dimensional chaos. If one considers the logical extreme, any signal sufficiently bandpass filtered will yield a simple sine wave. Unfortunately, dire consequences occur long before this limiting case is reached. Heavy filtering distorts the signal enough to give indications of a low fractal dimension where none actually exits. For this reason, in part, I go into some detail about the effects of linear filtering. An additional reason is that the analysis results on MST data are suggestive of a white noise signal which has been lowpass filtered. I will identify in this chapter the characteristics of such a signal for comparison with the data in chapter 6.

In order to illustrate the effects of linear filtering, I will use as examples three of the most common types used. (See [57] for a thorough discussion.) The Butterworth filter is the simplest to implement. Its virtue is that it has maximally flat ( $A_{in} = A_{out}$ ) amplitude characteristics in the passband, the tradeoff being that it has a slow transition region from passband to stopband. A cousin is the elliptic filter where the flatness of the passband is compromised somewhat in order to achieve a steeper transition region. Finally, the Bessel filter, or constant delay filter, has poor amplitude characteristics (a very slow transition region), however, it has a linear phase relation with respect to frequency well into the stopband. The amplitude and phase characteristics of the Bessel and Butterworth filters are plotted in figure 4.6.

The power spectrum of the Lorenz system is plotted in figure 4.7. It is broadband and exhibits an exponential fall off in power which is common in chaotic systems. Power spectra for the Mackey-Glass

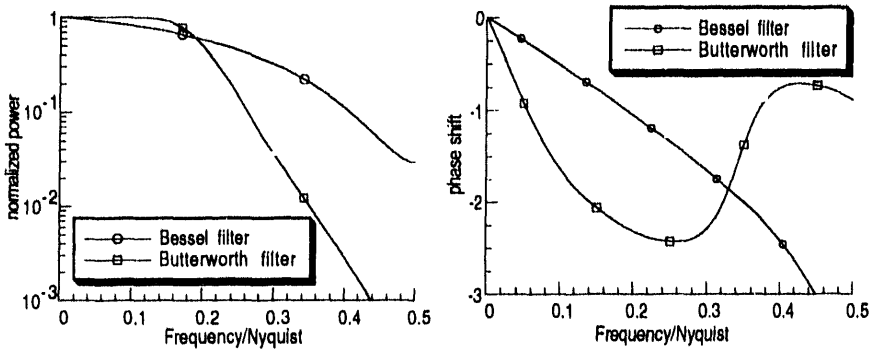


**Figure 4.6.** The amplitude and phase characteristics of the Bessel and Butterworth filters. The Butterworth filter has good amplitude characteristics, but distorts the phase. Bessel filters have a nearly linear phase response until well into the stopband, but poor attenuation performance.

system are very similar. This provides another obstacle for linear filters: Linear filters are generally designed as power law functions, though not exclusively so.

In figure 4.8 the top plot shows the power spectrum of the Lorenz time series when corrupted by 50% rms added Gaussian white noise. The original spectrum is plotted in gray for comparison. Beneath it are the effects of an 8-pole elliptic filter and 8-pole Bessel filter on the corrupted spectrum. In both cases the cutoff frequency was chosen to match the original power spectrum as closely as possible. Although

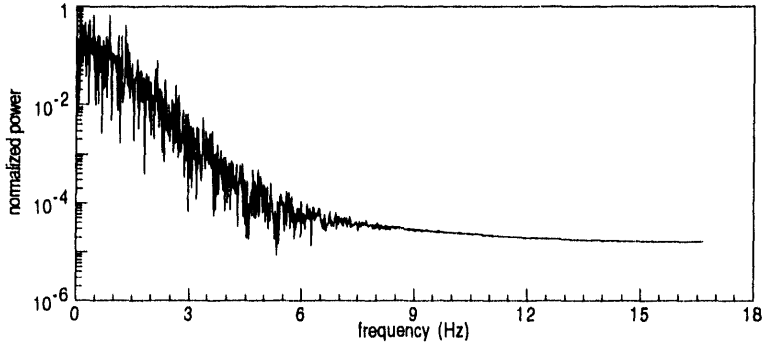


**Figure 4.7.** The power spectrum for the Lorenz attractor. It is broadband and shows an exponential falloff in power which is common in chaotic systems.

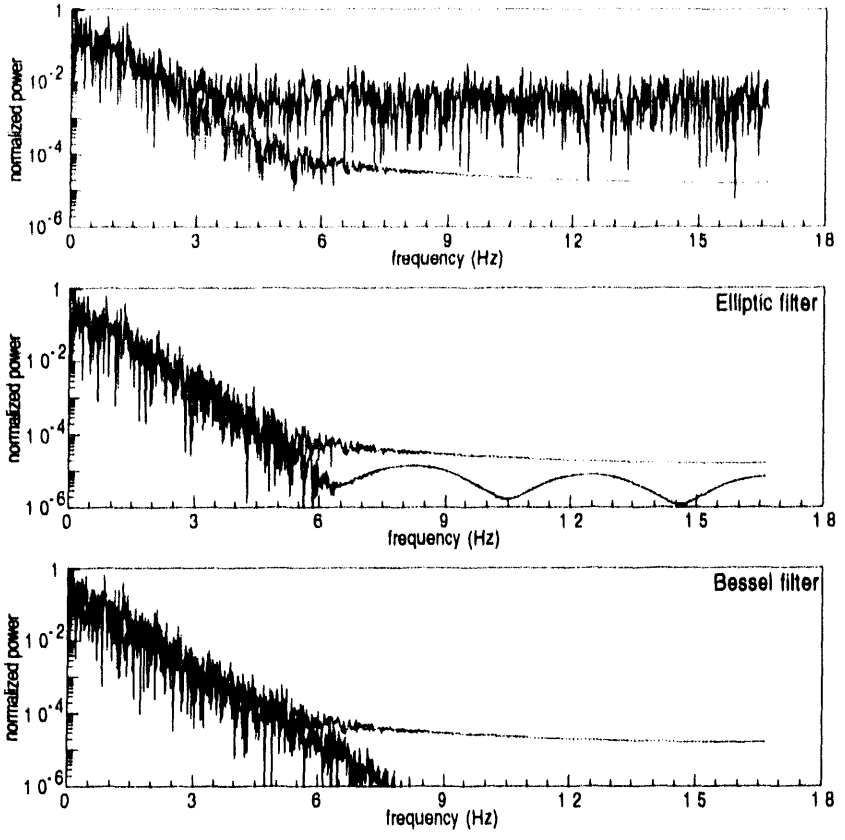


**Figure 4.8.** The top plot shows the power spectrum of the Lorenz attractor corrupted by noise. The lower two plots show the resulting spectra when noise reduction is attempted with an elliptic and a Bessel filter, respectively.

both do a fairly good job over much of the region, neither is able to recover the shape of the original spectrum at high frequency.

The filtered signals are plotted in figure 4.9. Both show significant improvement over the original noisy signal plotted in figure 4.5. This similarity, however, does not indicate whether the relevant simple determinism has been recovered. As will be demonstrated in the next section, neither filtering method

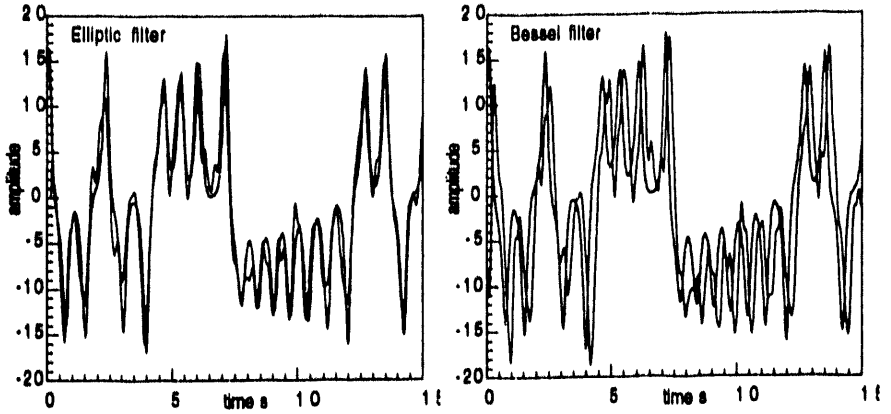


**Figure 4.9.** The noise corrupted signal of the Lorenz attractor as processed by two linear filters. The original signal is outlined in gray. Qualitatively, the two signals appear nearly identical, though the filtering methods are very different in principal. Note the delay introduced by the Bessel filter.

is able to recapture the underlying chaotic dynamics of the original signal.

### 4.2.3. Nonlinear Noise Reduction

While simple lowpass filtering may be appropriate in some cases, in general it is an inferior method. This is because linear filters do not take into account the inherent nonlinear dynamics of the system being filtered. The method simply attenuates all signal components greater than a certain frequency. This may, however, attenuate some of the relevant dynamics of the system, while emphasizing spurious components at lower frequencies.

Several similar alternative methods of filtering specifically aimed at reducing noise in chaotic systems have been developed[58-64]. The methods make use of the spatial structure of the underlying attractor and are similar in implementation to the prediction methods outlined in section 2.3. In a nutshell, the time record of a single component of the system is embedded using the method of lags. For each point in the embedding space the nearest neighbors are found. The average local trajectory of these points is found which becomes the functional map of the point being filtered.

The method as outlined lacks self consistency, however. One begins with a single time record and creates from it an array of time records, one corresponding to each dimension of the embedding space. The method for correcting this constitutes the various approaches to the filtering. One approach simply updates only a few of the components in the embedded space. For a given point in the embedded space $[x(t), x(t+\tau), x(t+2\tau), \ldots]$, the filtered image point is $[y(t+\Delta t), y(t+\Delta t+\tau), \ldots x(t+\Delta t+n\tau), \ldots]$, where $y$ is the filtered signal. Thus, each new basis vector consists of some components from the filtered trajectory and the remaining components from the original signal. My own investigations indicate that updating only one, the first component, yields the best results. The method achieves excellent results for sets of ODEs with modest noise levels (<100%), recovering the original trajectory almost exactly. The method is iterative, with several iterations required for best results. Unfortunately, the method does not work well with maps. A slightly modified version appears to achieve very good results with maps, yet fails for ODEs. With this method, one updates the leading component in the embedded space so that the trajectory is mapped to $[x(t+\Delta t), x(t+\Delta t+\tau), \ldots, y(t+\Delta t+m\tau)]$. This has the effect that after several filter steps the trajectory is completely different from that of the original signal. With both methods the global properties of the system – fractal dimension and largest Lyapunov exponent – are recovered to a close approximation.

More sophisticated methods[58,63] to achieve self consistency use a window of $p$ points and find the best fit trajectory using a least squares method. In practice they achieve results no better than the above method and require significantly more computation time. I'll stick with the simpler method.

An alternative filtering method developed by Sauer[60] makes use of singular value decomposition and local lowpass digital filtering. A window of $w$ points on the trajectory is lowpass filtered by zeroing all but the $n/2$ lowest components of the FFT. The inverse FFT returns a vector $x$ in $\Re^n$. Neighborhoods are constructed in this space and SVD is applied to the vectors in each local group. The vectors are projected onto the right singular vectors corresponding to the largest eigenvalues. The process is then reversed to extract a filtered version of the original trajectory of $w$ points. The method is somewhat

complicated to implement, and as such, Dr. Sauer agreed to try to process time series records from the MST. At the time of this dissertation, however, he had not managed to carry this out.

Figure 4.10 shows the signal resulting from nonlinear filtering on the same noisy signal used in testing the linear filters. Results are clearly better, especially with respect to recovering the original power spectrum. Qualitatively, at least, nonlinear filtering appears to do a better job of noise reduction.

Crucial, however, is that regardless of appearance, the dynamics of the original system must be preserved. In order to test this the correlation dimension was computed for all four filtering methods. Results are plotted in figure 4.11. The poorest method is principal component analysis, which may not be surprising, since the filtered signal looked the "least clean". Further, singular value decomposition is a linear method, with all its inherent drawbacks. The two other linear filtering methods, elliptic and Bessel, show nearly identical results. There is some tendency to saturate to a plateau at large radii, which quickly disappears at small scales; linear filtering methods cannot recover the small scale

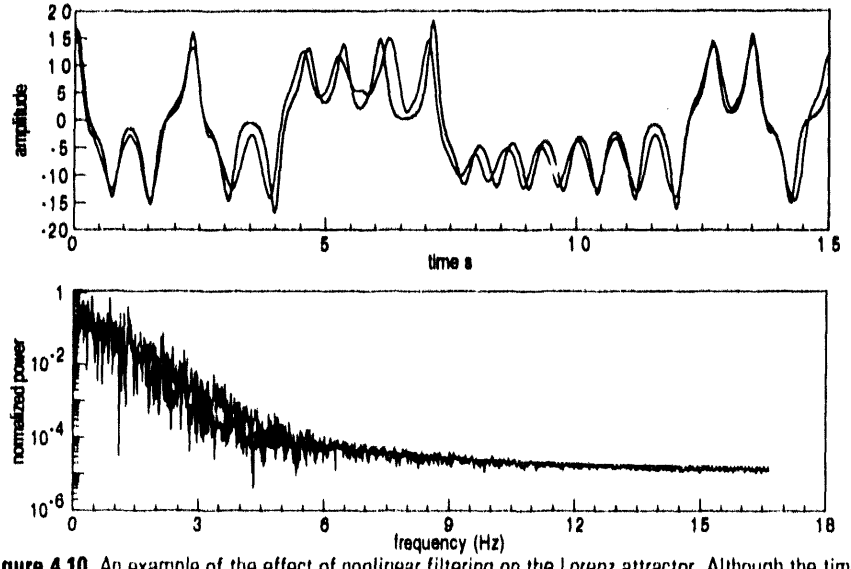


**Figure 4.10.** An example of the effect of nonlinear filtering on the Lorenz attractor. Although the time series looks comparable to that obtained with linear filtering, the power spectrum much more closely matches the original.

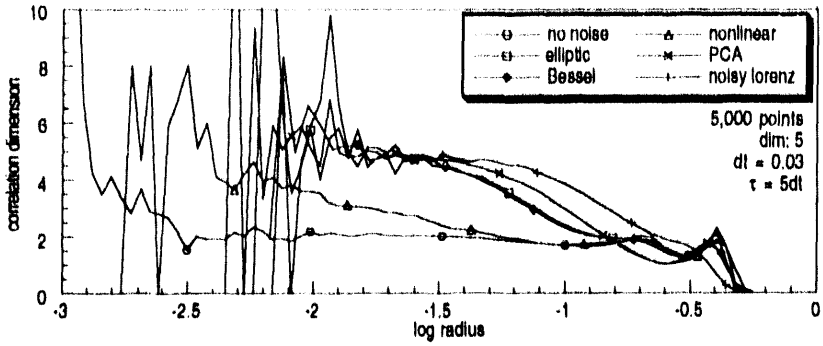


**Figure 4.11.** Correlation dimension for noisy Lorenz data after processing with various filtering methods. None of the linear methods, elliptic, Bessel, or PCA are able to recover the nonlinear dynamics of the original system. The nonlinear method yields a credible plateau of at least one decade.

microstructure of nonlinear systems. The result is curious in that Bessel filters better preserve the critical phase information of the original (noisy) signal. One might have naively thought it would produce better results than the elliptic filter, which is not the case. The nonlinear method clearly does best, yielding a credible plateau over at least one decade and a slow rise at small radii where the small scale structure could not be completely recovered.

As an additional test, the prediction error was checked for all four methods. This is plotted in figure 4.12. No method even remotely recaptures the short term predictability of the original signal. The nonlinear method does show evidence of limited short term predictability, though this quickly vanishes after 3 time steps. The other three methods have the prediction behavior of the original noisy system.

### 4.3. Correlated Noise

As mentioned several times, correlated noise, and in particular noise which has been lowpass filtered can give indications of low dimensional chaos or simple determinism where none is present. Colored noise can be generated by integrating Gaussian white noise. Lowpass filtering is a similar, but distinctly different process. Because the pole in a lowpass filter is located off-axis in the complex plane it distorts the phase information in the signal. (Integration doesn't require complex algebra.)

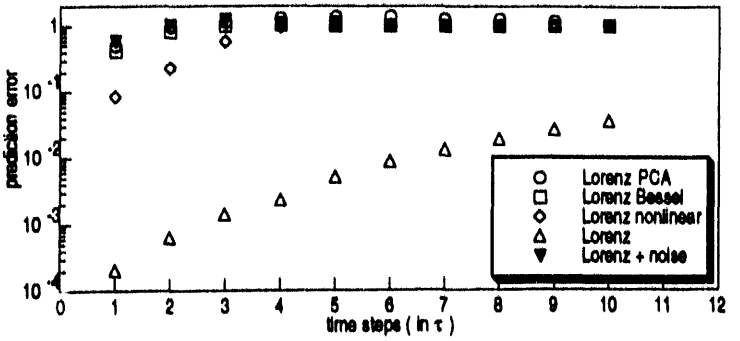


**Figure 4.12.** The prediction error for the various filtered signals. Only the nonlinear method shows any predictability different from correlated noise.

To illustrate this effect, figure 4.13 presents the correlation dimension of Gaussian white noise, lowpass filtered with a two pole Butterworth filter. The filter knee was at 10 kHz for a random process "digitized" at 500 kHz. As mentioned previously, Butterworth filters do not have a particularly steep transition region, especially with only 2 poles. There appears to be a short saturation region in all embeddings at a value of about 6. Without further investigation, one might wrongly conclude one was analyzing a chaotic system. The obvious admonition is to be particularly suspicious of filtered data.

In chapter 6, I will present the analysis of experimental data from MST and argue that the signals are

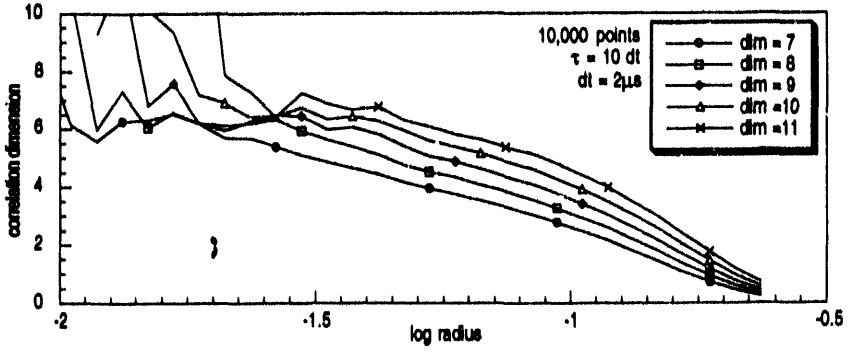


**Figure 4.13.** The correlation dimension of heavily filtered Gaussian white noise. There appears to be spurious saturation at a dimension near 6 in all embeddings.

more typical of correlated noise processes rather than deterministic systems. (This is not to say that there is no information in them!) I present an example here to which the MST data will be compared.

Figure 4.14 shows the time record and the power spectrum of filtered Gaussian white noise. The data were generated at 500kHz, and then filtered with an elliptic filter with a bandpass of 0-60kHz. This signal is contrived in this way because it very nearly reproduces the power spectrum of both $\dot{B}_{tw}$ and $\dot{I}_p$. The signal itself also strongly resembles these signals in its structure.

Figure 4.15 shows the translation error for the lowpass filtered noise signal along with that for Gaussian white noise. As mentioned in section 4.1, the translation error is a poor measure of simple determinism for high dimensional systems. As shown plotted here, without the benefit of a corresponding surrogate plot one might suspect there was some degree of simple determinism. As remarked above, for high dimensional signals, even surrogates cannot help in clearly distinguishing random from coherent processes. Because of this, for the remainder of this dissertation I will not use the translation error as a measure of simple determinism.

Table 4.1 in section 4.1 shows the Lyapunov exponents obtained from filtered Gaussian noise in an embedding dimension of 9. The Kaplan-Yorke dimension is approaching a constant value even though

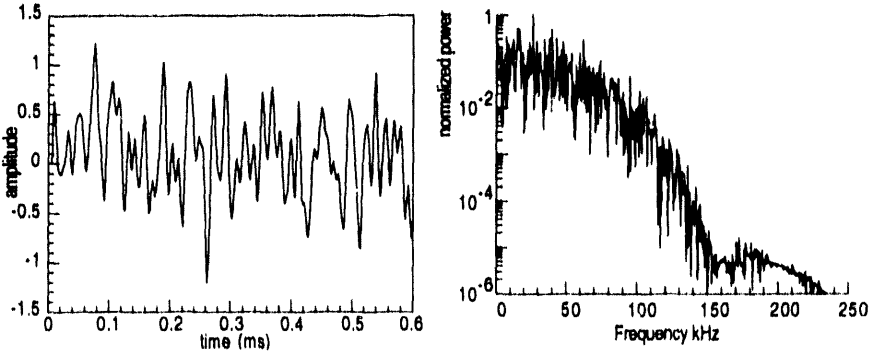


**Figure 4.14.** The signal from lowpass filtered noise shows a time behavior similar to the MST signals analyzed in chapter 6. The power spectrum has been contrived to closely match that of $\dot{B}_{tw}$ and $\dot{I}_p$.

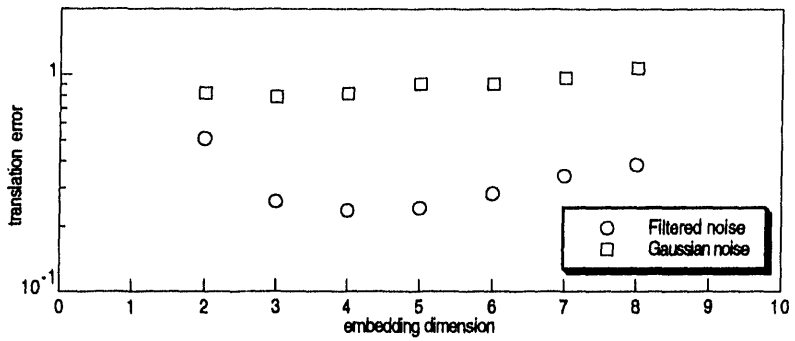


**Figure 4.15.** The translation error for filtered noise and Gaussian white noise. Correlations in the filtered noise lead to short term correlation in the system flow which gives an artificially low translation error. This is often indistinguishable from high dimensional chaotic systems. (see figure 3.10)

the system is random. Two things help to distinguish this system from a deterministic process. The spectrum is augmented by both positive and negative exponents as the embedding dimension increases, and no credible zero exponent is apparent, which would indicate the system is continuous in time.

Finally, I plot in figure 4.16 a comparison of the original filtered noise signal and the same signal after processing with one iteration of the nonlinear filtering algorithm. The purpose in this is to show that the

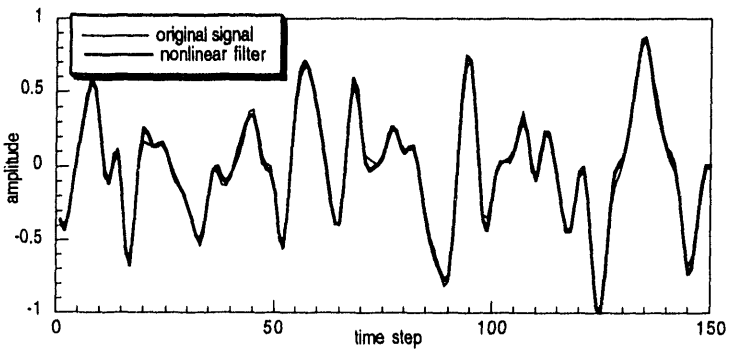


**Figure 4.16.** A comparison of lowpass filtered noise with the same signal after processing with the nonlinear filtering method. The signals are nearly identical, a phenomenon also seen in MST data.

two signals nearly overlay. This same phenomenon occurs when processing the MST signals, and seems unique to them. Neither white nor colored noise exhibits this behavior. It is exceedingly curious, since the filtering algorithm typically uses 40 nearest neighbors in a nine dimensional embedding space. A check reveals that neighbors are distributed throughout the time record, quelling the idea that this is an artifact resulting from correlations of points close in time.

This behavior seems to occur in systems with a non-zero correlation time when the "noise" time scale is comparable to the "system" time scale. The noise reduction method is most effective if the noise fluctuations are faster by about 3 to 4 times the fluctuations of the underlying dynamical system. Correlated noise *is* the dynamical system, and hence a "random noise" component cannot be filtered out.

### 4.4. Stationarity

Another problem, similar in nature to noise is the issue of stationarity. The filtering methods outlined above are effective only for additive noise: noise corruption that occurs independently of the dynamical system. The issue of stationarity is one of internal noise to the system. During the evolution of the dynamical system some of the control parameters may change. This can be minimized with a proper experimental situation. However parameter drift can never be completely eliminated.

There is little work in the literature dealing with the problem of stationarity and internal system noise. My own studies with the Lorenz attractor have shown that even relatively slow perturbations of modest amplitude can increase the fractal dimension of the attractor by as much as 1 or even destroy completely any evidence of chaos.[42] Figure 4.17 illustrates the problem. Depicted on the left is the Hénon attractor generated by eq. (2.4). To the parameter $a$ was added a random fluctuation with an amplitude of $\pm 0.1$. One can see in comparing figure 4.17 with 2.6 that the trajectory now has a "fuzzy" quality. The right plot shows the effect of this perturbation on the correlation dimension. The long plateau has been destroyed, leaving a scaling region of at most half a decade. Nonlinear noise reduction cannot correct this problem because the noise is inherent in the system, not external. From

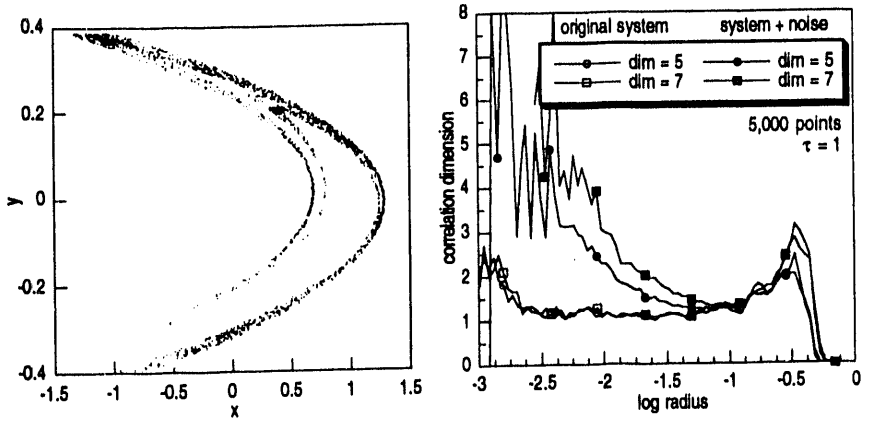


**Figure 4.17.** The Hénon attractor after perturbing the parameter $a$ with a small random component. The attractor is now "fuzzy", while the correlation dimension shows a very poor scaling region.

the data, one might guess that the system is low dimensional, but the evidence is not convincing.

For parameter fluctuations which are deterministic in nature, for example parameters which drift as functions of time, the problem is not as severe. Even with the non-stationary parameters the system is still deterministic, with a dimension increase of one for each additional dynamical variable added to the original system. A parameter that fluctuates as a function of the existing system variables and time would increase system dimension by at most two: one dimension corresponding to the parameter itself and one to time. Unfortunately, there is not much that can be done to correct this non-stationarity, since one is basically asking to eliminate one (or several) of the system variables. The real problem is that the number of points now required to reliably estimate the dimension increases a factor of 2.5 for each fluctuating quantity (using the Tsonis criteria $N_{min} \propto 10^{2+0.4D}$ ). For a system with a modest dimension (greater than 5) where several of the quantities are perturbed the requirement on the number of points needed quickly becomes unrealistic.

This issue is particularly relevant to studies of phenomena such as pulsed discharge plasmas in the MST. Even if a low dimensional attractor does govern the system, does the system ever achieve a

stationary regime during the discharge?

### 4.5. Summary

As demonstrated, noise corruption can pose a considerable problem when trying to identify low dimensional chaos and simple determinism in a system. Standard linear filtering techniques are inappropriate for most applications because 1) chaotic signals are typically broadband and 2) linear filters distort the phase information crucial to the small scale correlations. Nonlinear noise reduction techniques do show some success in reconstructing the original dynamics with modest noise levels (<100%). However some information is irrevocably lost resulting in a shortened plateau for the correlation dimension and poorer short term predictability. Another consequence of linear filtering is that in certain circumstances it can give indications of low dimensional chaos where none exits.

The issue of system stationarity poses an essentially insurmountable problem. If one or several of the ostensibly constant system parameters fluctuate or drift during the experiment the dimension of the system can increase dramatically. Although the system remains chaotic, this dimension increase may mean an impractical number of points is needed to identify the chaos and simple determinism.

## 5. Numerical Simulations of Plasmas

In this chapter I present analysis results for data from two numerical simulations of plasma processes. The first data set is from a code that models global RFP dynamics. The second model is for drift wave turbulence, a process thought to be responsible for transport in the core of tokamaks. Both models show strong evidence of low dimensional chaos and simple determinism.

### 5.1. DEBS Code

The DEBS code is a 3 dimensional magnetohydrodynamic (MHD) numerical simulation, which with proper initialization will model reversed field pinch (RFP) discharges.[65,66,67,68] The model has helped considerably in understanding long wavelength oscillations in RFP plasmas, specifically in understanding tearing mode fluctuations. As mentioned in the introduction, bispectral analysis of tearing mode fluctuations from both the code and experiment reveal a nonlinear coupling process from the $m$ =1 to $m$ =2 modes. This corroboration lends credibility to the code's ability to model real plasma processes.

Although the simulation correctly models these phenomenon, there are some limitations. The model is pressureless, and thus does not include pressure driven modes. In addition, in order to have a reasonable computation time, the model uses a rather small value for the magnetic Reynolds number, or Lundquist number $S = \tau_r / \tau_A$ . $\tau_r$ is the resistive diffusion time, given by $\tau_r = 4\pi a^2/c^2\eta$ , where $a$ is the scale size of the system and $\eta$ is the plasma resistivity. $\tau_A$ is the Alfvén time and is equal to $a$ divided by the Alfvén speed $v_A = B_0/\sqrt{4\pi\rho_0}$ where $\rho_0$ is the density. The Lundquist number measure the ratio of the time it takes the magnetic field to diffuse resistively outward to the time it takes a perturbation to travel along the field lines. Larger values of $S$ increase the computation time significantly because the system becomes more turbulent and requires a smaller time step size to accurately follow the wave dynamics. In the simulation presented here, the Lundquist number was set

to $S \approx 6\text{x}10^3$. This is particularly small, since $S$ for the experiment is measured to be of the order of $10^6$. Despite this low value, the simulation required over 60 hours of computation time over the space of 1 1/2 years on a CRAY-II computer in order to accumulate a time record of sufficient length for the analysis. When this project was begun it was hoped to try several values of $S$ in order to investigate scaling laws of dimension versus Lundquist number. This has proved impractical.

5.1.1. The Model

The code solves a reduced set of the MHD equations via the semi-implicit method. This allows for the use of relatively long time steps to track the nonlinear phenomena of interest by modifying the evolution of the destabilizing fast time-scale Alfvén modes. Details of the method can be found in the references. The dimensionless equations solved are:

$$\frac{\partial A}{\partial t} = SV \times B - \eta J$$
$$\rho \frac{\partial V}{\partial t} = -S\rho V \cdot \nabla V + SJ \times B + \nu \nabla^2 V \qquad (5.1)$$

The magnetic field $B$ is measured in units of the characteristic field strength $B_0$. $V$ is the fluid velocity in units of the Alfvén speed. $A$ is the vector potential and $J$ is the current density. $\rho$ is the mass density measured in units of $\rho_0$. Finally, $\nu$ is the viscosity coefficient $\nu = \nu_0 \tau_r / a^2$, where $\nu_0$ is the characteristic viscosity. Both the viscosity and the mass density are assumed to be spatially constant; furthermore, the mass density is not evolved. The equations are solved in cylindrical geometry which is periodic in the $z$ direction.

The equations were solved for 9 toroidal and 3 poloidal modes with 127 radial mesh points. The system was monitored at regular intervals during which nine quantities were recorded. These were the parallel electric field $E_{\|}$, the average electric field $E_{ave} = -S\langle V \text{x} B \rangle$, and the ohmic electric field $E_R = \eta J$ at both the edge and the core, and the average toroidal and poloidal magnetic fluctuations, $dB_t/dt$ and $dB_p/dt$, and toroidal loop voltage $V_{loop}$. Because of the long autocorrelation times of the signals the 160,000 plus data points were reduced to about 20,000 for each signal. The records span about 1.65

resistive diffusion times. Direct comparison with MST discharges is not possible because of the compressed time scales used in the code. However, by comparing tearing mode time scales, one arrives at a duration corresponding to about 55 ms for a standard MST discharge.

### 5.1.2. Analysis

The top plot in figure 5.1 shows the time history of average poloidal magnetic field fluctuations. Time is measure in units of the resistive diffusion time $\tau_r$. The trace may be compared with figure 6.2 which shows a plot of the raw magnetic fluctuation data from MST. Figure 5.1 shows evidence of flux jumps – bursts of magnetic field energy – which are also characteristic of MST discharges. Beneath is shown the power spectrum. The signal is broadband, indicating that it is not periodic. The falloff is similar to both the Lorenz and Mackey-Glass systems, although the shape of the power spectrum is not an indicator of low dimensional chaos.

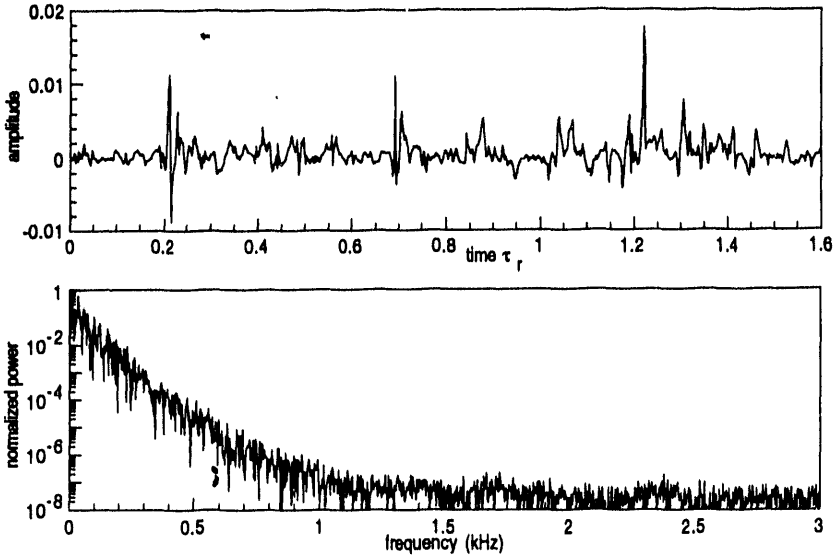


**Figure 5.1.** The top plot is the time trace for the fluctuations of the average poloidal magnetic field. It is in many respects similar to data from the MST experiment. The lower trace shows the corresponding power spectrum.

A phase-delay plot is depicted in figure 5.2. It is not very informative, indicating only that any dimension is likely greater than 2. The neighboring Poincaré section, obtained by embedding the system in 3 dimensions and inserting a plane at $x(t+6)=0$, suggests that the reduced system is nearly linear. That would imply the original system is nearly 2-dimensional. However, this effect may be due to lack of points rather than low dimensionality. Only 182 "punctures" were obtained from the data record.

The correlation dimension for several of the signals analyzed is presented in figure 5.3. Most signals, including $\dot{B}_p$, $E_{\|}$, and $E_R$ showed long saturation regions (at least a decade) at a dimension between three and four. $E_R$ and $E_{ave}$ showed identical behavior. The top two plots compare the correlation dimension for $\dot{B}_p$ and its phase randomized surrogate. The original signal shows a long clear plateau region. The surrogate shows a short region of spurious low dimension which is similar to the behavior seen in correlated noise. One can conclude that these signals show good evidence of low dimensional chaos. The bottom left figure shows the correlation dimension for $V_{loop}$. No clear saturation region is evident. This is probably to be expected. The simulation constrains the current to remain within a predetermined narrow range. In order to achieve this, the loop voltage is adjusted as the current drifts

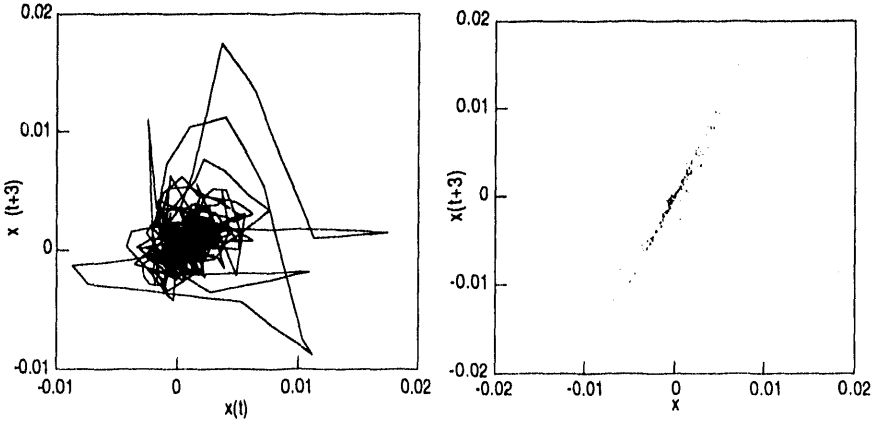


**Figure 5.2.** The phase delay plot and Poincaré section from $dB_p/dt$. The Poincaré section suggests that the reduced system is nearly linear.

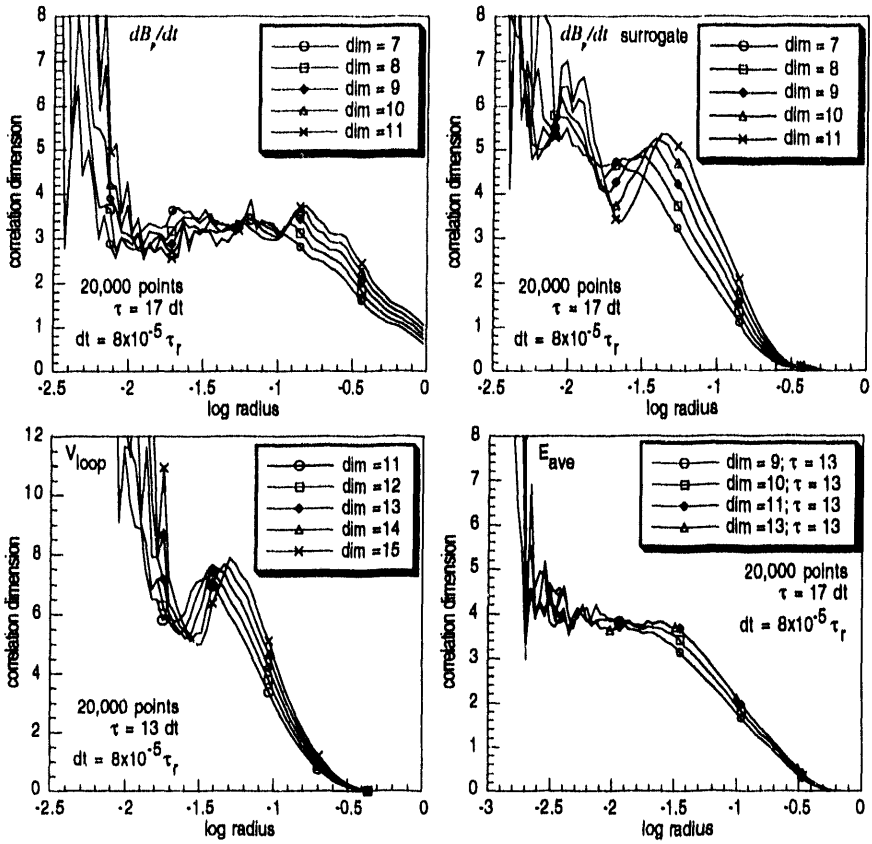


**Figure 5.3.** Correlation dimension for several signals from the DEBS code simulation. The top two plots compare the $\dot{B}_p$ signal with its phase randomized surrogate. The original shows a clear scaling region not present in the surrogate. The plot for $V_{loop}$ shows no saturation, which is expected. $E_{ave}$ also shows a good scaling region.

outside these limits. The correction is essentially an occasional kick, evident in the loop voltage signal, which shows rapid oscillations over a narrow range.

The prediction error for several of the signals is plotted in figure 5.4. The left plot shows the prediction error for $\dot{B}_p$, $E_R$ and their surrogates. Both signals show fair predictability, better by a factor of three than their corresponding phase randomized surrogate. However, an embedding greater than 18 was

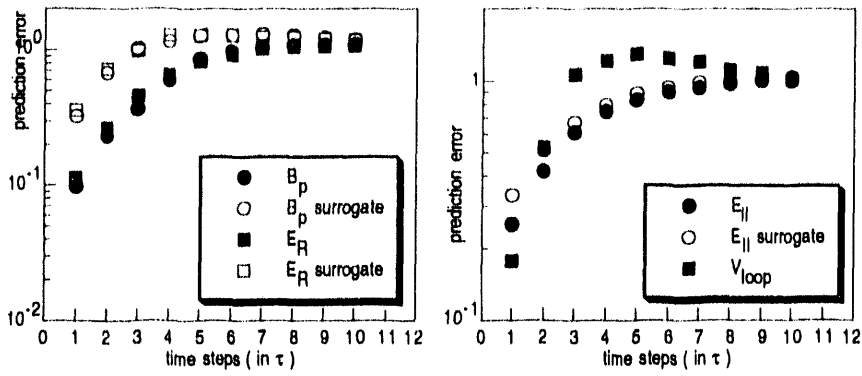


**Figure 5.4.** The left plot show reasonably good predictability for both $\dot{B}_p$ and $E_R$, better by a factor of three than their surrogates. The right plot shows that neither $E_{||}$ nor $V_{loop}$ shows any predictability.

required before any evidence of short term predictability was seen. The behavior is odd considering that the dimension of the system is no greater than 5, requiring an embedding of at most 11 to reconstruct the attractor faithfully . This may be attributable to the small number of points available to reconstruct the attractor. As seen in the right plot, $E_{||}$ shows very poor predictability; the surrogate and original signal are nearly identical. Again, this may be attributable to the small number of points. $V_{loop}$, as expected, also has poor predictability.

Table 5.1 shows the Lyapunov exponents calculated for two of the representative quantities. In both cases, the Kaplan-Yorke dimension asymptotes to a constant value, and the Lyapunov exponents remain relatively stable as embedding dimension increases. Both systems show a clear zero exponent value with a small magnitude and large standard deviation. All continuous systems must have at least one exponent equal to 0.

### 5.1.3. Summary

The simulation of an RFP discharge shows strong evidence for low dimensional chaos and simple determinism in nearly all signals. There are some anomalies, notably, the poor predictability of $E_{||}$,

| system | $\tau$ | $D_{KY}$ | Lyapunov exponents | | |
|---|---|---|---|---|---|
| $B_p$ | 0.96 | 5.31 | 0.3738 ± 3.3% | 0.1247 ± 7.3% | 0.0129 ± 76.8% |
| | | | -0.0535±21.0% | -0.2184 ± 8.1% | -0.7796 ± 4.4% |
| | 0.88 | 5.85 | 0.3638 ± 2.9% | 0.1341 ± 6.3% | 0.0113 ± 74.8% |
| | | | -0.0535 ± 17.8% | -0.1520 ± 7.1% | -0.3555 ± 4.1% |
| | | | -0.9002 ± 3.2% | | |
| $E_{ave}$ | 0.96 | 6.30 | 0.3569 ± 3.1% | 0.1537 ± 6.0% | 0.0262 ±31.6% |
| | | | -0.0033 ± 99.9% | -0.0760 ± 14.9% | -0.2296 ± 6.2% |
| | | | -0.7577 ± 3.5% | | |
| | 0.80 | 6.82 | 0.3680 ± 2.8% | 0.1951 ± 4.4% | 0.0404 ±18.7% |
| | | | -0.0091±89.8% | -0.0840 ±11.2% | -0.1988 ± 5.5% |
| | | | -0.3791 ± 3.8% | -0.9597± 3.0% | |

**Table 5.1.** The Lyapunov exponents for two of the quantities analyzed from DEBS code. Both show consistent exponent values at higher embeddings, a small "zero" exponent and saturation of the Kaplan-Yorke dimension.

which may be reconcilable with more data. By and large, however, the results indicate that low dimensional chaos might be expected in RFP discharges. There are several caveats, however. One is that the code simulation used a very small value for the Lundquist number and only a few modes were included. In addition, high frequency oscillations are not present in the code in order to model the more pertinent long wavelength oscillations in a reasonable time. Finally, the addition of a finite pressure could change these results considerably.

## 5.2. Dissipative Trapped Electron Mode Model (DTEM)

A topic of intense research in the fusion plasma community is the issue of anomalous particle and energy transport. In tokamaks, one mechanism possibly responsible for this transport is the long wavelength drift wave turbulence associated with dissipative trapped ion and electron modes. The existence of these modes is indicated by several experiments,[69,70,71] although their link to confinement is still speculative.

The specific model is probably not directly applicable to RFP physics, in part because the oscillations

are electrostatic. The magnetic topology in an RFP is too complicated to ignore magnetic effects. However, the basic structure of the model provides an instructive archetype for long wavelength turbulence in general. In particular, one of the nonlinearities, the polarization drift nonlinearity, has a direct correspondence to one of the MHD nonlinearities. Thus, although the model differs in the details, some of the global properties: saturation, spectral distribution of energy and transport, should be similar to those seen in RFP physics.

5.2.1. The Model

The DTEM model possesses two nonlinearities that govern its behavior. These are the $E\times B$ nonlinearity and the polarization drift nonlinearity. The interplay of these two nonlinearities was explored by Newman, who showed that the model has several spectral ranges where each of the nonlinearities and their cross terms dominate the dynamics.[72] The model equation is given by

$$\frac{\partial \tilde{n}}{\partial t} + v^* \frac{\partial \tilde{n}}{\partial y} + \gamma \tilde{n} + D\frac{\partial^2 \tilde{n}}{\partial y^2} - DL\nabla \frac{\partial \tilde{n}}{\partial y} \times z \cdot \nabla \tilde{n} + \rho c_s \nabla \tilde{n} \times z \cdot \nabla \rho^2 \nabla^2 \tilde{n} + \mu \nabla^4 \tilde{n} = 0, \tag{5.2}$$

where $\tilde{n}$ is the fluctuating ion density, $v^*$ is the diamagnetic drift wave velocity $(cT_e/eB)/L$, $L$ is a density gradient scale length, $\gamma$ is a long wavelength collisional damping coefficient, $\rho$ is the ion gyroradius evaluated at the electron temperature and $c_s$ is the ion sound speed. $D$ is a negative diffusivity describing the destabilization of DTEM modes with $D = \varepsilon^{3/2} v^{*2} (1+\frac{3}{2}\eta)/\gamma_e$ where $\gamma_e$ is the electron collisional damping coefficient and $\eta = d\ln T/d\ln n$ is the electron temperature gradient parameter. Finally, $\mu$ is the coefficient of hyper-viscosity introduced to model strong damping at high wavenumber $k$. The important nonlinear terms are the 5$^{th}$ term which is the $E\times B$ nonlinearity and 6th term, the polarization drift nonlinearity.

The code is purely spectral, meaning all computations are done in Fourier space. The system is initialized with a mode spectrum symmetric about the origin and allowed to evolve until transient behavior has vanished. The magnetic field is oriented along the $z$ axis and the density gradient is in the $x$ direction. In the jargon of the code, a 13x13 case contains the modes 0 though ±6 in both the $x$ and $y$

directions. For the work presented here the system was driven with a linear driving term (the 4th term) at long wavelengths and damped at short wavelengths. The intermediate wavelength range of no damping or driving is known as the inertial range. Nondriven/nondamped systems were examined and appear also to be chaotic, however I will concentrate here on the more physical model. Several cases were examined, including 13x13, 21x21 and 29x29. Most of the analysis results are presented for the 21x21 case, however the results are generally applicable. The 13x13 case has a very short inertial range (2 modes), and hence is a poor example, while obtaining sufficient points for proper analysis of the 29x29 case proved difficult. Reference will be made at appropriate points to results from other systems. The data records analyzed included the fluctuating energy from each of the modes in the inertial and damped regimes and the total fluctuating energy and enstrophy (mean squared vorticity). The results, which are presented below, indicate low dimensional chaos and simple determinism in most cases examined with a dimension dependent on the regime examined.

A similar model used to study $\eta_i$ turbulence has been investigated for low dimensional chaos by Persson and Nordman.[10] In contrast to the model investigated here, the $\eta_i$ model contains only one nonlinear term, the $E\times B$ nonlinearity. They examined individual mode energies in a system of 64x64 modes and found the dimension of the system to be high in the weak turbulence regime where the linear terms dominate and low, with a dimension less than 3, for the strong turbulence where the nonlinear terms dominate.

### 5.2.2. Analysis

In figure 5.5 is presented a typical time trace of a single mode energy of the 21x21 mode case; this one is the (0,8) mode. Here, the convention is $(y,x)$, in accordance with Newman. The mode is part of the damped regime. Below it is depicted the power spectrum. Although in no way indicative of chaos, it is interesting to note that the shape is very similar to that of both the Lorenz and Mackey-Glass systems.

The top two plots in figure 5.6 show the correlation dimension for the (0,8) mode and the correlation dimension for its phase randomized surrogate. There is a clear plateau region at a dimension between 8

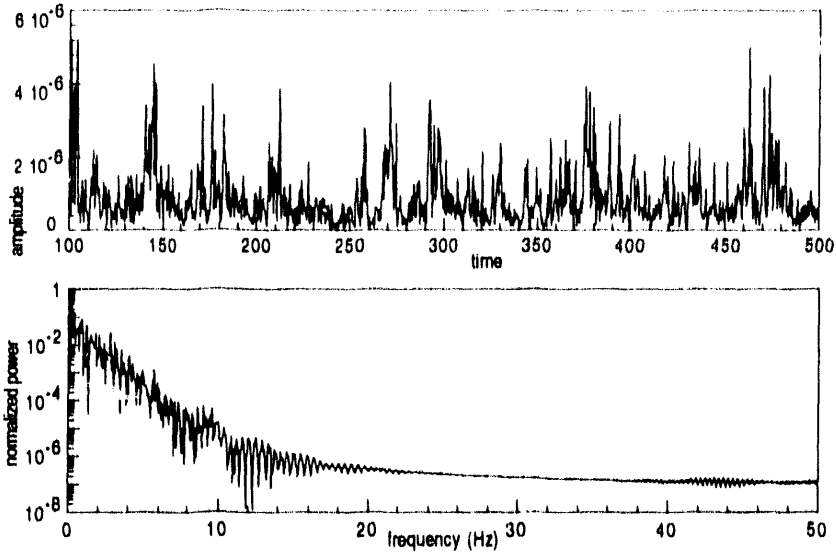


**Figure 5.5.** The energy of the (0,8) mode of a 21x21 mode system. This mode is in the damped regime. Beneath it is shown the power spectrum.

and 9 which is not evident in the surrogate plot. The low number of points available (40,000) accounts for the discrepancy between embeddings of 14 and 17, and the roll off to low dimension at small radii is for reasons similar to those discussed in connection with the Mackey-Glass system (see section 3.2). The divot seen in the surrogate plot near a dimension of 8 is typical of the spurious plateau seen with correlated noise as discussed in chapter 4 . The bottom two plots show the correlation dimension for the (0,6) mode, which is in the inertial range where no driving or damping is present, and the total energy. Both show a clear plateau region with a dimension around 6, while their surrogates (not shown) show a behavior similar to white noise.

Most signals examined from the DTEM system showed similar correlation dimension plots, with the inertial range having a dimension around 6 and the damped regime somewhat higher. This behavior is not unreasonable and is consistent with the results reported in [10]: the regime in which the linear terms dominate (damping, (0,8) mode) shows a higher dimension than does the nonlinear regime

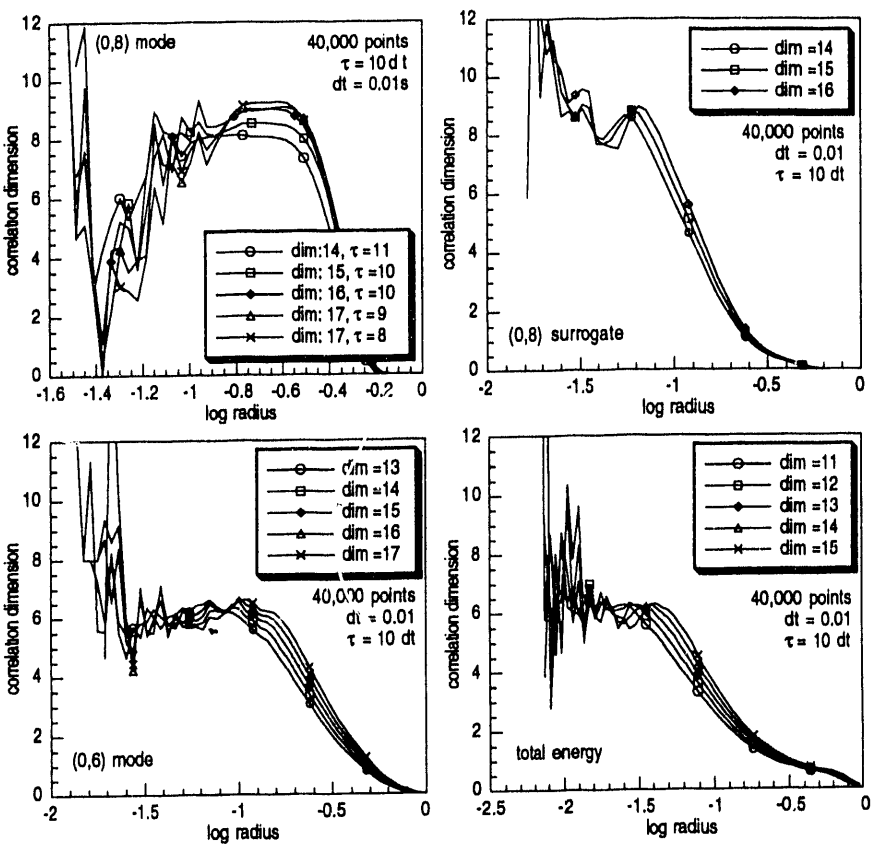


**Figure 5.6.** Plotted is the correlation dimension for several cases from the 21x21 mode spectrum. The top two plots compare the dimension of the (0,8) mode and its surrogate. There is a clear scaling region for the original signal at a dimension between 8 and 9. The dip in the surrogate is reminiscent of correlated noise as discussed in chapter 4. The lower two plots show the correlation dimension for the (0,6) mode and the total energy.

(inertial range, (0,6) mode). The results are also consistent with experimental results which indicate a dimension dependent on the wavenumber.[11] The different measured dimensions may be explainable on the basis of turbulence theory, however the explanation is still speculative. This will be discussed in more detail in the summary section at the end.

In the 13x13 case (not depicted) a saturation region was also apparent, though not as clearly defined. The dimension was somewhat lower, between 4 and 5. The poorer saturation may be due to the fact that the regimes are so close to each other that no stable transfer pattern is established. The 39x39 case showed some tendency to saturate at a dimension near 7, though many more points are needed before a reliable estimate can be made.

Figure 5.7 demonstrates the short term predictability of the signals. Plotted are the prediction error from the (0,6) mode, the (0,8) mode and the total energy and the error of their phase-randomized surrogates. One can see that the short term predictability of the (0,8) mode is especially good: at least an order of magnitude better than its surrogate. The predictability of the energy is also good, though not quite as dramatic as the (0,8) mode. The predictability of the (0,6) mode is poor, showing a high prediction error that is comparable to its surrogate's. The possible reasons for this will be discussed in the summary section at the end.

Table 5.2 shows the Lyapunov exponents for the (0,6) and (0,8) modes in several embedding dimensions. Both systems have positive exponents, indicating that the modes are chaotic. The (0,8) mode has a higher Kaplan-Yorke dimension before it saturates, as expected. The exponents are very

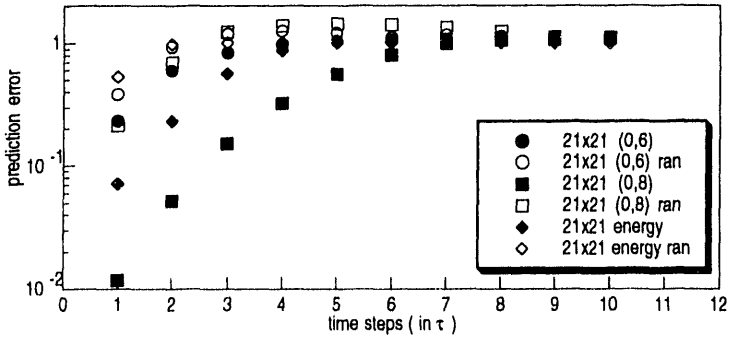


**Figure 5.7.** The prediction error for the (0,6), (0,8) modes and total energy of the 21x21 mode spectrum. Predictability is good for both the (0,8) mode and the total energy. It is poor for the (0,6) mode for reasons explained in the text.

| system | $\tau$ | $D_{KY}$ | Lyapunov exponents | | |
|---|---|---|---|---|---|
| mode (0,6) | 0.09 s | 8.10 | 1.7775 ± 2.4% | 1.0174 ± 3.1% | 0.5018 ± 5.5% |
| | | | 0.0950 ±27.4% | -0.0222 ±99.9% | -0.4130 ± 8.1% |
| | | | -0.9218 ± 4.3% | -1.6575 ± 3.4% | -3.8867 ± 2.8% |
| | 0.08 s | 8.55 | 1.7148 ± 2.2% | 0.9704 ± 3.1% | 0.4574 ± 5.7% |
| | | | 0.0757 ±31.0% | -0.0525 ±51.0% | -0.2167 ±13.4% |
| | | | -0.6746 ± 5.0% | -1.1945 ± 3.6% | -1.9802 ± 3.0% |
| | | | -4.4591 ± 2.6% | | |
| mode (0,8) | 0.05 s | 9.09 | 8.8462 ± 1.6% | 4.9430 ± 2.2% | 2.5281 ± 3.4% |
| | | | 1.1518 ± 7.3% | 0.0490 ±99.9% | -0.3610 ±27.6% |
| | | | -1.2486 ±10.0% | -3.9239 ± 7.3% | -9.2991 ± 5.5% |
| | | | -29.0221 ± 3.7% | | |
| | 0.04 s | 9.63 | 8.9888 ± 1.3% | 5.7238 ± 1.8% | 3.3122 ± 2.7% |
| | | | 1.3845 ± 6.3% | 0.1431 ±68.2% | -0.4498 ±26.3% |
| | | | -1.9071 ± 7.1% | -3.7892 ± 4.3% | -6.5160 ± 3.0% |
| | | | -10.8685 ± 2.3% | -23.4345 ± 1.7% | |

**Table 5.2.** The Lyapunov exponents for two modes of the DTEM model in several embedding dimensions.

stable from one embedding to the next, remaining at approximately the same value. This is a good indication that the values are probably very nearly correct. In addition, any system continuous in time must have at least one exponent equal to zero. Both show at least one and possibly two zero values with small magnitude and large standard deviation.

5.2.3. Summary

Analysis of the data from the DTEM model shows strong indications of low dimensional chaos and simple determinism. The individual mode energies and the total energy show a clear plateau region with a dimension dependent on which mode one examines. All signals show evidence of short term predictability, though the quality is mode dependent. Finally, the Lyapunov exponents yield a Kaplan-Yorke dimension which corroborates the results obtained from the correlation dimension.

Initially, one should expect a single system to have a single dimension characterizing its topological

structure. Although this should in no way be taken as fact, I can offer some speculation as to why the different modes show different dimensions and predictability. The DTEM model has two very different regimes which govern the dynamics of the system. The inertial range, modes 3 through 7 in the 21x21 case, contains no linear damping. The only dissipation is through the nonlinear coupling process to the other modes. The damping regime contains a large dominant linear damping term. In many ways the dynamics of the damping regime are independent of the inertial range; the reverse, however, is not true. One can make a loose analogy to an amplifier with a high input impedance: the input signal should be unaware of the amplifier's existence. Thus, it may not be unreasonable that the two regimes have different dimensions when examining the large scale structure. At very small scales this difference should disappear, reflecting the fact that it is coupled system. However, the number of points required and computational constraints restrict the ability to explore this limit of infinitesimal hypersphere radii. In any case, the difference in dimension is very small, about 2, in comparison to the number of equations used to describe the system: 441.

The difference in predictability may be explainable as follows. The inertial range is a much more turbulent regime, and in addition it is very nearly Hamiltonian. The only damping is from the nonlinear interaction with the other modes. Thus, the trajectory is not strongly drawn to the attractor. Through the interaction with the other modes it experiences a perturbation from the inertial manifold of the attractor, and cannot quickly converge back that manifold. The (0,8) mode is in the damped regime which is far less turbulent and thus more stable. This dissipation insures that the trajectory remains close to the inertial manifold, thus accounting for its superior predictability.

The Lyapunov exponents tend to corroborate this explanation. If one ignores probable zero values, those with large standard deviations, the least negative exponent (the one with smallest absolute magnitude) is larger for the (0,8) mode (-1.249) than for the (0,6) (-0.413). This value controls the collapse of the trajectory onto the inertial manifold (the topological region containing the attractor) of the attractor. This larger value for the (0,8) mode would imply a faster convergence to the attractor and hence better

predictability.

I must emphasize that these explanations are largely speculative. More work in this area is planned with the intention of trying to explain these phenomena. Clearly, however, the system is low dimensional, and one might therefore expect real plasma system to also show evidence of low dimensional chaos.

# 6. Experimental Data from the Madison Symmetric Torus

## 6.1. The Data

In order to ascertain whether simple determinism governs discharges of the Madison Symmetric Torus (MST) a wide range of signals was analyzed comprising both global and local measurements. Global signals included fluctuations in the average toroidal magnetic field at the wall, $dB_{tw}/dt$, fluctuations in the plasma current, $dI_p/dt$, chord averaged density fluctuations, both optical and soft x-ray radiation, and toroidal and poloidal gap voltages, $V_{tg}$ and $V_{pg}$. Local signals included local poloidal and toroidal magnetic field fluctuations, ion saturation current, $J_{sat}$, and plasma potential fluctuations. All the data analyzed cannot be presented here without severely compromising the reader's attention span. Rather, I will concentrate on a representative sample drawing from both groups.

As mentioned in the introduction, none of the analysis techniques applied yielded any evidence of simple determinism. On the contrary, circumstantial evidence would suggest that the signals analyzed are similar to lowpass filtered white noise. Results for the analysis will be presented in the same format as in the last chapter, and at the appropriate points I will remark about the similarities of the data to noise.

Comprising the global set of signals to be presented are fluctuations in the toroidal magnetic field at the wall and fluctuations in the plasma current. Because of the large voltage spikes in both gap voltages the digitizer resolution is poor, and the signals cannot be analyzed properly. The data for $dB_{tw}/dt$ were obtained from a set of four Rogowski coils around the feed legs for the poloidal current. The signal was first hardware filtered with a 6 pole Butterworth lowpass filter with a cutoff frequency at 157 kHz. The filtering proved unnecessary, since the natural bandwidth of the signal is well below this level. The signal was then attenuated by a factor of 3 and sampled at 500 kHz over the duration of the discharge. $dI_p/dt$ is obtained using a Rogowski coil located inside the torus. The signal was filtered and digitized in the same way as $dB_{tw}/dt$, however no attenuation was necessary. In view of

the effects of linear filtering presented in section 4.2.2, it should be noted that several signals which were *not* filtered have been analyzed yielding similar results.

The group of local measurements consists of the ion saturation current obtained from a Langmuir probe and the local fluctuating poloidal and toroidal magnetic field components obtained from the set of dense array coils. The dense array is a set of small, closely-packed magnetic pickup coils located at the wall designed to measure short, high frequency fluctuations and magnetic field correlations. The coil signals are amplified by a factor of 2 to 5 and then digitized at 250 kHz. One coil in each of the toroidal and poloidal field directions was used.

Table 6.1 summarizes the relevant parameters of the signals presented here. Notice that all signals with the exception of $J_{sat}$ have extremely short autocorrelation times. If this were due purely to the dynamics of the system, identification of the quantities characterizing the chaotic dynamics would be very difficult. As discussed in chapter 3, a reasonably large $\tau$ is necessary to properly estimate the correlation dimension, Lyapunov exponents, etc. Noting this, several of the quantities were remeasured using double the digitization rate to extend the autocorrelation time. There was no difference in the analysis results. The number of points available for analysis, by the Tsonis rule $N_{min} \propto 10^{2+0.4D}$, would mean it is possible to measure reliably a maximum dimension of 6 or so for $\dot{B}_{tw}$ and $\dot{I}_p$, 5 for the magnetics and 4 for $J_{sat}$.

The data for $dB_{tw}/dt$, $dI_p/dt$, and $J_{sat}$, were all taken on 22 September 1992. The flat-topping network was in operation for the data taken on this day, and peak plasma current was typically about

| Signal | $dt$ | Points during flat-top | Autocorrelation ($dt$ steps) | Date and Shot |
|---|---|---|---|---|
| $\dot{B}_{tw}$ | $2\times10^{-6}$ | 20,000 | 2 | 22 Sep 92, #41 |
| $\dot{I}_p$ | $2\times10^{-6}$ | 20,000 | 2 | 22 Sep 92, #41 |
| $J_{sat}$ | $1\times10^{-5}$ | 4,000 | 35-40 | 22 Sep 92, #41 |
| $\dot{B}_p$ | $4\times10^{-6}$ | 7,500 | 2-3 | 2 Jun 93, #124 |
| $\dot{B}_t$ | $4\times10^{-6}$ | 7,500 | 1 | 2 Jun 93, #124 |

**Table 6.1.** Summary of relevant parameters for the MST signals examined for simple determinism.

290 kA. I will concentrate on a particular shot, #41, although several others were analyzed with similar results. The magnetic fields during the discharge are depicted in figure 6.1 along with the chord averaged electron density from the FIR interferometer. There is a significant flat-top period extending from about 17 to 57 ms. The data were all analyzed during this period since it seems likely that if the plasma is to achieve "equilibrium", it would be during this period. Data from both startup and rampdown periods have also been analyzed with similar results. The data for the magnetic field fluctuations were taken on 2 June 1993. Again, flat-topping was operational, this time with peak plasma current around 400 kA. The flat-top period was somewhat shorter, owing to the higher currents, and extended from approximately 10 to 40 ms.

## 6.2. Analysis

The raw signals are plotted in figure 6.2. Digitization means all signal amplitudes are measured in volts.

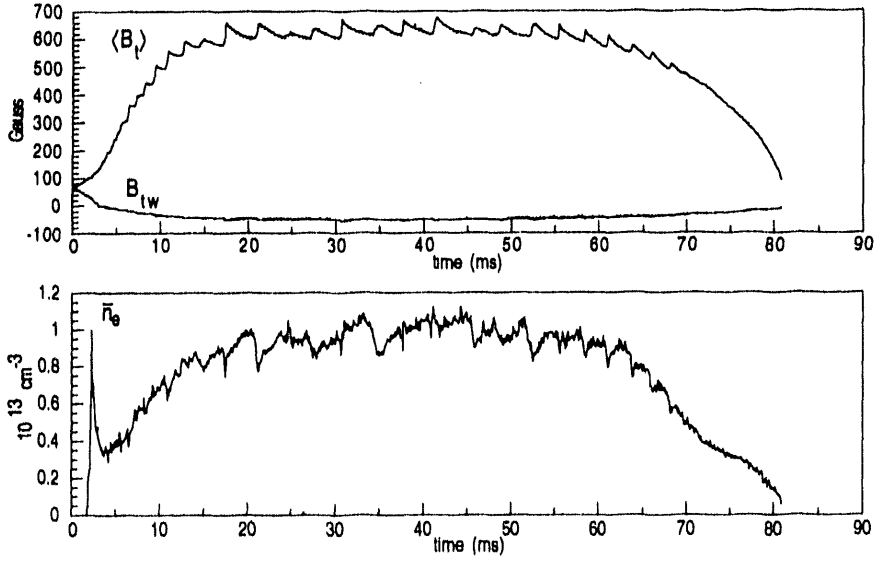


**Figure 6.1.** MST discharge #41, 22 September 1992. The top plot shows the average toroidal magnetic field and the toroidal field at the wall. The lower trace shows the chord averaged electron density. The data presented here were analyzed during the flat-top period from about 17-57 ms.

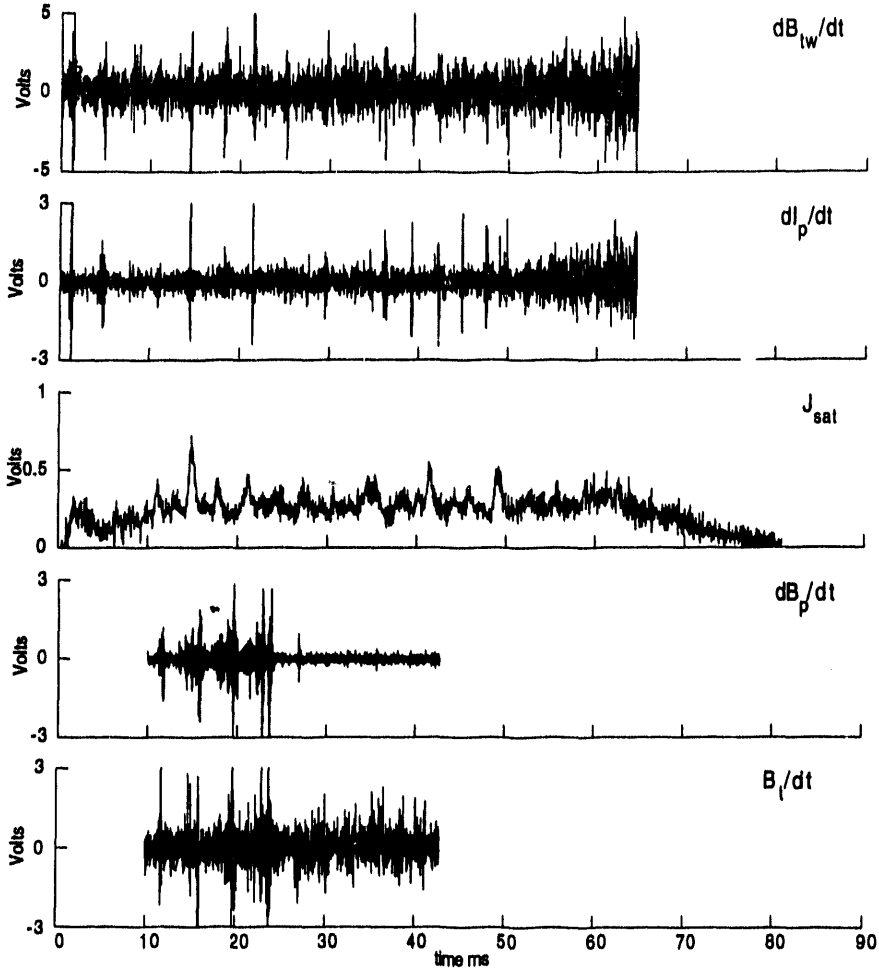


**Figure 6.2.** The raw signals from the MST to be analyzed in this chapter. The data represent both global and local quantities.

Evident in all signals are the flux jumps, bursts of magnetic field energy, characteristic of the MST discharges. Otherwise, except for in $J_{sat}$ , there is no other structure apparent in the signal. A detail of $dB_{rw}/dt$ is shown in figure 6.3 around the time of a flux jump. Although in no way indicative of the

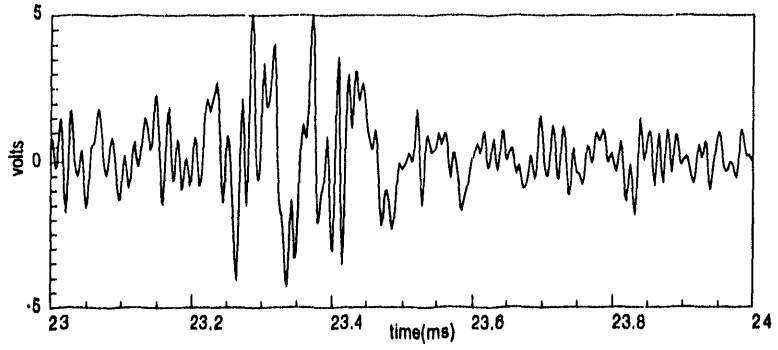


**Figure 6.3.** Detail of the $dB_{tw}/dt$ showing the structure during a flux jump. There is some qualitative structural similarity to lowpass filtered noise depicted in figure 4.3

lack or presence of simple determinism, the signal should be compared with figure 4.3, which shows a time trace of lowpass filtered Gaussian white noise. The two are qualitatively very similar in structure.

Figure 6.4 shows the power spectra of each of the signals over the flat-top region. The $B_t$ spectrum, not shown, is similar to $B_p$. All signals are clearly broad spectrum, which probably accounts for the short autocorrelation times. The power spectra are not at all similar to either the known chaotic systems or the numerical systems presented in the last chapter. Power spectra are not, however, in any way indicative of low dimensional chaos. One *can* conclude that the signals are not periodic, and thus at least candidates for chaos. By design, the power spectra for $dB_{tw}/dt$ and $dI_p/dt$ are qualitatively similar to that of lowpass filtered noise depicted in figure 4.14. Notice that the spectra for both $\dot{B}_{tw}$ and $\dot{I}_p$ fall off significantly before the hardware filter roll off frequency of 157 kHz.

The phase delay plots, shown in figure 6.5, show no apparent simple structure. The plot for $dB_{tw}/dt$ is a 3.4 ms window (1700 points) with a lag of 3 time steps. The $J_{sat}$ plot covers 10 ms and 1,000 points. Essentially, they appear as a ball of wool with occasional excursions into hyperspace during flux jumps. Again, phase portraits are typically only useful for dimensions less than 2.

Figure 6.6 presents the correlation dimension plots for all signals. There is no saturation with increasing

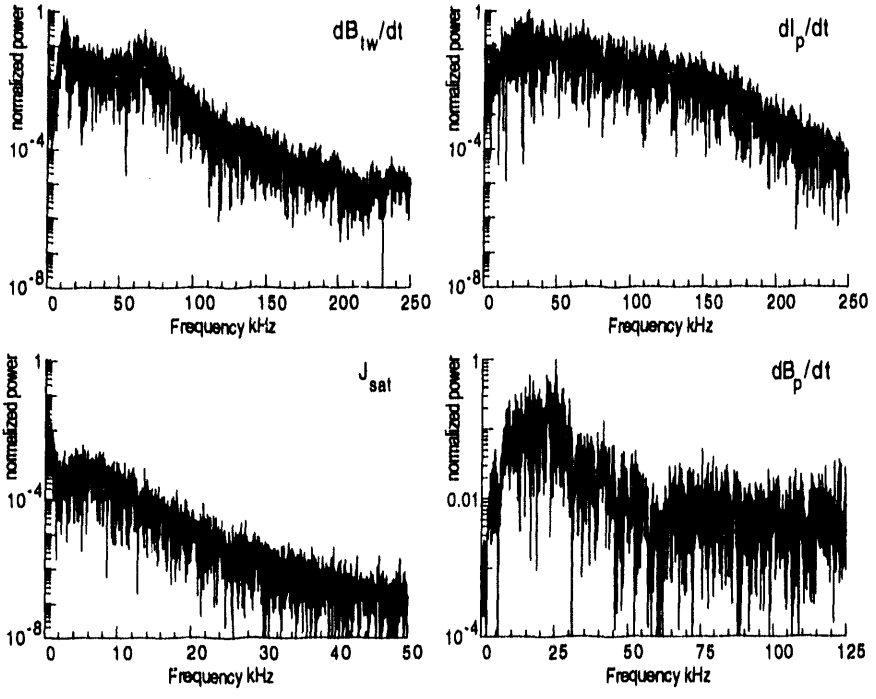


**Figure 6.4.** The power spectra for the MST signals.

embedding for any signal. These plots exhibit no evidence for low dimensional chaos or simple determinism in the raw signals from MST. All plots are typical of noise systems. There appears to be a hint of saturation in the $J_{sat}$ plot for an embedding of 9 at a dimension near 8. It disappears, however, in higher embeddings. The behavior is more typical of correlated noise, as discussed in section 4.3, rather than any real indication of low dimensional chaos. In addition, the number of points available would not allow for a credible determination of a dimension this high. Figure 6.7 shows a comparison of the correlation dimension of $\dot{B}_{tw}$ and its phase randomized surrogate. The two sets of curves are indistinguishable, confirming that $\dot{B}_{tw}$ is not a low dimensional chaotic process.

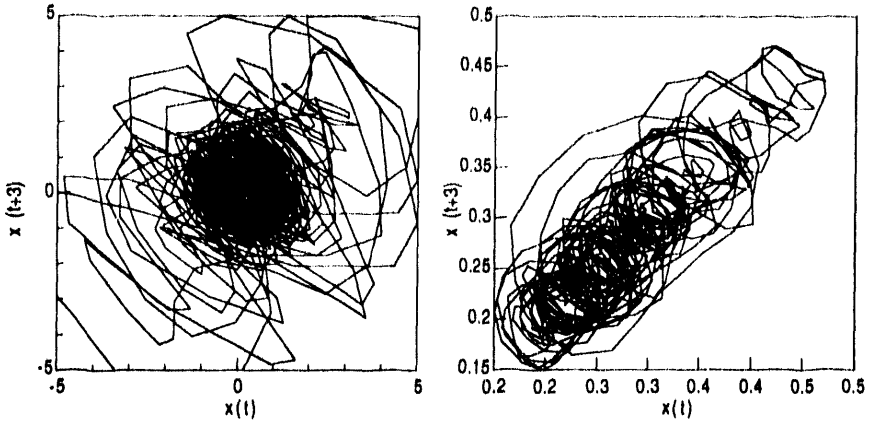


**Figure 6.5.** Phase delay plots for $\dot{B}_{tw}$ on the left and $J_{sat}$ on the right. For $\dot{B}_{tw}$ 1700 points are plotted covering 3.4 ms; for $J_{sat}$ there are 1000 points covering 10 ms. Phase delay plots for the other signals are just as illuminating.

Figure 6.8 shows the translation error of the MST signals along with their phase randomized surrogates. Recall that the translation error measures the coherence of flow in simple deterministic systems. The left plot shows the global signals $\dot{B}_{tw}$ and $\dot{I}_p$. Given only the data from the original signals, one might be persuaded that some degree of predictability and flow coherency exists. The values in several embeddings could (marginally) be considered small. However, the surrogate data shows an almost exactly similar trend, indicating that the presumed coherence is spurious. These small values are likely due to the choice of $\tau = 1$ for time lags. Even though the signal loses correlation on this time scale, this choice of $\tau$ means that neighbors are very likely to be on the same trajectory. Hence their flow is in a similar direction. This emphasizes the need to sample data frequently enough to have an autocorrelation time of several time steps. However, data sampled at a higher frequency, 1 MHz, allowing the use of a larger $\tau$ (21), did not yield significantly different results. As discussed in chapter 3, the translation error is a poor indication of simple determinism for even modestly high (>4 or 5) dimensional systems. It is presented here only in the interest of completeness.

The neighboring figure shows the local signals $J_{sat}$, $\dot{B}_p$, and $\dot{B}_t$. The same conclusions as above

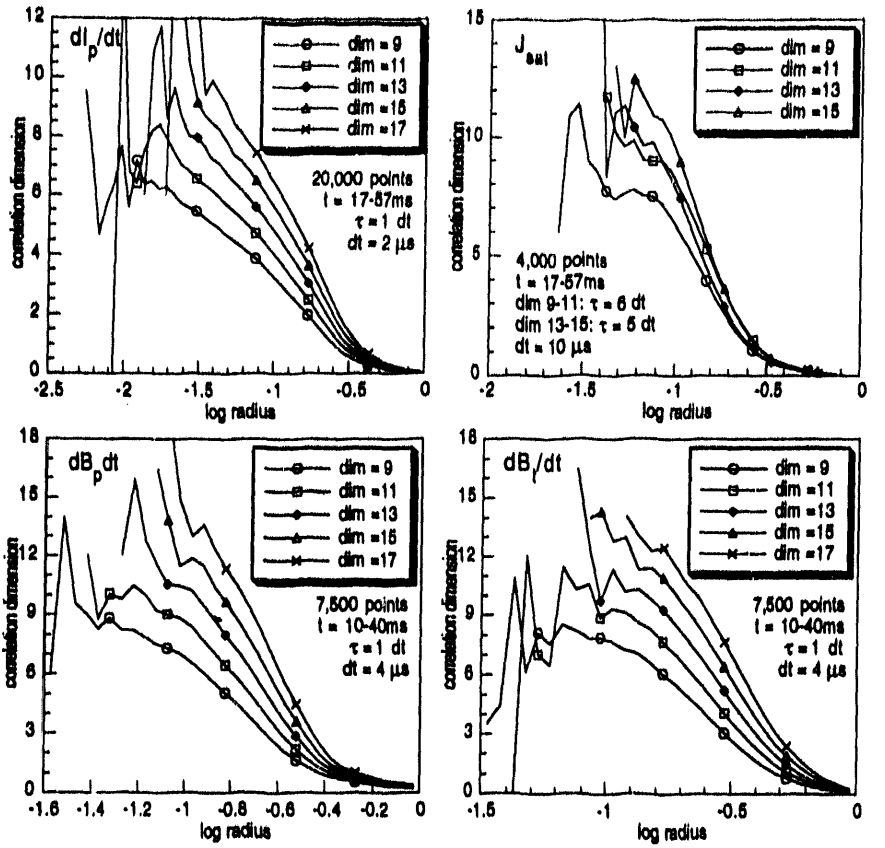


**Figure 6.6.** The correlation dimension of the MST signals. None show any evidence of saturating to a constant value which would indicate low dimensional chaos.

apply. Notice that since $J_{sat}$ has a relatively long autocorrelation time due to the fact that the signal is not differentiated, the proper choice of $\tau$ yields very large values for the translation error.

Figure 6.9 depicts the prediction error for the MST signals. The prediction error measures short term predictability, should be small for a simple deterministic system. In a nutshell, none of the signals are even remotely predictable in the short term. The steep rise from a modestly high value (20 – 30%) to saturation at 100% within 2-3 time steps is typical of correlated noise systems. As mentioned

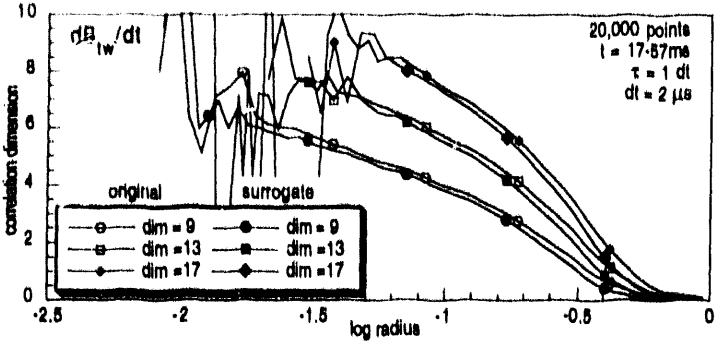


**Figure 6.7.** Comparison of the correlation dimension of $\dot{B}_{tw}$ with its surrogate data set. Both show very similar behavior, indicating that $\dot{B}_{tw}$ is not governed by a low dimensional chaotic process.

previously, the initial short term predictability is an artifact of the short term correlations seen when measuring time steps in units of $\tau$.

Table 6.2 presents the calculated Lyapunov exponents for the data. With each increase in embedding, the Kaplan-York (KY) dimension increases significantly, although it does not fill the embedding space.

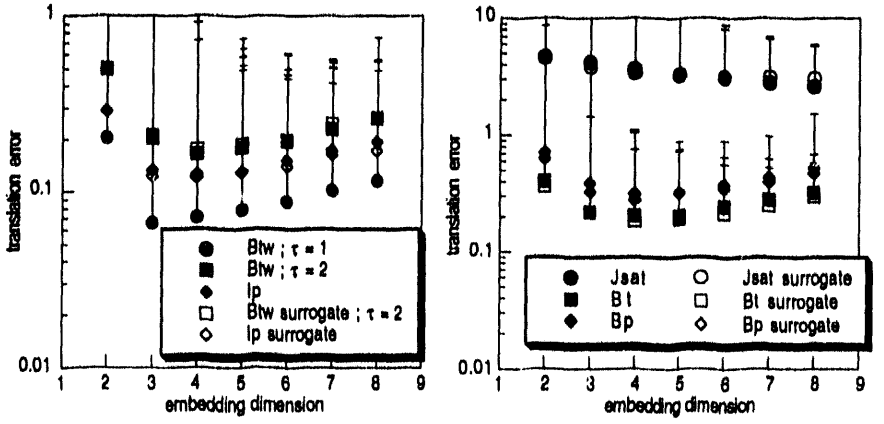


**Figure 6.8.** The translation error of global signals and their surrogates is plotted in the left figure. The same plot for local measurements is shown on the right. Neither shows any evidence of simple determinism.

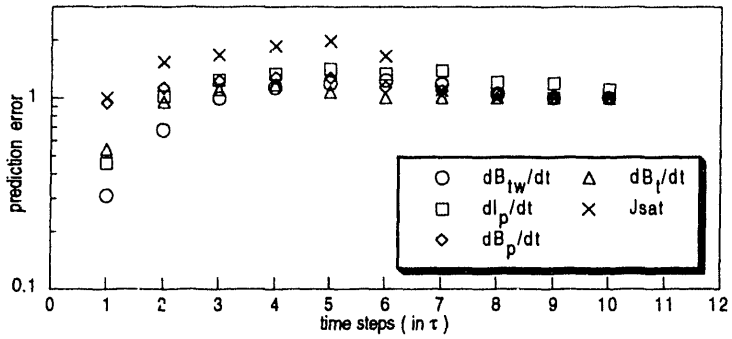


**Figure 6.9.** The prediction error for MST signals. The low values in some of the signals for the first step is due to spurious correlations due to measuring time steps in units of $\tau$.

Recall from section 4.3 that this behavior is typical of lowpass filtered noise. In contrast, several of the systems, $J_{sat}$, $\dot{B}_p$ and $\dot{B}_t$ show credible zero exponents values, which would indicate the processes are continuous in time. $\dot{B}_{tw}$ and $\dot{I}_p$ do not show a zero exponent. Because the KY dimension never stabilizes, the Lyapunov negative exponents cannot be considered to reflect any real value, despite the fact that some of the larger values appear relatively stationary. The positive values may be correct, and reflect the space filling property of the high dimensional or stochastic system.

In addition to time series analysis, MST discharges were analyzed spatially using the set of magnetic pickup coils distributed around the torus. Rather than using time-delay embedding to reconstruct the phase space, vectors were created by using signals from separate coils as individual vector components. The purpose was to address the issue of stationarity by analyzing data from a very short time period, and yet have a sufficient number of vectors for adequate analysis. The data were taken on 8 October 1992, and digitized at 500 kHz. Figure 6.10 show the correlation dimension obtained when using 2000 spatial vectors over a duration of 4ms of the discharge. The number of coils used corresponds to the embedding dimension. The results are consistent with the time series analysis: No evidence for simple determinism was seen in MST discharges.

| system | $\tau$ | $D_{KY}$ | Lyapunov exponents | | |
|---|---|---|---|---|---|
| $B_{rw}$ | 2 $\mu$ s | 4.02 | 0.1570 ± 0.7% | 0.0691 ± 1.7% | -0.0342 ± 5.2% |
| | | | -0.1790 ± 1.6% | -0.5480 ± 0.9% | |
| | | 6.15 | 0.1186 ± 0.7% | 0.0701 ± 1.2% | 0.0288 ± 3.2% |
| | | | -0.0162 ± 7.6% | -0.0569 ± 2.9% | -0.1134 ± 2.0% |
| | | | -0.2057 ± 1.4% | -0.4776 ± 0.9% | |
| $I_p$ | 2 $\mu$ s | 4.11 | 0.1589 ± 0.7% | 0.0670 ± 1.8% | -0.0205 ± 7.8% |
| | | | -0.1472 ± 1.8% | -0.5068 ± 0.9% | |
| | | 6.24 | 0.1227 ± 0.7% | 0.0726 ± 1.1% | 0.0296 ± 3.0% |
| | | | 0.0093 ± 12.2% | -0.0536 ± 3.0% | -0.1100 ± 2.1% |
| | | | -0.2157 ± 1.4% | -0.4987 ± 0.9% | |
| $J_{sat}$ $\lambda/10$ | 10 $\mu$ s | 4.09 | 0.0432 ± 4.8% | 0.0159 ± 13.0% | -0.0081±29.1% |
| | | | -0.0411 ± 7.9% | -0.1047 ± 5.6% | |
| | | 5.07 | 0.0509 ± 4.5% | 0.0232 ± 7.6% | 0.0019 ± 100% |
| | | | -0.0181 ±13.3% | -0.0481 ± 7.2% | -0.1427 ± 5.1% |
| $B_p$ | 4 $\mu$ s | 4.04 | 0.0670 ± 1.4% | 0.0257 ± 3.5% | -0.0149 ± 7.1% |
| | | | -0.0636 ± 2.3% | -0.1731 ± 1.6% | |
| | | 6.66 | 0.0567 ± 1.5% | 0.0342 ± 2.0% | 0.0147 ± 4.3% |
| | | | -0.0009 ± 72.9% | -0.0174 ± 4.5% | -0.0399 ± 2.5% |
| | | | -0.0723 ± 2.0% | -0.1751 ± 1.6% | |
| $B_t$ | 4 $\mu$ s | 4.19 | 0.0698 ± 1.5% | 0.0317 ± 2.9% | -0.0102±10.5% |
| | | | -0.0599 ± 2.6% | -0.1645 ± 1.7% | |
| | | 6.77 | 0.0581 ± 1.5% | 0.0350 ± 2.0% | 0.0169 ± 3.8% |
| | | | 0.0005 ± 100% | -0.0173 ± 4.5% | -0.0377 ± 2.5% |
| | | | -0.0718 ± 1.9% | -0.1708 ± 1.6% | |

**Table 6.2.** Lyapunov exponents for the MST signals, measured in $\mu$ s$^{-1}$. The Kaplan-Yorke dimension shows no indication of saturation in any embedding.

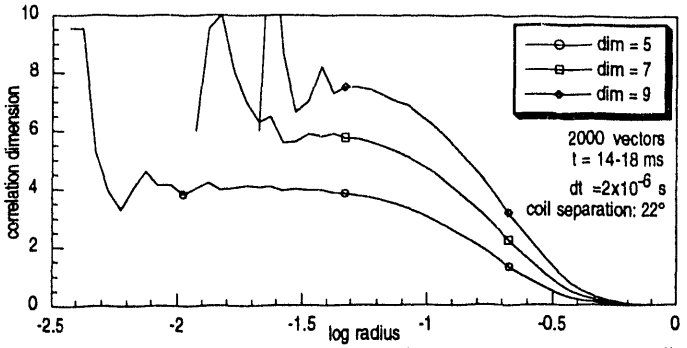


**Figure 6.10.** The correlation dimension derived by creating vectors from magnetic coils distributed around the MST vacuum vessel. It too shows no evidence of chaos.

## 6.3. Filtering

Although there is no evidence for simple determinism in the raw data, the possibility remains that the signals are noise corrupted. Thus, all signals were low pass filtered in order to extract any possible low frequency chaotic dynamics. Despite the admonitions against linear lowpass filtering presented in chapter 4, I first filtered with an 8-pole elliptical filter with the knee at 20kHz. The resulting phase delay plot for $\dot{B}_{tw}$ is shown in figure 6.11. The signal does appear to be cleaned up considerably, and the phase-delay portrait is quite a bit smoother then the comparable one in figure 6.5. However, as indicated in the right plot, there is still no evidence of low dimensional chaos. Plotted is the correlation dimension for the filtered signal and the phase randomized surrogate of the filtered signal. The two show nearly identical behavior, dispelling any hope that linear filtering may extract underlying chaotic dynamics. In chapter 4, however, I presented evidence that linear filtering often destroys rather than extracts simple determinism for a corrupted signal. The results obtained here are thus not too surprising.

The signals were next processed using principal component analysis (PCA) in hopes of recovering the relevant dynamics. As can be seen in figure 6.12, PCA has distinguished about four dominant dynamical components; there appears to he a break in the eigenvalue spectrum after the fourth component.

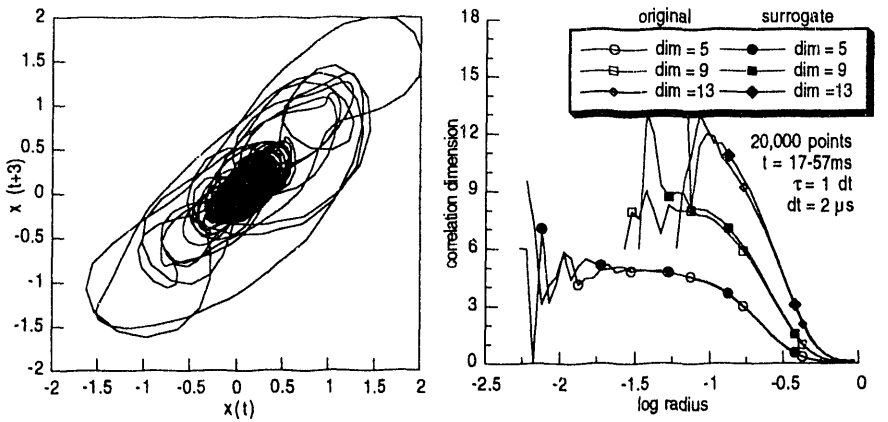


**Figure 6.11.** The left hand figure shows the resulting phase delay-plot when $\dot{B}_{hv}$ is filtered with a lowpass elliptical filter with the cutoff at 20kHz. It corresponds to the same time frame as in figure 6.5. Despite the more attractive "attractor" there is still no evidence for simple determinism, as seen in the right figure. The plot compares the correlation dimension for both the filtered signal and its phase randomized surrogate. The two are indistinguishable.

Plotted in the lower figure are the three largest eigenvectors multiplied by their respective eigenvalues. It appears that the original system can be separated into processes on different time scales. The dominant component has a much lower frequency than the other two. This would lead one to hope that there is some underlying low dimensional system, ca. 4–5, obscured by noise. PCA hopefully has relegated these noise components to the eigenvectors corresponding to the smallest eigenvalues, leaving the relevant dynamics to the largest few vectors.

Unfortunately, as shown in figure 6.13, this is not the case. Depicted is the correlation dimension for the largest eigenvector from the PCA of $\dot{B}_{hv}$. It shows no indication of saturation to a small correlation dimension value. The other two largest eigenvectors show similar behavior. In addition, I attempted a second processing of the largest eigenvector, hoping to achieve iterative "cleaning" of the signal. Results were similar to those from a single iteration.

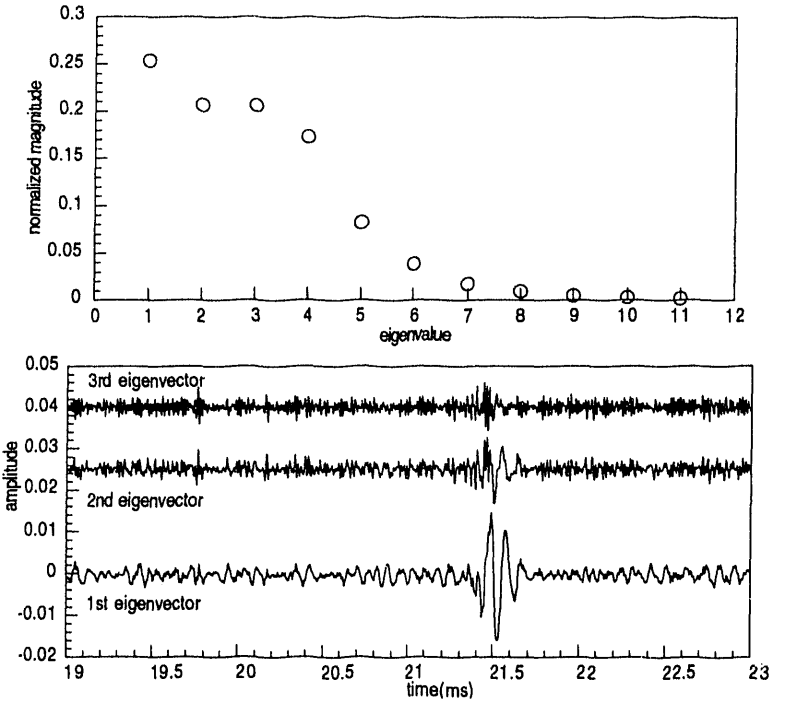


**Figure 6.12.** Principal component analysis of $\dot{B}_{tw}$. The upper plot shows the eigenvalue spectrum with what appears to be a break after 4th value. The three largest components are shown in the lower plot. The decomposition distinguishes a low frequency vector with the largest eigenvalue (amplitude) from several smaller high frequency components.

Nonlinear noise reduction, the process outlined in section 4.2.3, does not yield results different from the above. Plotted in the right of figure 6.14 is a detail from the $\dot{B}_{tw}$ time series compared with the same series after one iteration of the nonlinear filtering process. The signals are nearly identical. In section 4.3 I discussed this phenomenon in conjunction with lowpass filtered Gaussian white noise.

This behavior seems unique to the MST signals and the filtered noise signal. Possible reasons for this were discussed in that section. Although the evidence is purely circumstantial, it would indicate that MST signals are similar to filtered noise. The right plot of figure 6.14 show the result after six

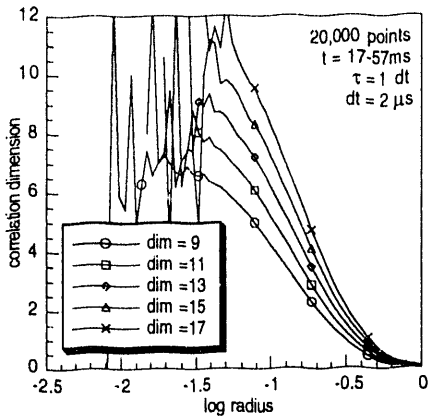


**Figure 6.13.** The correlation dimension for the principle component corresponding to the largest eigenvalue from the SVD of $\dot{B}_{tw}$. There is still no indication of chaotic dynamics.

iterations. Qualitatively, the two signals do not differ significantly from one another.

Figure 6.15 shows the correlation dimension for the MST signals after processing with the nonlinear

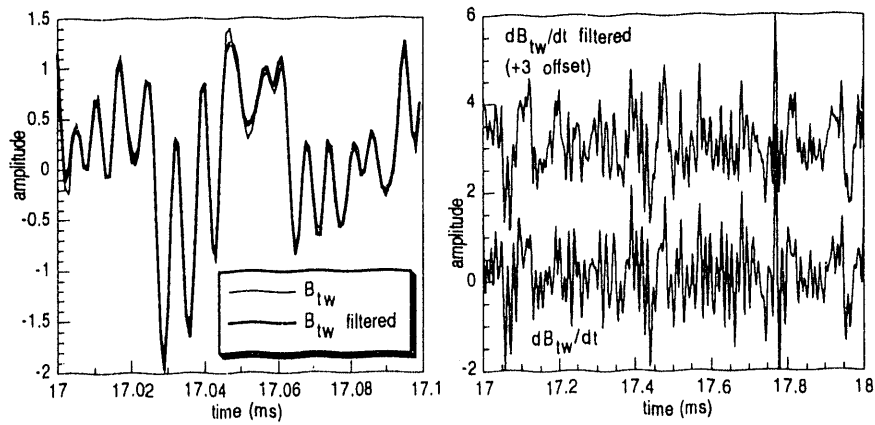


**Figure 6.14.** The effect of nonlinear filtering on $\dot{B}_{tw}$ is depicted. The left figure shows a detail after one iteration. It is nearly identical to the original signal. After six iterations, difference between the two are only superficial (right).

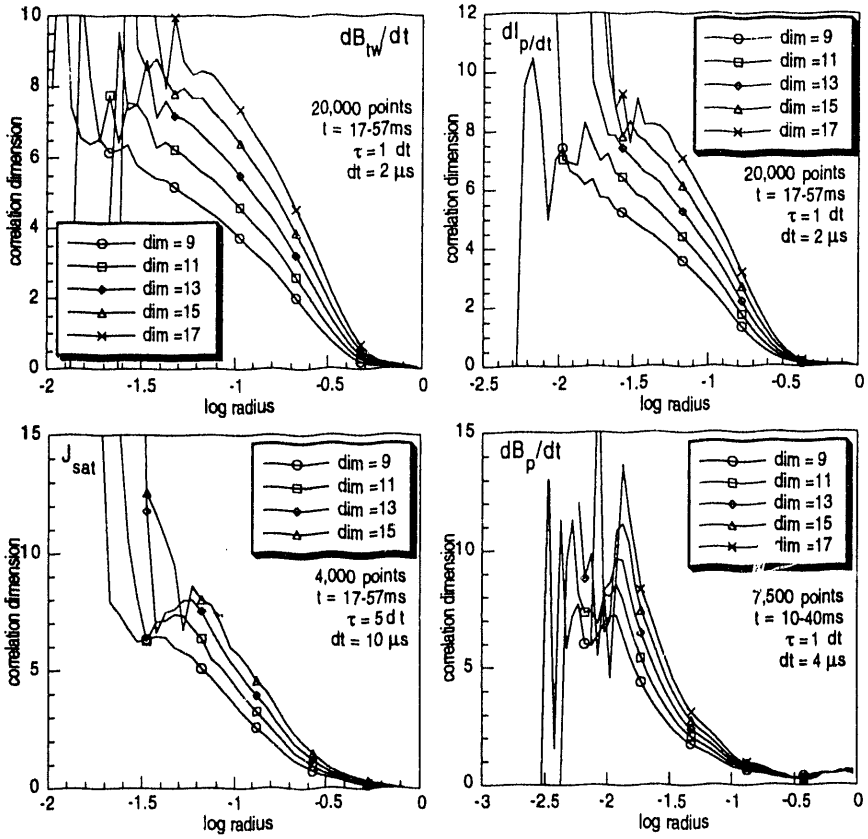


**Figure 6.15.** The correlation dimension for the MST signals after processing with the nonlinear noise reduction method. The are still no indications of low dimensional chaos.

filtering algorithm. $\dot{B}_t$, which shows similar behavior to $\dot{B}_p$, has been omitted. There is still no evidence of low dimensional chaos in any of the data.

The plot for $\dot{B}_p$ shows a curious behavior at large scales, with what looks like a plateau region of dimension less than one for $-1 < \log r \leq 0$. The origin of the behavior can be seen in figure 6.16. The nonlinear filtering has had a different effect on the local magnetic fluctuation signals ( $\dot{B}_t$ and $\dot{B}_p$ show

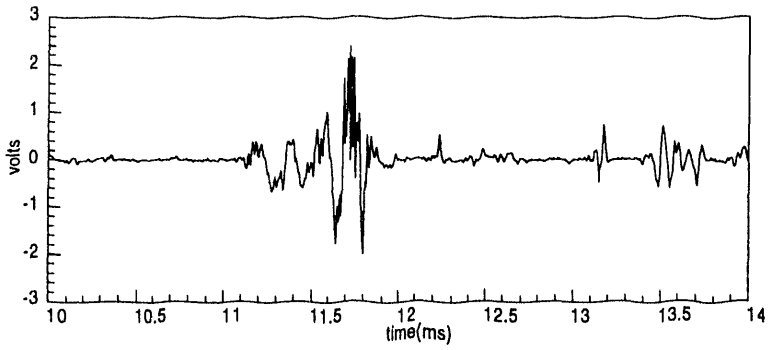


**Figure 6.16.** Shown is a detail from $\dot{B}_p$ after processing with the nonlinear filtering routine. All signal, save the bursts corresponding to flux jumps, has been nearly eliminated. This feature is responsible for the spurious $D_2 = 0$ region of the correlation dimension depicted in figure 6.15.

the same behavior) than on $\dot{B}_{tw}$. Essentially all signal has been eliminated except the bursts during flux jumps. The likely reason for this is the small amplitude of the signal between flux jumps. The signal level was less than 1/2 volt during this period, corresponding to less than 50 digitizer bits. Additionally, the sampling frequency of $\dot{B}_p$ was 1/2 that of $\dot{B}_{tw}$. This resulted in a shorter autocorrelation time, making the signal between flux jumps appear more like Gaussian noise. This "noise" was reduced by the noise reduction process, leaving only the large amplitude flux jump signal. Aside from the fact that the filtering has obviously severely distorted the signal, the plateau region can be discounted as indicating any real dimension on the basis that real systems must have a fractal dimension greater than two. The $J_{sat}$ signal also shows a hint of a plateau at a dimension near 7-8. This behavior is similar to that seen in correlated noise and is probably not indicative of chaos.

Prediction also indicates that no simple determinism is present. Figure 6.17 shows the prediction error for the MST signals after nonlinear noise reduction. They actually show poorer predictive behavior than before filtering was attempted.

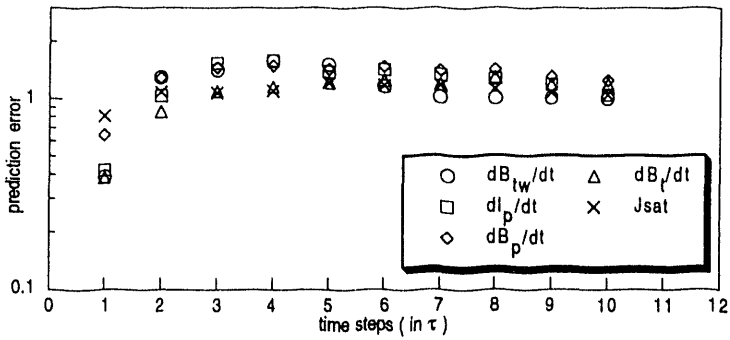


**Figure 6.17.** Prediction error for MST signals after processing with the nonlinear filter. Predictability has deteriorated in most signals relative to the unfiltered case (see figure 6.9).

## 6.4. Summary

Several quantities characterizing the discharges of the Madison Symmetric Torus (MST) have been analyzed for evidence of low dimensional chaos and simple determinism. These included global and local quantities: $\dot{B}_{tw}$, $\dot{I}_p$, $J_{sat}$, $\dot{B}_p$, and $\dot{B}_t$. Analysis of the raw signals shows no indications of low dimensional chaos from either the correlation dimension, Lyapunov exponents or short term predictability. The data were also filtered using a variety of linear and nonlinear filtering techniques. Nonetheless, evidence for simple determinism remained elusive. The analysis suggests, on the basis of circumstantial evidence (similarities in the signals' structure, power spectra, Lyapunov spectrum, translation error, the effect of nonlinear filtering) that the data more closely resemble lowpass filtered Gaussian white noise. The system is certainly high dimensional. Given the number of points available for analysis, one can place a lower bound of the fractal dimension of MST plasmas. Using the Tsonis criterion, $N_{min} \propto 10^{2+0.4D}$, at a minimum $D_2$ must be greater than 5.75. The ramifications of this result in light of the results of chapter 5 will be discussed in the final conclusions chapter.

# 7. Discussion and Conclusions

## 7.1. Summary

In this dissertation I have examined the possibility that low dimensional chaos and simple determinism govern the dynamics of fusion-caliber plasma discharges by looking at both numerical simulations and experimental data. Several previous studies have been done analyzing experimental or numerical data, but these have yielded conflicting results. The study presented here attempted to be more thorough by comparing experiment to simulation. In addition, since the time of most of these earlier studies several new analysis methods have been developed along with a better understanding of how to apply the existing techniques.

I examined data from two numerical simulations which model plasma processes. The first model, the DEBS code, is a numerical simulation of reversed field pinch discharges. Several quantities from the code were analyzed and found to show strong evidence of chaos. These were the toroidal and poloidal magnetic field fluctuations, the toroidal loop voltage and various manifestations of the global electric field. All signals, with the exception of loop voltage, showed evidence of low dimensional chaos with a long scaling region for the correlation dimension at a dimension of 3 to 4. This was corroborated by the spectrum of Lyapunov exponents which yielded a correspondingly low value for the Kaplan-Yorke dimension. The fact that the loop voltage showed no plateau region is not surprising since this quantity is advanced differently by the code than the others. Most signals also had good short term predictability, which is evidence of simple determinism. Notably, the parallel electric field did not.

Data from the DTEM model, which models long wavelength drift wave turbulence, were also examined. The energy of the individual modes was analyzed, and all modes showed a good correlation dimension scaling region with the dimension dependent on the mode. Dimensions ranged from 6 to 9. The total energy also showed evidence of a low correlation dimension. Predictability was good for all cases,

though better for modes in the linear regime than for those in the inertial range. As discussed in section 5.2.3, the different dimensions measured and the difference in predictability may be explainable. The measured Lyapunov exponents appear to corroborate these findings.

Several signals from the Madison Symmetric Torus were analyzed comprising both local and global quantities. Despite concerted effort, including the application of linear and nonlinear filtering techniques, no evidence of low dimensional chaos or simple determinism could be found. Moreover, circumstantial evidence suggests that the signals more closely resemble correlated noise rather than a deterministic process. This claim is on the basis of similarities in the signal's structure, the behavior of the Lyapunov exponents and short term predictability, and the action of the nonlinear noise reduction procedure on the signal.

## 7.2. Discussion

The fact that the experimental data from the MST show no evidence of simple determinism must be contrasted with the positive results of both the numerical simulations and previous results from other experiments. Addressing first the discrepancy between code and experiment, there are several likely origins. The DEBS code, although it seems to model some RFP processes well, makes several crucial simplifications. As mentioned earlier, the model includes no temperature or pressure effects. Although one cannot predict with certainty the effect of including a finite temperature, it seems reasonable to assume that including the additional quantities in the system of equations would result in an increase in the dimension of the system.

Another simplification is the small number of modes included in the system. The number of modes was 9 toroidal by 3 poloidal, a very limited subset. Results from the DTEM model indicate that the dimension no longer scales with the number of interacting modes once the system is large enough. However, this saturation is evident only after more than 400 modes are present. The 27 modes used in the DEBS code is probably far too few to model the highly turbulent system of the experiment.

The magnitude of the Lundquist number $S$ also probably contributes to the difference between the

experiment and simulation. The dynamics of the code change significantly as $S$ changes from $10^3$ to $10^4$.† In particular, the nonlinear interaction among the modes increases with increasing Lundquist number. One could reasonably expect that the dimension should also increase.

Finally, in order to efficiently model the long wavelength tearing modes of the plasma, the code does not treat fast time scale fluctuations correctly. Although most of the power is concentrated in low frequency oscillations, a significant fraction is in the higher frequency dynamics. This is apparent from the broadband nature of power spectra of all signals, and especially the prominent second peak seen in the $\dot{B}_{rw}$ spectrum at about 70 kHz (see figure 6.4).

The fact that low dimensional chaos is seen in the DTEM model and not in the experimental data from MST may not be too disconcerting. The simulation models a specific process, drift wave turbulence, which is believed not to be significant in RFP plasmas. Yet the model is in many ways general enough that one should expect to see similar results despite this difference. The code suggests that one should see simple determinism in individual mode amplitudes. Further, the simulation suggests that once a sufficient number of interacting modes is present the dimension is not strongly affected by increasing that number. However, analysis of individual mode amplitudes from magnetic fluctuations in MST yielded negative results. The simulation does, however, model only one of several processes occurring simultaneously in a real plasma. This omission could account for the difference.

One can probably account for the discrepancy of the experimental data and the numerical simulations on the basis of the simplifications made in the models. However, the results presented here also disagree with results obtained by several other groups working with data from experiments, including RFPs. In short, I think the inconsistency is due to improperly applied analysis techniques by several of the groups reporting positive results. When most of these results were reported the correlation dimension was essentially the only technique available for analysis, and it was relatively new. None of

† Private communication from Carl Sovinec.

the reported results include a plot of the slope $\log C(r)$ versus $\log r$, which aids in identifying the scaling region, and none shows a scaling region of at least one decade. One group reports identifying two scaling regions of different slopes,[11] which seems both an implausible result and an improper interpretation of the analysis. Verification of the results using phase-randomized data sets was not done. In my estimation, the only group that did a thorough examination of the data is Sawley, *et al.* [14] who reported negative results. As further confirmation, I point out that no group studying fusion-caliber plasmas has, to my knowledge, reported positive results in recent history (since 1987).

Thus far I have concentrated on explaining the inconsistency of the results by citing the faults in the numerical models and previous experimental results. Let me now focus on the experimental data to understand why no chaos is seen in it. Looking first just at the quality of the data, there are three concerns which are very closely related. These are the time length of the record, the number of points and the autocorrelation time. To the first issue: Typically, one requires several hundred cycle times of the "dominant" period of the system for proper estimation of the dimension. For the Lorenz attractor this period would be once around either of the lobes. Let us suppose that the dominant dynamics, the tearing mode fluctuations, are a low dimensional chaotic process. For MST data, one would need several tens of milliseconds *at a minimum* to determine the dimension. Higher dimensional systems require more cycles, and the interaction of the tearing modes with other modes may mean the cycle time is longer than the typical 2 to 5 ms between flux jumps. The duration of the flat-top period is about 40 ms, corresponding to only 10 to 15 flux jump periods.

At the opposite end of the spectrum, the time interval between data points is too long. As discussed in section 3.2, when using delay embeddings, proper choice of the time lag $\tau$ is crucial to proper estimation of the dimension, and this is linked to the autocorrelation time of the data. With the exception of $J_{sat}$ all the data had extremely short autocorrelation times, on the order of 2-3 time steps. In high dimensional embeddings, any correlation is probably lost even when choosing $\tau$=1 for the time lag. Finally, there are too few points available for analysis. The MST system is probably high

dimensional, and most authors estimate that the number of points required scales exponentially with the dimension of the system. Estimating the dimension of the Mackey-Glass system with $T$ =100s required 40,000 points for a reasonable plateau length at the accepted dimension of 7.5. For the 20,000 points available for analysis, one could possibly expect to measure a dimension of only 6-7 at most.

The latter two issues were addressed to some extent in data that were not presented here. 32,000 data points digitized at 1MHz for $\dot{B}_{tw}$ and $i_p$ were taken during the flat-top period of an MST discharge. The increased sampling time meant an autocorrelation time of 4-5 time steps. Analysis of these data yielded results nearly identical to those presented in chapter 6.

On the basis of this analysis, one must conclude that the system is probably high dimensional. I would estimate that it is very probably greater than a dimension of 15. This lower limit is based largely on conjecture from examining the data. Typically when analyzing a system, even if all parameters – embedding delay time, embedding dimension, number of points, etc. – are not optimally determined there is at least some indication of a plateau in the correlation dimension plots. The data from the MST show not the slightest hint of a plateau, even for embeddings up to 30. The behavior of the correlation plots is very similar to high dimensional or random data.

An issue separate from the data itself is whether the data are truly representative of the MST dynamical system. An obvious possible problem is that the signals are contaminated by noise. Even a small amount of noise can obscure the simple determinism, especially for high dimensional systems. The question is, what is the source of the noise? The diagnostic equipment used to gather the data is largely noise free, contributing a noise level of perhaps 1 to 2 parts in $10^3$ at most to the signal. Another possible source of noise is the plasma itself. The dominant dynamics are thought to be the 10 kHz oscillation of the tearing mode fluctuations. Yet there is significant power in higher frequency fluctuations as well. If the tearing mode dynamics are governed by a low dimensional chaos, perhaps these high frequency oscillations are obscuring the chaos.

One cannot, however, consider this a "noise" process in the sense that it is concealing the true

dynamics of the system. The high frequency oscillation as well as the tearing mode oscillations are part of the same dynamical system; they cannot be separated into dynamical and noise component. Although the two processes may occur on different scales as was suggested to explain the results of the DTEM model, they are presumably coupled, and so are both part of the dynamical system. Ultimately, the true dimension of the system is determined by the highest dimension process.

A second problem is the issue of stationarity. As demonstrated in section 4.4, even a very slight perturbation of the system can make the dimension immeasurable. In the DEBS code, both the plasma current and the toroidal loop voltage remain fairly constant during the discharge. This is not the case in MST discharges. With the flat-topping network operational the plasma current remains fairly constant over a period of up to 40ms. The loop voltage, however, fluctuates wildly during this period. The salient question is whether the system is in any sense "stationary" at any time during the discharge.

In part, I think the issue of stationarity begs the question. Assuming we have a noise free system (no random disturbances), then if one of the "parameters" fluctuates in time one needs to re-designate it as one of the "variables". This can increase the dimension by at most two if the fluctuations of the parameter are time dependent. If the loop voltage of the system fluctuates, then *that* is the dynamical system, not a lower dimensional system with non-stationary loop voltage.

The issue of stationarity does, however, become pertinent if one of the system parameters is modified randomly – or by a very high dimensional process – during the discharge by some mechanism independent of the system. I think this may be the case in MST. One such process is the influx of impurity ions into the plasma. The presence of impurities has a strong deleterious effect on the plasma's behavior, and substantial effort has been made to control the impurity fraction in the MST. Yet the process is largely uncontrollable. The interaction of the plasma with the MST containment vessel results in an influx of impurities by a process which is probably very high dimensional.

The plasmas of the MST constitute a highly turbulent system of weakly coupled modes and minimal damping. This corresponds in many ways to the inertial range of the DTEM model. Assuming an

attractor exists, if it has a weakly attracting inertial manifold, this impurity influx may perturb the trajectory from the attractor. As demonstrated in section 4.4, even small perturbations can result in a "fuzzy" attractor and destroy any simple determinism in the system. The impurity problem is only one example, and there may be other processes which also affect the stationarity.

My own feeling is that it is probably impossible to identify and quantify a low dimensional chaotic system in MST discharges. This is not to say that I believe that the system is stochastic. It has been shown that for hydrodynamic turbulence (in 2D) the maximum dimension of the system is proportional to the Reynolds number squared.[73] Assuming this applies to magnetohydrodynamic systems, this does puts an upper bound of $10^{12}$ on the dimension of the system. It may be much lower. The major difficulties I see in identifying this possible low dimension are the length of the flat-top period of the discharge and the related problem of stationarity. The former problem is a hardware/money problem, which in principle could be addressed. The latter may be impossible to remedy. Because of the nature of the system, even tiny random perturbations probably destroy any stationarity and dramatically increase the dimension of the system.

### 7.3. Future Work

For the future, I see several avenues which can be pursued in continuing to study chaos in plasmas and especially RFPs. Using the DEBS code, issues which should be addressed are the scaling of dimension with the Lundquist number and the number of modes in the system. A version of the code now exists which includes finite pressure effects. Pressure effects on the dimension should also be studied. In the DTEM model, we need to understand better how the dimension scales with truly large systems and why there are differences between the damping and inertial ranges. David Newman and I have plans to continue these investigations.

In the MST, despite the fact that deterministic chaos cannot be identified, continuing studies may still prove useful. Should the machine evolve so that system is more "stationary" – long flat-top period, reduced flux jumps and loop voltage spikes – it may be possible to identify a low dimensional attractor.

Also, with the development of new techniques, e.g. dimension densities, it may be possible to identify relatively high dimensional chaos in the MST at some time in the future. Finally, in controlling chaotic systems, one does not necessarily need to know the dimension of the system. It is only necessary that the system be deterministic. Investigations should continue into the feasibility of controlling the MST discharges using chaotic feedback and entrainment.

## 8. References


[1] Schuster, H.G., Deterministic chaos, VCH: Weinhein, Germany (1989).

[2] Krasner, S., ed., The ubiquity of chaos, AAAS: Washington, DC (1990).

[3] Brock, W., Hsieh, K., and LeBaron, B., Nonlinear dynamics, chaos and instability: statistical theory and economic evidence, MIT Press (1991).

[4] Horton, C.W. and Reichel, L., Statistical Physics and Chaos in Fusion Plasmas, John Wiley & Sons: New York (1984).

[5] Braun, T., Lisboa, J., and Gallas, J., "*Evidence of homclinic chaos in the plasma of a glow discharge,*" Phys. Rev. Lett., **68**, 18, 2770 (1992).

[6] Qin, J., Wang, L., Yuan, D., Gao, P., and Zhang, B., "*Chaos and Bifurcations in Periodic Windows Observed in Plasmas,*" Phys. Rev. Lett., **63**, 2, 163 (1989).

[7] Cheung, P. and Wong, A., "*Chaotic Behavior and Period Doubling in Plasmas,*" Phys. Rev. Lett., **59**, 5 (1987).

[8] Chu, J.H. and I, L., "*Quasiperiodic transition to spatiotemporal chaos in weakly ionized magnetoplasmas,*" Phys. Rev. A, **39**, 1, 233 (1989).

[9] Strohlein, G. and Piel, A., "*Experimental evidence of a low-dimensional attractor in the coupling of drift- and ion-sound waves,*" Phys. Fluids B, **1**, 6, 1168 (1989).

[10] Persson, M. and Nordman, H., "*Low-Dimensional Chaotic Attractors in Drift-Wave Turbulence,*" Phys. Rev. Lett., **67**, 24, 3396 (1991).

[11] Arter, W. and Edwards, D.N., "*Non-linear Studies of Mirnov Oscillations in the DITE Tokamak: Evidence of a Strange Attractor,*" Phys. Lett., **114A**, 2, 84 (1986).

[12] Barkley, H.J., Andreoletti, J., Gervais, F., Olivain, J., Quemeneur, A., and Truc, A., "*Estimate of the Correlation Dimension for Tokamak Plasma Turbulence,*" Plasma Phys Controlled Fusion, **30**, 1, 217 (1988).

[13] Gee, S.J. and Taylor, J.B., "*Dimension Measurement of Fluctuations in HBTX1A,*" in 12th European Conference on Controlled Fusion and Plasma Physics, September (1985).

[14] Sawley, M.L., Simm, W., and Pochelon, A., "*The Correlation Dimension of Broadband Fluctuations in a Tokamak,*" Phys. Fluids, **30**, 1, 129 (1987).

[15] Assadi, S., Prager, S.C. and Sidikman, K.L., "*Measurement of nonlinear mode coupling of tearing fluctuations,*" Phys. Rev. Lett., **69**, 2, 281 (1992).

[16] Jackson, E.A., Perspectives of nonlinear dynamics, vol. 1-2, Cambridge U Press: Cambridge (1989).

[17] Ott, E., Grebogi, C., and Yorke, J., "*Controlling chaos,*" Phys. Rev. Lett., **64**, 11, 1196 (1990).

[18] Shinbrot, T., Ott, E., Grebogi, C., and Yorke, J., *"Using chaos to direct trajectories to targets,"* Phys. Rev. Lett., **65**, 26, 3215 (1990).

[19] Ditto, W., Rauseo, S., and Spano, M., *"Experimental control of chaos,"* Phys. Rev. Lett., **65**, 26, 3211 (1990).

[20] Jensen, R., *"Chaos,"* in Encyclopedia of Physical Science and Technology, Academic Press, Inc. (1992), p. 83.

[21] Hénon, M., *"A two-dimensional mapping with a strange attractor,"* Comm. Math. Phys., **50**, 69 (1976).

[22] Lorenz, E., *"Deterministic Nonperiodic Flow,"* J. Atm. Sci., **20**, 130 (1963).

[23] Takens, F., *"Detecting Strange Attractors in Turbulence,"* in Dynamical Systems of Turbulence, Rand, D.A. and Young, L.S., Eds., Springer: Berlin (1981), p. 366.

[24] Moon, F., Chaotic vibrations, Wiley & Sons: New York (1987).

[25] Mandelbrot, B., The fractal geometry of nature, Freeman: San Francisco (1982).

[26] Eckmann, J.P. and Ruelle, D., *"Ergodic Theory of Chaos and Strange Attractors,"* Rev. Mod. Phys., **57**, 3, 617 (1985).

[27] Shannon, C.E. and Weaver, W., The mathematical theory of information, U. Illinois Press: Urbana (1949).

[28] Grassberger, P. and Procaccia, I., *"Characterization of Strange Attractors,"* Phys. Rev. Lett., **50**, 5, 346 (1983).

[29] Wolf, A., Swift, J., Swinney, H., and Vastano, J., *"Determining Lyapunov Exponents from a Time Series,"* Physica D, 16, 285 (1985).

[30] Haken, H., *"At Least One Lyapunov Exponent Vanishes if the Trajectory of an Attractor Does Not Contain a Fixed Point,"* Phys. Lett., **94A**, 2, 71 (1983).

[31] Eckmann, J.P., Kamphorst, S.O., Ruelle, D., and Ciliberto, S., *"Lyapunov Exponents for Time Series,"* Phys. Rev. A, **34**, 6, 4971 (1986).

[32] Kaplan, J. and Yorke, J., *"Chaotic behavior of multidimensional difference equations,"* Springer (1979), p. 204

[33] Rowlands, G. and Sprott, J.C., *"Extraction of dynamical equations from chaotic data,"* Physica D, **58**, 251 (1992).

[34] Cremers, J. and Hübler, A., *"Construction of differential equations from experimental data,"* Z. Naturforsch, **42a**, 797 (1987).

[35] Farmer, J.D. and Sidorowich, J., *"Predicting Chaotic Time series,"* Phys. Rev. Lett., **59**, 8, 845 (1987).

[36] Sgihara, G. and May, R., *"Nonlinear forcasting as a way of distiguishing chaos from measurement error in time series,"* Nature, **344**, 734 (1990).

[37] Wayland, R., Bromley, D., Pickett, D., and Passamante, A., *"Recognizing Determinism in a Time Series,"* Phys. Rev. Lett., **70**, 5, 580 (1993).

[38] Mackey, M. and Glass, L., *"Oscillation and Chaos in physiological control systems,"* Science, **197**, 287 (1977).

[39] Tsonis, A., Chaos: From theory to applications, Plenum: New York (1992).

[40] Sprott, J.C., Strange attractors: Creating patterns in chaos, M&T Books: New York (1993).

[41] Watts, C., *"An efficient method for calculation of the correlation integeral"*, University of Wisconsin - Madison, PLP-1122 (1993).

[42] Watts, C. and Sprott, J.C., *"The Effect of Non-Equilibrium Conditions and Filtering on the Dimension of the Lorenz Attractor"*, University of Wisconsin - Madison, DOE/ER 53198-175 (1991).

[43] Albano, A.M., Muench, J., and Schwartz, C., *"Singular-value decomposition and the Grassberger-Procaccia algorithm,"* Phys. Rev. A, **38**, 6, 3017 (1988).

[44] Theiler, J., *"Spurious Dimension form Correlation Algorithms Applied to Limited Time-series Data,"* Phys. Rev. A, **34**, 3, 2427 (1986).

[45] Grassberger, P. and Procaccia, I., *"Measuring the strangeness of strange attractors,"* Physica D, **9**, 189 (1983).

[46] Havstad, J.W. and Ehlers, C., *"Attractor dimension of nonstationary dynamical systems from small data sets,"* Phys. Rev. A, **39**, 2, 845 (1989).

[47] Smith, L., *"Intrinsic Limits on Dimension Calculations,"* Phys Lett A, **133**, 6, 283 (1988).

[48] Ruelle, D., *"Deterministic Chaos: the Science and the Fiction,"* Proc. R. Soc. Lond. A, 427, 241 (1990).

[49] Briggs, K., *"An Improved Method for Estimating Lyapounov Exponents of Chaotic Time Series,"* Phys. Lett. A, **151**, 1,2, 27 (1990).

[50] Wilkinson, J.H. and Reinsch, C., Linear Algebra, Springer: Berlin (1971).

[51] *LAPACK FORTRAN Routines*, available by anonymous ftp from netlib@research.att.com.

[52] Bauer, M., Heng, H., and Martienessen, W., *"Characterization of spatiotemporal chaos from time series,"* Phys. Rev. Lett., **71**, 4, 521 (1993).

[53] Brandstäter, A. and Swinney, H.L., Phys. Rev. A, **35**, 2207 (1987).

[54] Schreiber, T., *"Determination of the noise level of chaotic time series,"* Phys. Rev. E, **48**, 1, 13 (1993).

[55] Press, W.H., Flannery, B.P., Teukolsky, S.A., and Vetterling, W.T., Numerical Recipes, Cambridge U. Press (1989).

[56] Broomhead, D., Hulke, J., and Muldoon, M., "*Linear filters and nonlinear systems,*" in Proceedings: Interpretation of time series from nonlinear mechanical systems, Warwick, England (1991).

[57] Daniels, R., Approximation methods for electronic filter design, McGraw-Hill: New York (1974).

[58] Kostelich, E.J. and Yorke, J.A., "*Noise reduction in dynamical systems,*" Phys. Rev. A, **38**, 3, 1649 (1988).

[59] Schreiber, T. and Grassberger, P., "*A simple noise-reduction method for real data,*" Phys. Lett. A, **160**, 5, 411 (1991).

[60] Sauer, T., "*A noise reduction method for signals from nonlinear systems,*" Physica D, **58**, 193 (1992).

[61] Cawley, R. and Hsu, G.H., "*Local-geometric-projection method for noise reduction in chaotic maps and flows,*" Phys. Rev. A, **46**, 6, 3057 (1992).

[62] Grassberger, P., Hegger, T., Kantz, H., Schaffrath, C., and Schreiber, T., "*On noise reduction methods for chaotic data,*" Chaos, **3**, 2, 127 (1993).

[63] Enge, N., Buzug, T., and Pfister, G., "*Noise reduction on chaotic attractors,*" Phys. Lett. A, **175**, 178 (1993).

[64] Schreiber, T., "*Extremely simple nonlinear noise-reduction method,*" Phys. Rev. E, **47**, 4, 2401 (1993).

[65] Harned, D.S. and Schnack, D.D., "*Simi-implicit method for long time scale magnetohydrodynamic computations in three dimensions,*" J. Comp. Phys., **65**, 57 (1986).

[66] Kirby, P., "*A simulation code for 3-dimension non-linear incompressible resistive MHD in a periodic cylinder,*" Comp. Phys. Comm, **47**, 17 (1987).

[67] Schnack, D.D., Barnes, D.C., Mikic, Z., Harned, D.S., and Caramana, E.J., "*Semi-implicit Magnetohydrodynamic Calculations,*" J. Comp. Phys., **70**, 330 (1987).

[68] Ho, Y.L., "*Behavior of the reversed field pinch with nonideal boundary conditions,*" Ph.D. thesis, UW-Madison, 1989.

[69] Fonck, R.J., Paul, S.F., adn Y.J. Kim, D.R.R., Bretz, N., Johnson, D., Nazikian, R., and Taylor, G., in 18th European conference of controlled fusion and plasma physics, vol. 15C, Bachmann, P. and Robinson, D.C. ed., Berlin (1991) p. I-269.

[70] Cripwell, P. and Costley, A.E., in 18th European conference of controlled fusion and plasma physics, vol. 15C, Bachmann, P. and Robinson, D.C. ed., Berlin (1991) p. I-17.

[71] Brower, D.L., Peebles, W.A., and Luhmann, N.C., Nucl. Fusion, **27**, 2055 (1987).

[72] Newman, D., *"The dynamics of interacting nonlinearitiesgoverning long wavelength drift wave turbulence,"* Ph.D. thesis, UW-Madison, 1993.

[73] Arnold, V.I., Geometrical methods in the theory of ordinary differential equations, vol. 250, Grundlehren der mathematischen wissenschaften, Springer: Berlin (1988).

## 9. Bibliography

This bibliography presents a condensed list of what I found to be the most useful references for the study of nonlinear dynamics and related analysis techniques. It is in no way meant to be complete, but only a guide for a basic introduction to the field.

### Chaos in General

J.P. Eckmann and D. Ruelle, "*Ergodic Theory of Chaos and Strange Attractors*," Rev. Mod. Phys., **57**, 3, 617 (1985).

E.A. Jackson, Perspectives of nonlinear dynamics, vol. 1-2, Cambridge U Press: Cambridge (1989).

R. Jensen, "*Chaos*," in Encyclopedia of Physical Science and Technology, Academic Press, Inc. (1992), p. 83.

S. Krasner, ed., The ubiquity of chaos, AAAS: Washington, DC (1990).

B. Mandelbrot, The fractal geometry of nature, Freeman: San Francisco (1982).

G. Mayer-Kress, Dimensions and Entropies in Chaotic Systems: Quantification of Complex Behavior, Springer: Berlin (1986).

F. Moon, Chaotic vibrations, Wiley & Sons: New York (1987).

H.G. Schuster, Deterministic chaos, VCH: Weinhein, Germany (1989).

A. Tsonis, Chaos: From theory to applications, Plenum: New York (1992).

### Time Series Analysis

D. Broomhead and R. Jones, "*Time-series Analysis*," Proc. R. Soc. Lond A, 423, 103 (1989).

A. Fraser and H. Swinney, "*Independent Coordinates for Strange Attractors from Mutual Information*," Phys. Rev. A, **33**, 2, 1134 (1986).

A. Fraser, "*Reconstructing attractors from Scalar Time Series: A Comparison of Singular System and Redundancy Criteria*," Physica D, 34, 391 (1989).

E. Lorenz, "*Deterministic Nonperiodic Flow*," J. Atm. Sci., **20**, 130 (1963).

N. Packard, J. Crutchfield, J. Farmer, and R. Shaw, "*Geometry from a Time Series*," Phys. Rev. Lett., **45**, 9, 712 (1980).

J. Roux, R. Simoyi, and H. Swinney, "*Observation of a Strange Attractor*," Physica D, 8, 257 (1983).

**Correlation Dimension**

A.M. Albano, J. Muench, and C. Schwartz, "*Singular-value decomposition and the Grassberger-Procaccia algorithm,*" Phys. Rev. A, **38**, 6, 3017 (1988).

M. Bauer, H. Heng, and W. Martienessen, "*Characterization of spatiotemporal chaos from time series,*" Phys. Rev. Lett., **71**, 4, 521 (1993).

P. Grassberger and I. Procaccia, "*Characterization of Strange Attractors,*" Phys. Rev. Lett., **50**, 5, 346 (1983).

P. Grassberger and I. Procaccia, "*Estimation of the Kolmogorov Entropy form a Chaotic Signal,*" Phys. Rev. A, **28**, 4, 2591 (1983).

P. Grassberger and I. Procaccia, "*Measuring the strangeness of strange attractors,*" Physica D, **9**, 189 (1983).

E.N.L. Lorenz, "*Dimension of Weather and Climate Attractos,*" Nature, **353**, 241 (1991).

D. Ruelle, "*Deterministic Chaos: the Science and the Fiction,*" Proc. R. Soc. Lond. A, 427, 241 (1990).

J. Theiler, "*Spurious Dimension form Correlation Algorithms Applied to Limited Time-series Data,*" Phys. Rev. A, **34**, 3, 2427 (1986).

**Lyapunov Exponents**

G. Benettin, L. Galgani, A. Giorgilli, and J.S. S., "*Lyapunov Characteristic Exponents for Smooth Dynamical Systems and for Hamiltonian Systems; a Method for Computing All of Them. Part 1: Theory,*" Meccanica, 9 (1980).

G. Benettin, L. Galgani, A. Giorgilli, and J.S. S., "*Lyapunov Characteristic Exponents for Smooth Dynamical Systems and for Hamiltonian Systems; a Method for Computing All of Them. Part 2: Numerical Application,*" Meccanica, 21 (1980).

K. Briggs, "*An Improved Method for Estimating Lyapounov Exponents of Chaotic Time Series,*" Phys. Lett. A, **151**, 1,2, 27 (1990).

J.P. Eckmann, S.O. Kamphorst, D. Ruelle, and S. Ciliberto, "*Lyapunov Exponents for Time Series,*" Phys. Rev. A, **34**, 6, 4971 (1986).

J.D. Farmer, "*Chaotic attractors of an infinite-dimensional dynamical system,*" Physica, **D**, 4, 366 (1992).

H. Haken, "*At Least One Lyapunov Exponent Vanishes if the Trajectory of an Attractor Does Not Contain a Fixed Point,*" Phys. Lett., **94A**, 2, 71 (1983).

M. Sano and Y. Sawada, "*Measurement of the Lyapunov Spectrom from a Chaotic Time Series,*" Phys. Rev. Lett, **55**, 10, 1082 (1985).

A. Wolf, J. Swift, H. Swinney, and J. Vastano, "*Determining Lyapunov Exponents from a Time Series,*" Physica D, 16, 285 (1985).

X. Zeng, R. Eykholt, and R.A. Pieke, "*Estimating the Lyapunov - Exponent Spectrum from Short Time Series of Low Precision,*" Phys. Rev. Lett, **66**, 25, 3229 (1991).

**Principal Component Analysis**

D.S. Broomhead and G P. King, "*Extracting qualitative dynamics from experimental data,*" Physica D, **20**, 217 (1986).

**Nonlinear Prediction**

J.D. Farmer and J. Sidorowich, "*Predicting Chaotic Time series,*" Phys. Rev. Lett., **59**, 8, 845 (1987).

G. Sgihara and R. May, "*Nonlinear forcasting as a way of distiguishing chaos from measurement error in time series,*" Nature, **344**, 734 (1990).

R. Wayland, D. Bromley, D. Pickett, and A. Passamante, "*Recognizing Determinism in a Time Series,*" Phys. Rev. Lett., **70**, 5, 580 (1993).

**Noise and Nonlinear Noise Reduction**

R. Badii, G. Broggi, B. Derighetti, and M. Ravani, "*Dimension Increase in Filtered Chaotic Signals,*" Phys. Rev. Lett., **60**, 11, 979 (1988).

R. Cawley and G.H. Hsu, "*Local-geometric-projection method for noise reduction in chaotic maps and flows,*" Phys. Rev. A, **46**, 6, 3057 (1992).

N. Enge, T. Buzug, and G. Pfister, "*Noise reduction on chaotic attractors,*" Phys. Lett. A, **175**, 178 (1993).

P. Grassberger, T. Hegger, H. Kantz, C. Schaffrath, and T. Schreiber, "*On noise reduction methods for chaotic data,*" Chaos, **3**, 2, 127 (1993).

J.W. Havstad and C. Ehlers, "*Attractor dimension of nonstationary dynamical systems from small data sets,*" Phys. Rev. A, **39**, 2, 845 (1989).

E.J. Kostelich and J.A. Yorke, "*Noise reduction in dynamical systems,*" Phys. Rev. A, **38**, 3, 1649 (1988).

F. Mitschke, M. Möller, and W. Lange, "*Measuring Filtered Chaotic Signals,*" Phys. Rev. A, **37**, 11, 4518 (1988).

A. Passamante, T. Hediger, and M. Gollub, "*Fractal dimension and local intrinsic dimension,*" Phys. Rev. A, **39**, 7, 3640 (1989).

T. Sauer, "*A noise reduction method for signals from nonlinear systems,*" Physica D, **58**, 193 (1992).

T. Schreiber and P. Grassberger, "*A simple noise-reduction method for real data,*" Phys. Lett. A, **160**, 5, 411 (1991).

T. Schreiber, "*Extremely simple nonlinear noise-reduction method,*" Phys. Rev. E, **47**, 4, 2401 (1993).

T. Schreiber, "*Determination of the noise level of chaotic time series,*" Phys. Rev. E, **48**, 1, 13 (1993).

EXTERNAL DISTRIBUTION IN ADDITION TO UC-20

S.N. Rasband, Brigham Young University
T. Dolan, EG&G Idaho, Inc.
R.A. Moyer, General Atomics
J.B. Taylor, Institute for Fusion Studies, The University of Texas at Austin
E. Uchimoto, University of Montana
F.W. Perkins, PPPL
O. Ishihara, Texas Technical University
M.A. Abdou, University of California, Los Angeles
R.W. Conn, University of California, Los Angeles
P.E. Vandenplas, Association Euratom-Etat Belge, Belgium
Centro Brasileiro de Pesquisas Firicas, Brazil
P. Sakanaka, Institute de Fisica-Unicamp, Brazil
Mme. Monique Bex, GANIL, France
J. Radet, CEN/CADARACHE, France
University of Ioannina, Greece
S. Ortolani, Istituto Gas Ionizzati, EURATON-ENEA-CNR Association, Italy
R. Andreani, Associazione EURATOM-ENEA sulla Fusione, Italy
Plasma section, Energy Fundamentals Division Electrotechnical Laboratory, Japan
Y. Kondoh, Gunma University, Kiryu, Gunma, Japan
H. Toyama, University of Tokyo, Japan
FOM-Instituut voor Plasmafysica "Rijnhuizen," The Netherlands
Z. Ning, Academia Sinica, Peoples Republic of China
P. Yang, Shandong University, Peoples Republic of China
S. Zhu, University of Science & Technology of China, People's Republic of China
I.N. Bogatu, Institute of Atomic Physics, Romania
M.J. Alport, University of Natal, Durban, South Africa
R. Storer, The Flinders University of South Australia, South Australia
B. Lehnert, Royal Institute of Technology, Sweden
Librarian, CRPP, Ecole Polytechnique Federale de Lausanne, Switzerland
B. Alper, Culham Laboratory, UK
A. Newton, UK

2 for Chicago Operations Office
4 for individuals in Washington Offices

INTERNAL DISTRIBUTION IN ADDITION TO UC-20
80 for local group and file

# END

DATE
FILMED
12/14/93